Fall 11-14-2016

ENGINEERING SMALL MOLECULE BASED DIMERIZATION TO INDUCE TRANSLATION AND PROVIDE OPTOGENETIC CONTROL

Catherine Wright

Catherine Wright

Candidate

Chemistry and Chemical Biology

Department

This dissertation is approved, and it is acceptable in quality and form for publication:

Approved by the Dissertation Committee:

Fu-Sen Liang , Chairperson

Charles Melancon

Lina Cui

David Peabody

ENGINEERING SMALL MOLECULE BASED DIMERIZATION TO INDUCE TRANSLATION AND PROVIDE OPTOGENETIC CONTROL

by

CATHERINE WRIGHT

B.A. Biochemistry, University of New Mexico, 2008

DISSERTATION

Submitted in Partial Fulfillment of the
Requirements for the Degree of

Doctor of Philosophy

Chemistry

The University of New Mexico
Albuquerque, New Mexico

December 2016

Acknowledgements

I would like to thank my mentor and advisor, Fu-Sen Liang, for providing me the opportunity to learn in his lab. I have appreciated his wealth of knowledge that he has shared with me to help me in my research. He has supported me in my curiosity and is patient with mistakes. He has guided me by sending me articles and talking through our ideas. For all of this and more, I am grateful that he has let me learn from his expertise.

I want to thank all the faculty and students that have given me questions or comments on me research to help me better understand the material. This especially includes my committee members Dr. Charles Melancon, Dr. Lina Cui, and Dr. David Peabody. Their knowledge and support has allowed me to look at my experiment and information in ways I would have never thought of alone.

Lastly, but not least I would like to thank my family for the lifelong support that has allowed me the opportunity to pursue my doctorate. You have always believed in me even when I did not, and have helped me when times were hard. The only reason I have made it to this point is the help of very many friends, family and faculty and I cannot express my gratitude enough.

Engineering Small Molecule Based Dimerization to Induce Translation and Provide Optogenetic Control

by

Catherine Wright

B.A. Biochemistry, University of New Mexico, 2008
PhD Chemistry, University of New Mexico, 2016

Abstract

We wanted to develop a system that combines the spatial control of photoactivation and control of translation to build a tool to spatially control translation in neurons. This kind of tool could be used to investigate the role of spatially controlled translation of any protein in neural behavior. In this way the development and growth of neural processes could be studied to elucidate the mechanisms for spatially sensitive events such as pathfinding, repair, or long-term potentiation.

Chemically induced dimerization was used to install a switch into the activation of translation for specific genes. An abscisic acid (ABA) dependent dimerization of the proteins PYL and ABI was engineered to control the proximity of the translation machinery to an RNA sequence by fusing the C-terminus of

eIF4G to PYL and fusing the MS2 coat protein to ABI. This produced ABA dependent translation of a reporter gene downstream of the MS2 stem loop. The expression of the reporter protein was low without ABA and increased within hours of addition of ABA.

ABA dependent dimerization of two proteins, PYL and ABI, was engineered to be photoactivatable. ABA was caged with protecting groups, DMNB and DEACM, that can be cleaved by light. This was used to control the activation of biological events with light. We were able to achieve temporal control over the activation of biological activity, but were unable to spatially control this activity.

The photoactivation of ABA dimerization could possibly be used in combination with the activation of translation. This could provide optical control over translation and possibly provide a tool that is capable of studying translation on a sub-cellular scale.

Table of Contents

List of Figures

List of Abbreviations

2MA	2xMS2-ABI
2MIF	2xMS2-eIF4G
4E-BP	EIF4E binding protein
ABA	Abscisic acid
ABI	ABA insensitive
CB1G	mCherry-BoxB1-GFP
CB2G	mCherry-BoxB3-GFP
ChR	Channelrhodopsin
CIB	Cryptochrome interacting basic helix-loop-helix
CM1G	mCherry-MS21-GFP
CM3G	mCherry-MS23-GFP
CPE	Cytoplasmic polyadenylation element
CPEB	CPE binding protein
CRY	Cryptochrome
DAP-5	Death associated protein-5
DEACM	7-Diethoxy aminocoumarin
DMNB	1,2-Dimethoxy-4-nitrobenzene
DMNPP	2-(4,5-dimethoxy-2-nitrophe- nyl)propyl
EANBP	2-(4’-bis((2-methoxyethoxy)ethyl)amino)-4-nitro-[1,1’-biphenyl]-3-yl)propan-1-ol
eIF2	Eukaryotic translation initiation factor 3
eIF3	Eukaryotic translation initiation factor 3
eIF4A	Eukaryotic translation initiation factor 4 A
eIF4E	Eukaryotic translation initiation factor 4 E
eIF4G	Eukaryotic translation initiation factor 4 g
ERK	Extra cellular signal-related kinase
FAD	Flavin adenine dinucleotide
FKBP12	FK506 binding protein 12
FKF1	Flavin binding kelch repeat F-box 1

FMN	Flavin mononucleotide
FMRP	fragile X mental retardation protein
FRB	FKBP-rapamycin binding
FUS	fused in sarcoma
G3BP	GAP SH3 domain binding protein
GA3	Giberellic acid
GAI	Giberellin insensitive
GAL4BD	Gal4 binding domain
GI	Gigantea
GID1	Giberellin insensitive dwarf 1
IRE	Iron response element
IRES	Internal ribosome entry site
IRP	Iron response protein
LOV	Light oxygen voltage
MA	MS2-ABI
MAPK	Mitogen activated protein kinase
MCP	MS2 coat protein
MIF	MS2-eIF4G
mTOR	Mammalian target of rapamycin
NES	Nuclear export sequence
ORF	Open reading frame
PCB	Phycocyanobillin
PHY	Phytochrome
PI3K	Phosphoinositide 3-kinase
PIF	Phytochrome interacting factors
PIF	PYL-eIF4G
PIFi2MA	PYL-eIF4G-ires-2xMS2-ABI
PYL	Pyrabactin-like regulatory component
RBP	RNA binding protein
RNP	Ribonucleoprotein particles
SG	Stress granules

SMN	Survival motor neuron
TALE	Transcription activator-like effector
TDP-43	TAR DNA binding protein-43
TIA-1	T-cell-restricted intracellular antigen-1
TIAR	TIA-1 related
UTR	Untranslated region
ZBP1	Zipcode binding protein
ZFP	Zinc finger protein
λN	Bacteriophage Lambda N protein
λNIF	2xλN-eIF4G

Chapter 1 – Controlling Translation and Optogenetics

Protein translation is highly regulated in the cell to control the specific time and place that a protein is produced. The regulation of translation to a specific location is particularly important for neural growth. In order to investigate this process we must possess a tool that is capable for sub-cellular activation of translation for specific transcripts. There are tools for controlling the expression of specific transcripts, but none that have control on the sub-cellular scale.

The field of optogenetics has been used to induce signaling on a sub-cellular level using precise activation with light, and maybe a similar technique could be applied to activate translation. Optogenetics is the use of light combined with the expression of a gene that encodes a photo responsive protein system. Combining optics and genetics provides greater control over the activation of the system.

Photo inducible dimerization of proteins is a branch of optogenetics that is highly adaptable to controlling biological events that depend on the proximity of two components. Engineering photo inducible dimerization to control protein translation could provide the ability to investigate the role of a protein in a spatially sensitive natural process.

1.1 Sub-Cellular Control of Translation

Introduction

There are two main parts to gene expression: transcription and translation. The transcription of the DNA into RNA is heavily regulated by the specific condition of the cell. Transcription of any gene can be controlled in time, but since all of transcription occurs in the nucleus, it is generally not a spatially controlled process. The time of translation of an mRNA can be controlled, but in addition translation can be limited to a specific sub-cellular location. The production of a given protein can be restricted to a subcellular region in order to fulfill a very localized purpose.

There are general tools for repressing all cellular translation with drugs such as rapamycin (1). There are even tools for activating translation of a specific transcript (2) and degrading specific sequences (3). A tool that has spatial control of translation of a specific transcript is necessary to investigate the natural functions of localized mRNA in cells. Spatially sensitive translation could be further understood if there were more tools for studying it. There is a need for a tool that will allow subcellular manipulations to learn about the function of localized translation (4).

Importance of Spatially Controlled Translation

There are ways to control the global translation in a cell that tune the level of activity depending upon the conditions. There are also ways a cell can control translation on a more transcript specific level. Global control of translation is achieved by modifying the activity of translational machinery. While mRNA specific control is modulated through the interactions of the mRNA sequences and proteins that bind it.

Translational control is extremely important in the oocyte and early embryo. Early embryos are often transcriptionally silent, but employ a rapidly changing cast of proteins to regulate development processes. Localized mRNAs are seen in many cell types and play a role in establishing polarity and structure (5). The accumulation of different mRNAs is seen at distinct stages in development (5), and it was found that 71% of mRNA's are expressed in spatially distinct patterns in early embryos, Figure 1.1 (6).

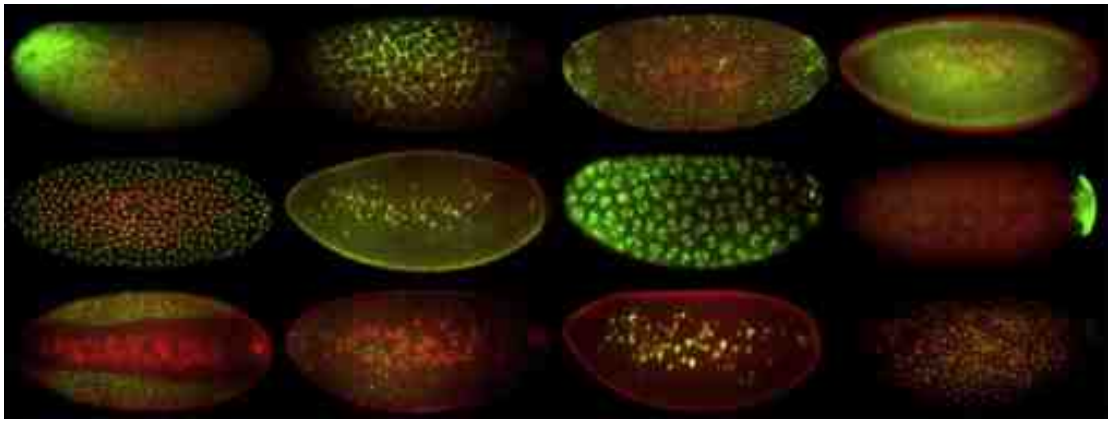

Figure 1.1 Fluorescent *in situ* hybridization of mRNA during early embryogenesis in Drosophila shows the localization of different transcripts. (6)

Localized mRNA causes the accumulation of a protein at the destination of the transcript. This restricts the expression of a protein to a subcellular location, and it can be temporally controlled with stimuli to produce rapid responses. The localization of a transcript allows the cell to be efficient for the specific expression of a protein.

Localized translation is used by cells to establish polarity in embryos. The Xwnt-11 mRNA initiates establishment of the body axes in Xenopus (7). Its spatially controlled translation results in the accumulation of the protein along the dorsal-ventral axis (8). The mRNA for oskar and nanos are specifically expressed in the posterior in Drosophila embryos (9-10). Their translation is controlled by a host of RBPs such as, Bruno, Staufen, and Vasa (12-13). The Nanos and Oskar proteins in turn regulate the expression of other transcripts. The regulation of translation in a single cell is crucial for the development of polarity for the entire organism.

Neurons control the translation of many proteins spatially and temporally through complex mechanisms that allow them to follow guidance cues or avoid repulsive cues. Studies using microarrays have shown that thousands of transcripts are present in axons and dendrites (14). Synaptic activity controls the distribution of mRNAs and the RNA binding proteins (RBPs) present in the neuronal processes (15). Localized translation at synapses establishes what proteins are produced, which is important for the specific activity of the synapse. Local translation occurs at synapses during long-term potentiation and is

triggered by trans synaptic chemical signals (16). Localized translation is essential for the function and growth of neurons.

Several mRNAs from cytoskeletal proteins including β-actin, peripherin, vimentin, γ-tropomyosin 3, and cofilin 1 are present in the axon of dorsal root ganglia (DRG) neurons (17). Also found in the axons are mRNAs for heat shock proteins, endoplasmic reticulum proteins, proteins associated with neurodegenerative disease, anti-oxidant proteins, and metabolic proteins (17). Treatment with neurotrophins increased the levels of cytoskeletal mRNAs only by selectively increasing transport to the axon (17). In addition, repulsive cues induce the axonal translation of cytoskeletal regulators, Rho A and cofilin, to control actin polymerization (18). The localized production of proteins is rapid and occurs in a matter of minutes and allows the cell to rapidly react to changes in its environment.

Mechanisms of Regulating Translation

The translation initiation complex is made up of many proteins. These proteins function to bring the mRNA into proximity with the ribosome so that translation can begin. There is a translation initiation complex composed of eukaryotic initiation factor proteins, such as eIF4E, PABP, eIF4G, eIF4A and eIF3. The mRNA circularizes because the cap binding protein, eIF4E, and the poly A binding protein, PABP, will both bind to eIF4G to bring the head and tail together. The translation initiation factor eIF4G is the connection between the initiation factors that bind the mRNA, PABP and eIF4E, and the factors that bind

the small subunit of the ribosome, eIF4A and eIF3, Figure 1.2. The 40S ribosomal subunit is recruited to the initiation complex. Once it is bound it scans along the RNA until it reaches the first start codon, AUG.

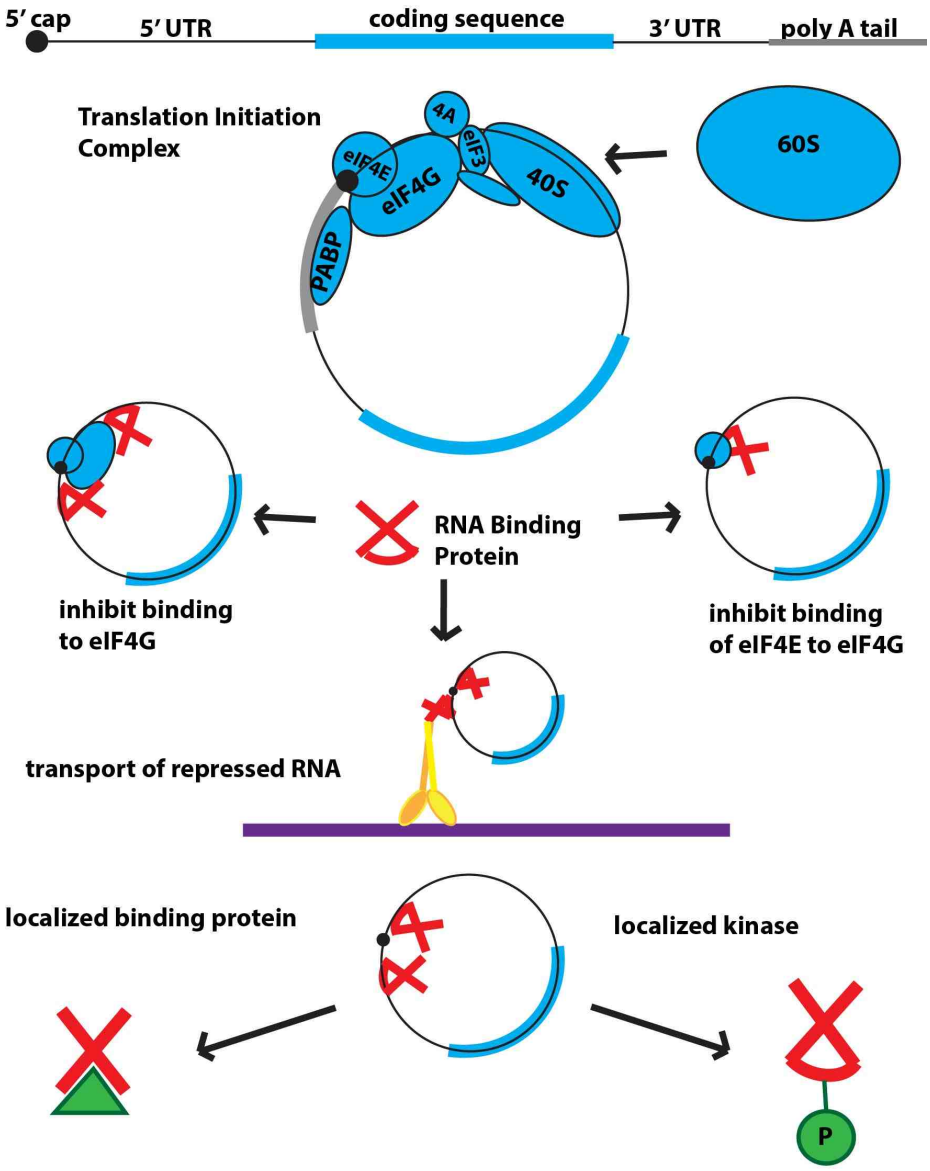

Figure 1.2. Translation of an mRNA requires the translation initiation complex. Regulation of translation occurs by interrupting the formation of the complex. RNA binding proteins are capable of inhibiting translation and localizing the transcript. Activation of translation occurs through inhibition of the repressor protein and release of the mRNA.

The factor eIF4E is a critical regulator for cell growth, development and differentiation (19). Phosphorylation activates the proteins ability to participate in translation and is induced by growth factors, hormones, and mitogens (19). Dephosphorylation occurs in response to serum deprivation, viral infection, and heat shock (19), which globally suppresses cap-dependent translation to protect the cell. The phosphorylation of eIF4E is often used to spatially control the translation of transcripts in a given area, but is not specific to the mRNA it activates.

One way that cells control translation of specific transcripts is to have a RBP that binds a specific mRNA and localizes it to a given subcellular compartment, Figure 1.2. The RBPs block translation of an mRNA until it reaches the proper destination (20). The sequences that regulate localization and repression are most often found in the 3' untranslated region (UTR) of the mRNA (21). Repressors often target the binding of eIF4G and eIF4E, Figure 1.2. A repressor may bind eIF4E to block eIF4G (22) or bind eIF4G to block its ability to recruit the translation complex (23).

The eventual release of the repressors results from a spatially restricted activator protein. The translation activation has been shown to be a result of spatially controlled kinases that inhibit the translational repression through phosphorylation (20). Spatially controlled proteins that bind the translation repressors are also able to cause the release of the mRNA and activation of translation (24).

Localized mRNAs are translated in neurons in response to synaptic activation and guidance cues (25). The guidance cue is received as a signal and transmitted through receptor-coupled kinases, ERK and mTOR (25). The kinase mTOR phosphorylates the eIF4E binding protein 1 (4E-BP1), which causes the dissociation of the 4E-BP1 and eIF4E to activate the translation machinery (26-27). Rapamycin, an FDA approved drug, inhibits translation by preventing the phosphorylation of 4E-BP1 (28). 4E-BP1 is a small protein that competes with eIF4G for binding to eIF4E and prevents the formation of the initiation complex (29). eIF4E and 4E-BP are both phosphorylated in growth cones induced by guidance cues (25). Nerve growth factor and netrin-1 induce a rapid increase in 4E-BP1 phosphorylation in growth cones (30).

RBPs bring together RNA-protein complexes to form RNA granules that prevent translation (31). Some RBPs, such as cytotoxic granule-associated RNA binding protein (TIA-1), TIA-1 related protein (TIAR), GAP SH3 domain binding protein (G3BP), are responsible for reversible aggregation and contain glutamine and asparagine rich domains that readily aggregate to form RNA granules. There are three different kinds of granules: ribonucleoprotein particles (RNP) that function in the transport and the storage of mRNAs, stress granules (SG) that sequester nonessential mRNAs to promote translation of stress response proteins, and processing bodies (P-bodies) that regulate degradation of mRNAs (31). P-bodies often contain miRNA machinery and decapping enzymes (32). Survival motor neuron (SMN) protein is important for the formation of stress granules (33) and is found in RNP complexes with fragile X mental retardation

protein (FMRP) (34). FMRP and the RBP Pumilio function in dendritic transport and repression of mRNAs (35). The primary components of SG are the proteins TIA-1, TIAR, G3BP and SMN, but other disease related proteins associate with SG as they expand such as FMRP, fused in sarcoma (FUS), TAR DNA binding protein-43 (TDP-43), and ataxin-2 (36).

The most well studied RBP is zipcode binding protein 1 (ZBP1) which regulates the β-actin mRNA by directing its localization and expression through binding to a sequence in the 3'UTR of the mRNA (37). β-actin mRNA has been found localized to axonal growth cones using *in situ* hybridization (38). ZBP1 localizes it to regions of high actin polymerization (20). ZBP1 prevents translation of the mRNA until it reaches the periphery of the cell where Src phosphorylates ZBP1 and releases the mRNA for translation (20).

FMRP is known to mediate mRNA delivery and translational repression of certain mRNAs in dendrites (39). FMRP associates with the RNA induced silencing complex and miRNAs (40). FMRP plays a role in growth cone collapse through translational suppression of microtubule associated proteins (41).

An RNA sequence known as cytoplasmic polyadenylation elelment (CPE) is found in the 3'UTR of some transcripts, and is recognized by the protein CPE binding protein (CPEB). This protein regulates the expression mRNAs through cytoplasmic polyadenylation and localization (42). CPEB binds specific sequences to repress translation, but elongates the poly-A tail in response to signaling events to promote translation (43).

Iron response protein (IRP) functions to regulate the expression of genes containing the iron response element (IRE) such as ferritin (44), erythroid 5-aminolevulinate synthase (45), mitochondrial aconitase (46), and succinate dehydrogenase-iron protein (47) in order to control iron homeostasis (44). The IRE is close to the 5' cap in these mRNA and the binding of the initiation complex is prevented when IRP is bound (48).

Cap-Independent Translation

The internal ribosome entry site (IRES) was first discovered in picornaviruses (49). The pseudoknot structure of the RNA is essential for IRES function (50). Picornaviral IRESes show binding for eIF3 and eIF4G (51). The IRESes from hepatitis C and swine fever viruses bind the 40S ribosomal subunit without the need for any of the initiation factors (52). Other IRESes interact with proteins that are not the typical translation initiation factors, but may facilitate recruitment of the ribosome. These non-canonical initiation factors include heterogeneous nuclear ribonucleoproteins, a polypyrimidine-tract-binding protein that is a regulator of splicing (53), La, an autoantigen involved in RNA metabolism (54), death associate protein (DAP5), an eIF4G analog (55). DAP5 is homologous to the C-terminal two thirds of eIF4G and is capable of suppressing both cap-dependent and IRES mediated translation (56). Different viral classes may require different factors to mediate translation (49).

The IRES can control translation of a downstream open reading frame (ORF) of a bicistronic mRNA without affecting the translation of the upstream

ORF, Figure 1.3 (57). Translation at an IRES still occurs even when cap-dependent translation is impaired (58). During picornaviral infection a protease cleaves eIF4G in half and cap-dependent translation is shut down in the host. This allows the virus to focus the translation machinery upon its RNAs using the C-terminal half of eIF4G for IRES mediated translation (59). Encephalomyocarditis virus and poliovirus prevent the phosphorylation of 4E-BP1, which represses cap-dependent translation, but which has no effect upon IRES related translation.

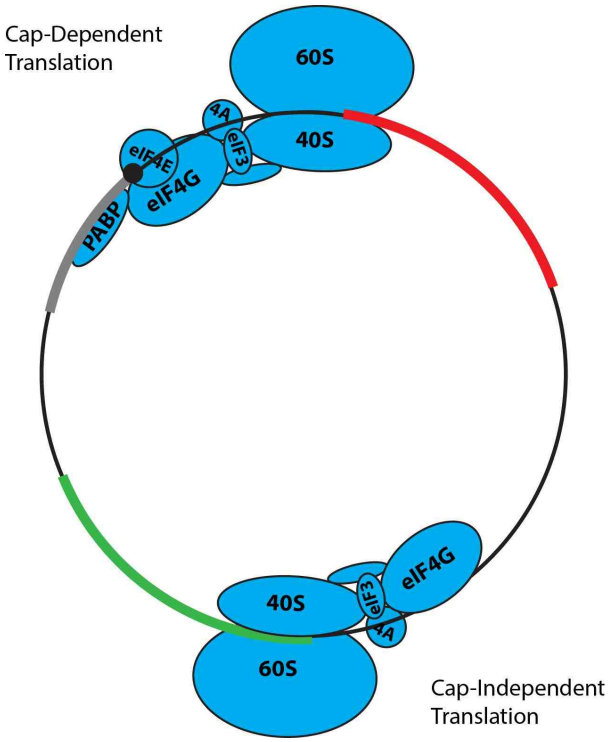

Figure 1.3. Cap-independent translation does not require the RNA binding proteins, eIF4E and PABP, of the initiation complex. Some of the other initiation factors may be necessary to recruit the ribosome. Cells used cap-independent translation during periods when cap-dependent translation is silenced.

Functional cellular IRES's have been found in yeast, Drosophila, birds and mammals. IRES dependent translation is a regulatory method that cells use to cope with stress. Cellular IRES elements are found to be active even when cap-dependent translation is silenced during mitosis, quiescence, differentiation, and stress such as γ-irradiation (54), hypoxia (60) and amino acid starvation (61).

Cap-independent translation can be regulated by its own factors for control of expression completely independent from cap-dependent translation levels. The controlled activity of these factors is capable of regulating the time and place of translation, and has been shown to temporally control translation during certain periods of the cell cycle.

Cap-independent translation may even play a role in spatially controlling the translation of certain mRNAs. Proteins that make up the cap-binding complex are present in low concentrations in dendrites compared to the soma. Five neuronal mRNAs are found to be translated in dendrites through IRES dependent initiation (62).

Dysregulation of Translation in Disease

The proper expression of proteins is essential for normal cellular function. Uncontrolled production of certain genes is the cause for many disease states. Lots of attention has been focused on the transcription level expression of genes

and how it affects disease states. Excessive or insufficient translation in a certain region of the cell can contribute to disease states.

Mutation in FMRP causes fragile X syndrome, which is the most common genetic cause of intellectual disability and autism (63). FMRP is expressed only in the brain and is found with ribosomes or in RNPs and in dendritic spines, but small amounts are also present in the nucleus (64). Absence of this protein leads to over expression of FMRP associated mRNAs in dendrites.

In neurons, synaptic stimulation induces protein synthesis (65). Disruption of protein synthesis impairs long-term potentiation (66). mTOR regulates cap-dependent translation during LTP and memory consolidation (67). Dysregulation of the mTOR pathway is implicated in the mechanisms of neurological disorders including autism and epilepsy (68).

Conclusion

A cell's ability to control translation in a sub-cellular manner allows it to produce proteins in a spatially controlled manner. This process is highly regulated and functions to keep the cell healthy, and is important for many developmental processes. Spatially controlled translation is especially important in neuronal cells for guidance of neurites and synaptic activity. Problems with the regulation of sub-cellular translation are implicated in many diseases. Therefore more tools to study the translation of a specific gene are needed to study the importance and mechanism of these processes.

1.2 Optogenetic Control of Biological Events

Introduction

The field of optogenetics has shown how much can be learned from new tools to manipulate cellular behavior. Optogenetics is a broad field encompassing many techniques that employ optics and genetics in combination. This applies to light responsive proteins as well as other biological systems engineered to respond to light. Optical control lends investigators the ability to precisely deliver activation from light in time and space. By combining the genetic control of the system's protein expression and a light activation, the method has the ability to control the responses spatially, temporally, and biologically.

Optogenetics addresses the need to control defined events in defined cell types at defined times in intact animal systems. Because of this the use of optogenetic tools has shown great promise as a tool for very specific activation. Much has been learned from the sub-cellular application of optogenetics in neurons. What is learned from optogenetic systems in general show the versatility and adaptability of optogenetics as a tool.

Optogenetics of Rhodopsins

One of the most influential tools developed in optogenetics uses light activated ion channels to manipulate the synaptic activity of neurons. The ion channels were originally discovered in bacteria where there are a large variety of species that use photo responsive proteins (69). These proteins use retinal as cofactor to respond to light and thus they are collectively called rhodopsins. The most popularly used rhodopsin is channelrhodopsin (ChR), one that allows the passive transport of cations from irradiation with blue light (70), which has been used in neurons to depolarize the cell membrane.

Control from Optogenetics

Optogenetics has achieved specificity for a target in several ways including, targeting certain cell types based upon expression of a specific promoter, by spatially restricted delivery of virus to target a specific neural structures, and by precisely controlling the delivery of light to activate the system (71).

Viral infection has been used with many optogenetic tools because it is an efficient way to deliver gene components into living animals. The area of injection can control the general organ or substructure of an organ that is infected, Figure 1.4. In addition, it is possible to illuminate an axon far from the cell body where the opsin was introduced because the opsins are trafficked down

the axon, Figure 1.5. This provides the ability to control the projections of cells to select the cells of interest without any genetic knowledge of the cell (72).

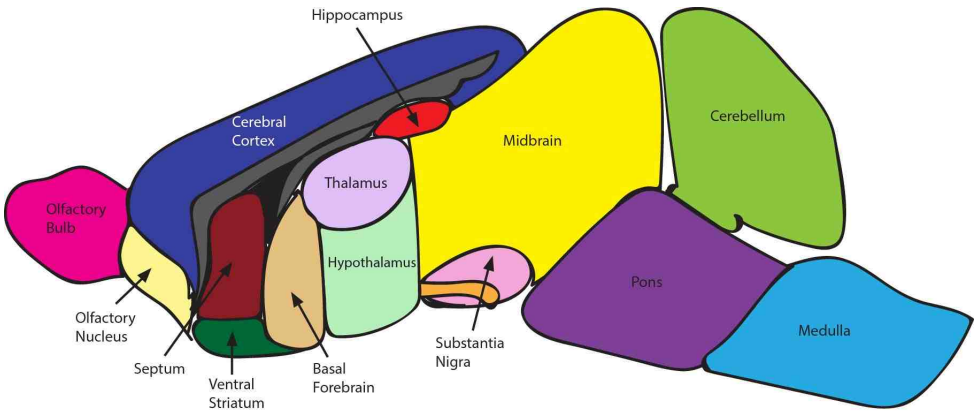

Figure 1.4. Different regions of the brain can be targeted for delivery because of the spatial separation of the anatomical structures. An optogenetic construct can be virally delivered such that the infection is localized near the region of delivery. This allows the expression of this gene only in the specific area of delivery.

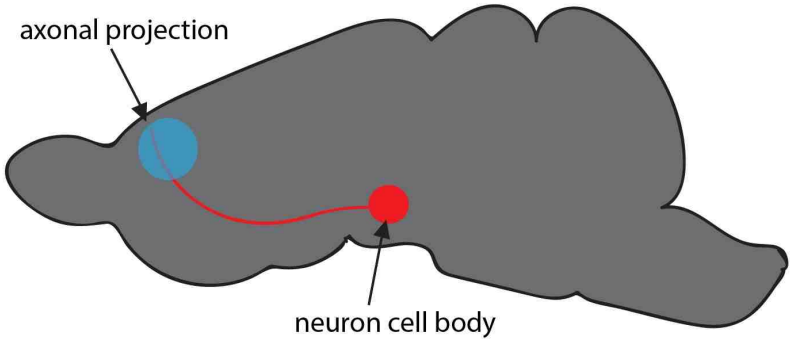

Figure 1.5. Light activation of optogenetics allows sub-cellular control through optical precision. The axons of neurons may extend across the brain such that the process and the cell body are well separated in space. Studies in intact brains can illuminate neuron projections to target protein activity on a subcellular level. This allows specific spatial control over the activation of optogenetic proteins.

Because they employ a genetic component, these tools can be controlled by the genetic context they are given. Therefore cell type specific promoters can control the expression of the system. In this way the CamKII expressing neurons have been targeted to selectively express genetic components, Figure 1.6A. The use of specific promoters can be somewhat difficult when using viruses because the payload is usually less than 4kb, while strong and specific promoters may often be too large for this.

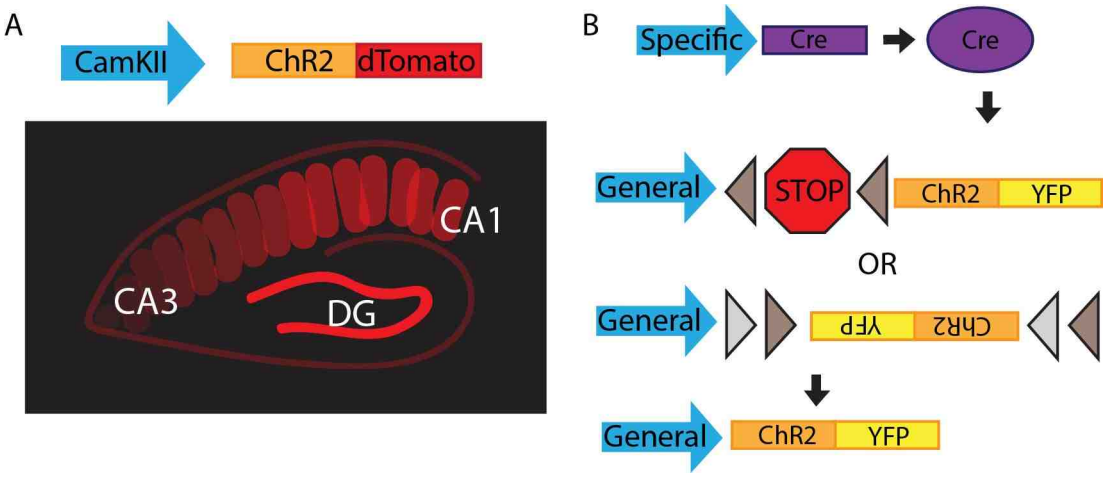

Figure 1.6. (A) Using a cell type specific promoter can control expression of optogenetic tools. A specific subset of cells in the hippocampus express the CamKII promoter. Only these cells will express an optogenetic protein, ChR2, fused to a red fluorescent protein, dTomato. The Cornu Ammonis areas CA1 and CA3 show some expression of this promoter, while the dentate gyrus (DG), shows strong expression of the CamKII promoter. (B) Transgenic mouse lines expressing recombinase enzymes under a specific promoter can be used in conjunction with recombinase dependent optogenetic expression. This allows the use of a small and strong promoter when infecting the optogenetic component, ChR2 fused to YFP. The optogenetic protein will only be expressed in cells where the recombinase is present.

This issue has been somewhat mediated by using transgenic animals that express the recombinase Cre under specific promoters. The restricted presence of the recombinase causes the restricted expression of recombinase dependent constructs, Figure 1.6B. In this way the field of optogenetics can be combined with the plethora of transgenic recombinase expressing animals.

Channelrhodopsin was first used to depolarize hippocampal neurons to induce synaptic events (73). Later optogenetic control was feasible even in intact mammalian brain tissue (74) and freely moving mammals (75). This allows researchers to learn about the roles of cells by how they transform the given input information that we give them and how that transformation changes based upon biological conditions.

Optogenetics has been used to study how different cell types contribute to the function of certain pathways and interactions. There have been studies into mechanisms of deep-brain stimulation for Parkinson's disease (76) and the role of nucleus accumbens in modulating cocaine reward (77). It has been used to study the contribution of hypothalamic hypocretin neurons to sleep and wakefulness (75), to examine dopamine-modulated addiction (78), to do functional mapping of the motor cortex (79), and to investigate the amygdala neurons in regulating anxiety (80). The most important impact of optogenetics is from use as a research tool to obtain insights into complex tissue function.

Photo Inducible Dimerization

Protein dimerization is a modular switch that can be inserted into processes controlled by protein proximity. Inducible dimerization has become an increasingly popular tool for controlling biological processes because of its versatility. Engineered dimerization has allowed the investigation of many processes because it is adaptable to any situation that can be controlled by the proximity of two proteins such as signaling network interaction or protein complex formation.

Chemically induced dimerization has already been shown to activate transcription, reconstitute a functional protein from separated domains, and control protein translocation to cellular organelles. Photo induced dimerization is based upon photo activation of chemical changes that induce protein binding and should be able to do anything that has been controlled with chemically inducible dimerization, but additionally provides greater spatial and temporal control.

Controlling dimerization is more generally applicable than pharmacological and photochemical tools because it can be adapted to diverse biological situations and has specifically controlled interactions that have less off-target effects. Other kinds of light regulated proteins (channelrhodopsin) or caged compounds (glutamate) have specific purposes and may not be good for engineering biological outcomes based upon protein proximity, but have shown the benefits of using light to control activity.

There are two ways in which researchers have developed photocontrolled dimerization of proteins. In one scenario the light-sensing molecule is unbound but can interact with the protein; in the other the light-sensing molecule is integral to the protein. Of the first variety there are many ligands that induce dimerization but just a few that have been caged by light cleavable moieties, making a light dependent dimerization system. Of the second variety there are a number of light activated dimerizing pairs that have been taken from their natural functions and put to new uses.

Photocaging Chemical Dimerizers

Photo cages allow spatially and temporally resolved manipulation through controlled delivery of light. Many biologically relevant small molecules have been photo caged. Caged calcium chelators were used to observe the effects from calcium concentrations on muscle contraction, neurotransmitter release and ion-channel gating (81). Caged glutamate was used to explore the function of AMPA and NMDA receptor and in long term potentiation in synapses, and could be used to activate individual dendritic spines (82). Caged ATP was the first caged molecule used in biology (83) and has since been used to study sodium/potassium pumps (84). There has been use of caged nucleic acids to temporally control gene expression (85).

A photo cage must be removable by light and yet must also be stable enough to not be cleaved under biological conditions. It also has to block

biological activity of the caged molecule (e.g. inducing protein dimerization). The photocages need to be cleavable by common wavelengths used in fluorescence microscopy. Other characteristics that make a good cage are good solubility in aqueous solution, long wavelength absorption and high absorption coefficient.

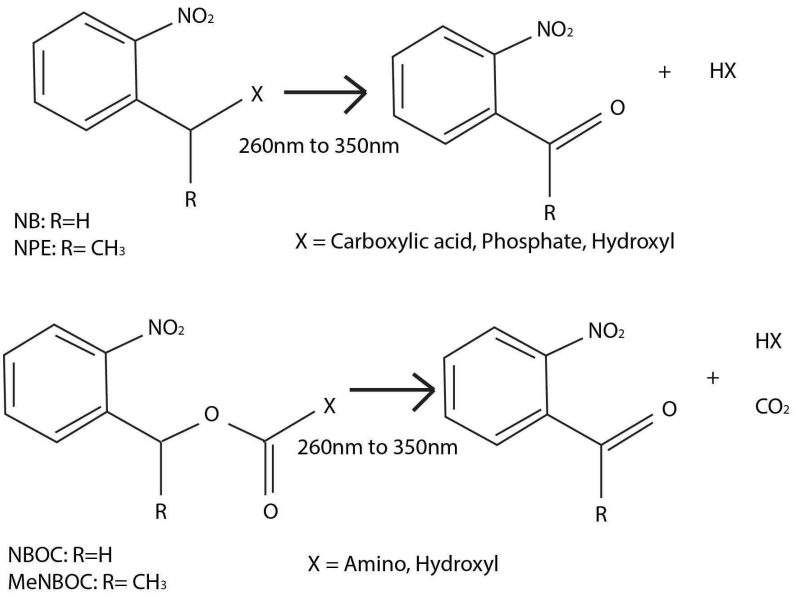

Figure 1.7. Nitrobenzene derivatives are the most commonly used photo caging groups. They can be conjugated to many types of functional groups such as carboxylic acids, phosphates, hydroxyls, and amines. These groups can be cleaved with light to produce the free caged molecule and a nitrosobenzene product.

The most commonly used photo cage is nitrobenzene and its derivatives, Figure 1.7. This group of photo cages is cleaved by light from 260nm to 350nm depending upon the structure of the cage and the ligand (86). These can be attached to a variety of different functional groups, Figure 1.7. There are other classes of photo cages including p-hydroxyphenacyl and coumarin. The

coumarin compounds have the advantage that they can be cleaved with longer wavelength light, 320nm to 400nm (86).

Photocaging of chemical inducers of dimerization takes a small molecule dependent protein-binding event and puts it under the control of light. The small molecule is covalently linked to a large molecule in such a way as to block its ability to interact with the protein pair and therefore cage it in the dark state, Figure 1.8. Upon irradiation these photocaging groups access a high-energy state that facilitates the breaking of the linkage to the small molecule allowing it to interact with its protein pair and induce dimerization.

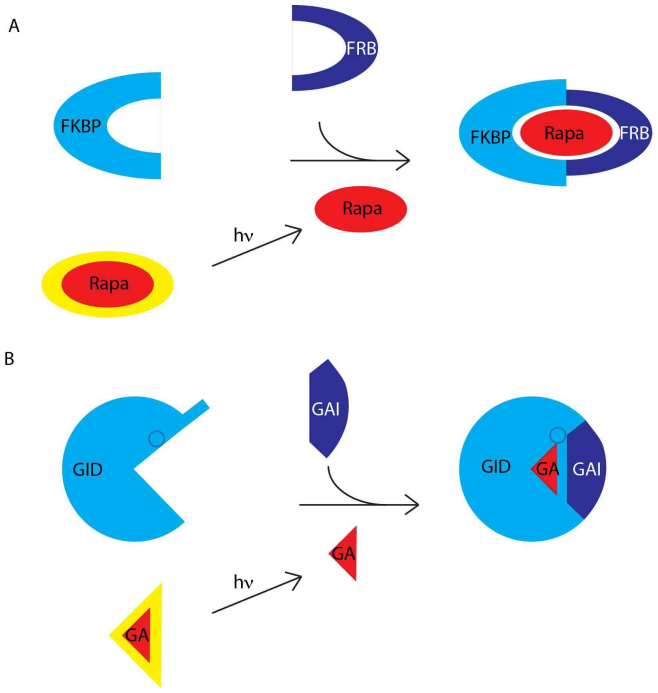

Figure 1.8. Chemical dimerizing systems use a small molecule to induce the binding of two proteins. Several chemical dimerization systems have been engineered to be light responsive including rapamycin (A) and gibberellin (B) dependent dimerization. The ligands, rapamycin and gibberellin, have been caged to block the interaction with the dimerizing protein pair. Irradiation of the cage causes release of the small molecule, which can then induce dimerization.

Rapamycin

Rapamycin is the most widely used chemical inducer of dimerization in engineered systems. Rapamycin is a macrolide bacterial natural product that binds the FK506 binding protein 12 (FKBP12) and this complex binds an FKBP-rapamycin binding (FRB) domain, Figure 1.8 (87). There are endogenous FRBs and FKBPs present in mammalian cells that are affected by rapamycin. A well known protein that is involved in the regulation of translation is named the mammalian target of rapamycin (mTOR) and contains an FRB domain. Rapamycin inhibits translation of proteins from binding mTOR and endogenous FKBPs and has immunosuppressive and anti-proliferative effects.

The hydroxyl group at C-40 was caged to prevent intermolecular contacts to FKBP12. The simple caging of rapamycin does not reduce the affinity enough to prevent binding to FKBP12 and FRB. Both the caged and free rapamycin induced dimerization with wild type FKBP12 with or without UV. Hence there is sufficient dimerization of the proteins that there is no “off” state in the dark. Several strategies were used to circumvent the difficulty in caging rapamycin.

It was thought that the complex was not sensitive enough to be perturbed by the caging. A mutant form of FKBP12 termed iFKBP, was used because it has increased flexibility in the loop that is next to C-40 of rapamycin, Figure 1.9. Caged rapamycin binds to iFKBP and distorts the proteins conformation in order to make extra contacts with the molecule, and is not able to bind FRB. Irradiation with 365nm light was able to release rapamycin and induce dimerization (88).

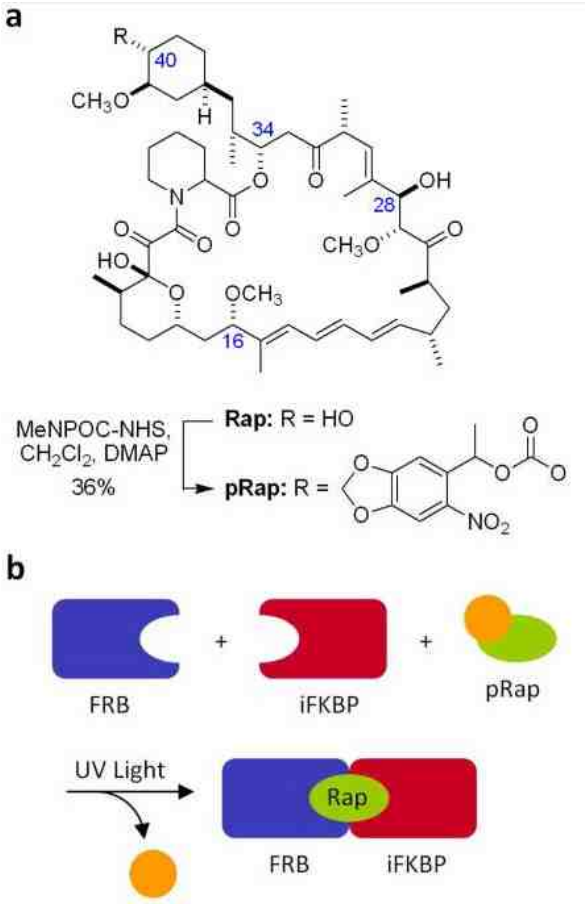

Figure 1.9. Rapamycin was caged at C-40 with a nitrobenzene derived photoprotecting group. The cage did not prevent dimerization of wildtype FKBP and FRB in the dark. FKBP was mutated so that dimerization did not occur when rapamycin was caged, but did occur once the cage was released.

Another group attached biotin to the photo cage and incubated it with streptavidin, Figure 1.10. This structure was unable to permeate cell membranes, but once cleaved the free rapamycin was able to cross and interact with its protein pair (89). This strategy works best when the target is at or near the membrane, and for short periods of time because of diffusion.

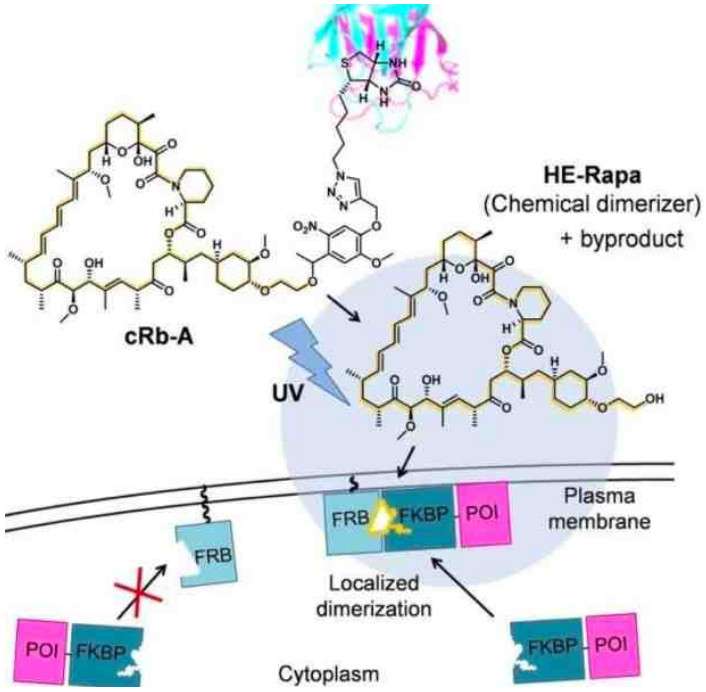

Figure 1.10. Rapamycin was caged at C-40 with a nitrobenzene derivative. The nitrobenzene was linked to biotin and incubated with streptavidin. The presence of the large moiety prevented the molecule from crossing the membrane, essentially sequestering it. This prevented the interaction of rapamycin with FKBP or FRB in the cell until the cage was cleaved, and then free rapamycin was able to enter the cell.

In addition, a rapamycin dimer was created with a photo cleavable linker in between. This dimer was capable of homodimerization of FKBP12, but could induce heterodimerization between FKBP12 and FRB once cleaved (90).

Gibberellin

Gibberellic acid (GA_3) is a pentacyclic diterpene that promotes growth and elongation of plant cells. GA_3 binds to a receptor protein gibberellin insensitive dwarf 1 (GID1) in plants causing a conformational change in the protein so as to

be able to bind the protein gibberellin insensitive (GAI). GID1 has a tight binding pocket for GA_3, which makes it easy to install a molecular cage for GA_3. GA_3 itself is not membrane permeable, but esterified versions of it are (91). The cages allow the molecule to cross the membrane and once cleaved free GA_3 is unable to leave the cell.

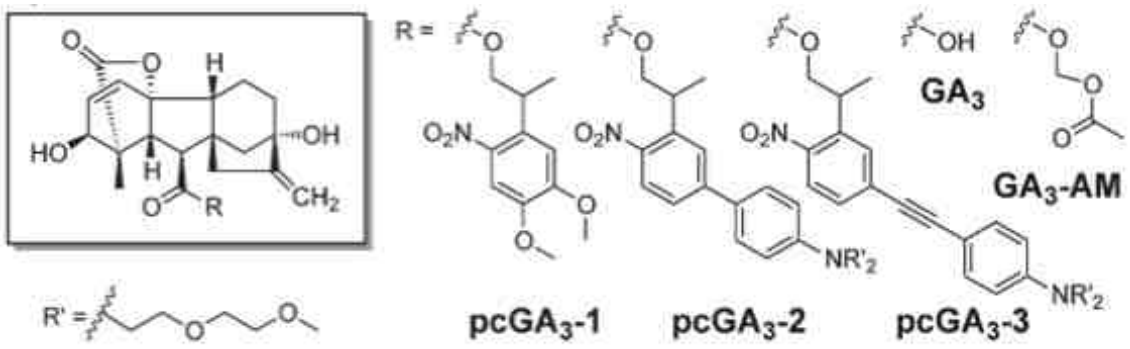

Figure 1.11. Giberellin was caged with nitrobenzene derivatives. Substitution of nitrobenzene derivatives is capable of tuning the physical properties of the compound. Methoxy groups increase solubility in aqueous solutions and enable cleavage with slightly longer wavelengths for the DMPP caged compound $pcGA_3$-1. The addition of phenyl groups an extended pi networks in EANBP and π-extended NPP gives better two-photon absorption and uncaging for the $pcGA_3$-2 and $pcGA_3$-3.

GA_3 was caged with 2-(4,5-dimethoxy-2-nitrophe- nyl)propyl (DMNPP), 2-(4'-bis((2-methoxyethoxy)ethyl)amino)-4-nitro-[1,1'-biphenyl]-3-yl)propan-1-ol (EANBP), and 2-(o-nitro-phenyl)propyl to allow one and two photon uncaging, Figure 1.11. The cages were stable against cellular esterases and could be cleaved with either 412nm light for one photon uncaging or 800nm light for two

photon uncaging. The caged molecule only needs to be irradiated for seconds to be released (92).

Light Responsive Proteins

Photosensitive proteins bind molecular cofactors that can undergo isomerization or formation of bonds upon absorption of a photon; the rearrangement of the cofactor is felt by the protein and propagated to the rest of its structure. These proteins are used in nature to initiate signaling cascades to allow organisms to detect and react to light. The light signaling pathways have been used with phytochromes, and flavin proteins, Figure 1.12.

Photodimerizing proteins have been used to control biological activity in a similar manner as chemically induced dimerization. The small molecule that responds to light is integral to the protein, therefore the activity is mediated by the presence of the photoactivated protein. A large protein will diffuse more slowly than a small molecule and therefore there have been several photodimerizing systems used to control activity on the sub-cellular level.

In addition to the advantage of increased sub-cellular control, there are some drawbacks to using photodimerizing proteins. Researchers have aimed to use longer wavelength activation in cells to minimize photo toxicity. Because of the specificity of the protein for its chromophore, the molecule cannot be altered and therefore its properties cannot be easily tuned in the way a photocage can. The chromophores of some systems may not be bioavailable from the host cell

and must be added in some cases (93). Some proteins will homo-oligomerize with themselves instead of hetero-dimerizing with their partners complicating the outcomes of biological investigations (194).

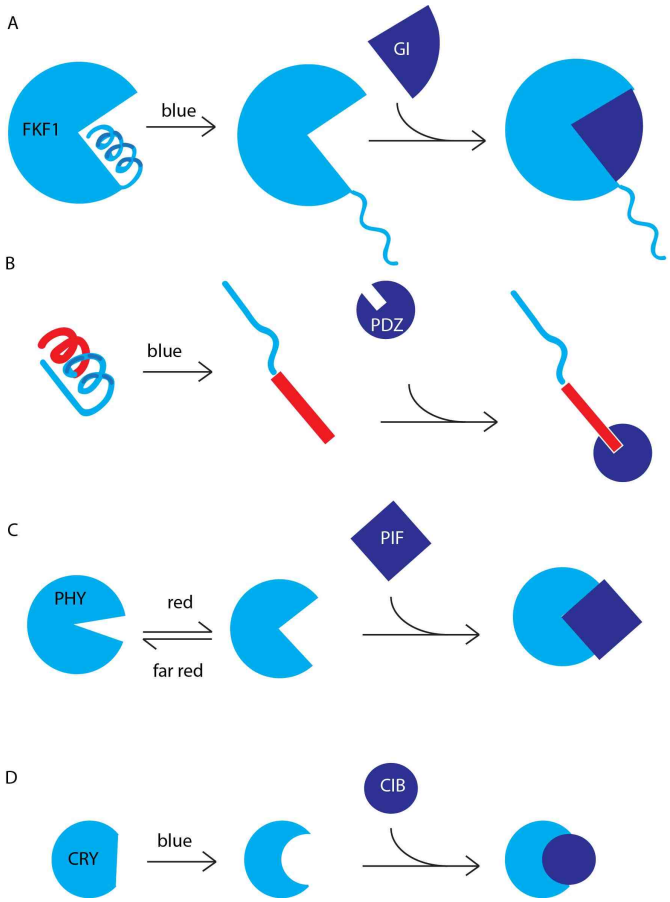

Figure 1.12. Photodimerizing systems have been borrowed from nature and engineered as optical switches. (A) The light-oxygen-voltage domain is found in natural proteins, such as FKF1. This domain unravels a helix in response to light, which exposes a binding site for the protein GI. (B) The LOV domain was fused to a peptide tag (red) such that the tag is unable to bind its cognate protein, PDZ, in the dark. Upon irradiation the helix containing the tag unfolds and is able to bind PDZ. (C) Upon absorption of red light phytochrome proteins, PHY, undergo a conformational change that creates a binding site for the protein PIF. The PHY protein will also absorb far-red light to revert back to the non-dimerizing state. (D) Cryptochrome proteins, CRY,

absorb blue light, which results in a conformational change that allows the binding of the protein CIB.

LOV DOMAIN

Proteins containing the light-oxygen-voltage (LOV) domains are found in plants and bacteria and are found to have many diverse roles in signaling. In the LOV domain the specific cofactor is a flavin mononucleotide (FMN). Upon absorption of blue light the FMN forms a covalent bond between the C(4a) and a cysteine in the LOV domain, Figure 1.13 (95). The formation of the bond propagates a conformational change to the LOV domain. This change causes unfolding of the C terminal helix, Jα, which confers the signal to the effector domain.

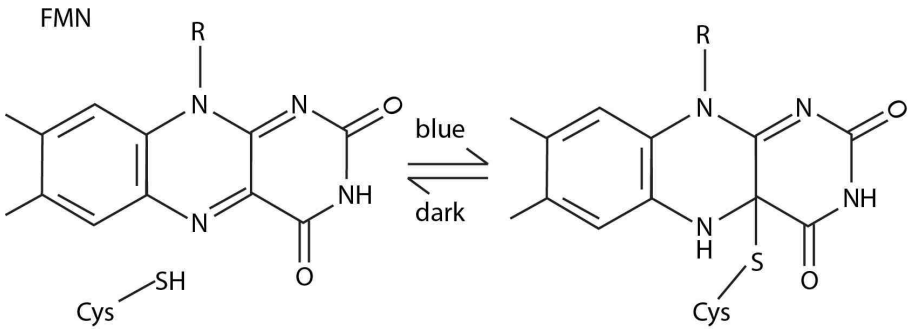

Figure 1.13. FMN forms a bond with the sulfur of cysteine from the LOV domain upon absorption of blue light photons. Spontaneous reversion from cleavage of the cysteine adduct occurs in the dark.

FKF1 GIGANTEA

The flavin binding kelch repeat F-box 1 (FKF1) protein uses a LOV domain to sense light in Arbadopsis thaliana. Upon irradiation the conformational changes in the LOV domain of FKF1 expose a binding site for the protein gigantean (GI). Proteins had visibly dimerized five minutes after irradiation and stayed associated for one and a half hours. Spontaneous reversion occurs with the hydrolysis of the FKF1-FMN bond and the disassociation of the proteins. This system requires up to 30 minutes for maximum effect and has slow spontaneous reversal kinetics (96).

The proteins showed noticeable levels of dimerization in the dark, especially when both were expressed in high levels. Mutations improved background dimerization in the dark by destabilizing the protein-protein interface. The mutation showed no decrease of the ability of the protein pair to associate through photoactivation. Additionally, even though the LOV domain is only 125 amino acids the full length FKF1 is 1,173 amino acids and may be difficult to use in some scenarios because of its size.

LOV PDZ

In the dark state a peptide tag fused to the end of the Jα is sterically blocked by the folded structure. Upon irradiation the Jα helix undocks from the core and unfolds. The unfolding of Jα allows the tag to be exposed and able to bind a protein a protein named PDZ. This results in light inducible dimerization of LOV domain and the PDZ protein (97).

PDZ domains are used to organize protein complexes. They bind to a short peptide sequence on the C terminus of a specific protein. Because PDZ is naturally occurring, there could be cross talk with endogenous signaling pathways.

Phytochromes

Phytochrome (PHY) proteins are used by plants, bacteria and fungi to regulate growth and development in response to light (98). Phytochrome is covalently bound to the tetrapyrrole chromophore bilin via the N-terminal region (98). Absorption of a red photon causes the E/Z isomerization from Pr to Pfr form of the molecule, Figure 1.14. Irradiation with far-red light causes another isomerization of the chromophore back to the Pr state. This molecular movement to the Pfr state translates into a physical change in PHY such that it binds to the protein PIF.

The two states, Pr and Pfr, are both relatively stable and so the dimerization can be turned off by light as well, and the switching is found to be indefinitely repeatable (99). A subcellular area was activated by red light while the area around it could be inactivated by far-red light, thus confining the area of activity (99). In this way they were able to control protein dimerization on the order of micrometers.

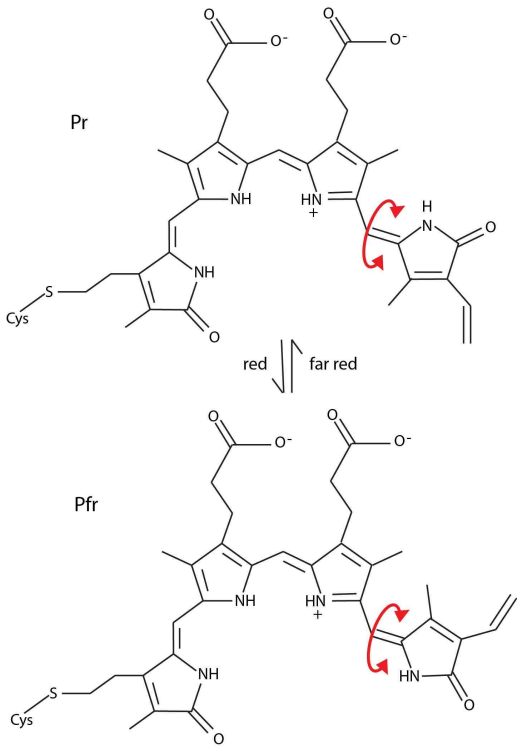

Figure 1.14. The Pr state of the billin chromophore in PHY isomerizes in response to red light to form the Pfr state. The Pfr state isomerizes back to the Pr state from absorption of far-red photons.

Unfortunately the chromophore is not endogenously expressed in mammalian cells and a precursor phycocyanobilin (PCB) must be incubated with cells for some time before the experiment for optimal excitation (93). It was shown to require a 30 min incubation with 5uM PCB for the molecule to be incorporated into the PHY protein (99).

Cryptochromes

Cryptochromes (CRY) are photoreceptors found in animals, plants, bacteria and fungi. These proteins sense light through a flavin adenine

dinucleotide (FAD) chromophore that changes oxidation state in response to absorption of blue light, Figure 1.15. The changes in FAD lead to conformational changes in CRY, which is then able to bind the protein CIB. Excitation with blue light gives dimerization within seconds and dissociation in ten minutes (94). This system can also be activated by 820-980nm light with two-photon excitation.

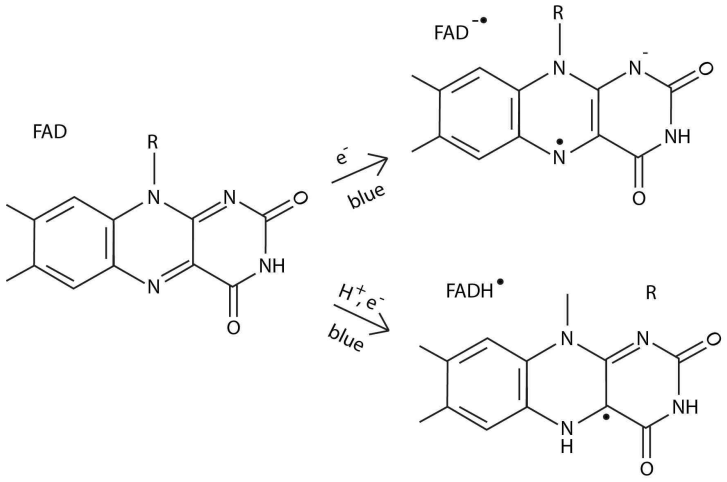

Figure 1.15. The mechanism of FAD signaling in cryptochromes is not completely resolved. Upon absorption of blue light the chromophore becomes reduced, but the exact species formed is still unclear.

Photoactivation of Biological Events

Photoinducible dimerization may be applicable to any biological event that can be controlled by protein proximity, but so far has only been applied to a select few events. Targeting proteins to specific subcellular locations based upon a protein anchor is a common feature in dimerization-based techniques. An anchored protein has been used to target the bud neck, nucleus, myosin ring

of bud, endosome, nucleolus, peroxisomes, spindle pole body and plasma membrane in yeast (100). Other protein anchors have been used to localize proteins to the mitochondria, centrosome, and kinetochores in mammalian cells (101). Targeting of active proteins to different sub-cellular compartments has been used to control their interactions with effector proteins (100). Commonly targeted areas are specific DNA sequences to control gene expression and the plasma membrane to control signaling cascades.

Targeting Functional Proteins to DNA Sequences

Localizing the transcription machinery to a specific gene is a common application of dimerizing proteins. It can be used to control the expression of reporter genes, such as luciferase and GFP, or functional genes. A DNA binding domain is fused to one of the dimerizing proteins to target a specific sequence and therefore a specific gene. The other dimerizing protein is fused to any protein that modulates expression of a gene, such as transcription activator, histone modifier, or recombinase. Activation with light causes the effector protein to be present at the gene's locus upon dimerization.

There is a large variety of DNA binding proteins available for use in targeting a specific gene. The Gal4 DNA Binding Domain (GAL4BD) has often been used to localize one protein partner to the GAL upstream activating sequence. A zinc finger protein (ZFP) can be used to target a specific sequence (102). The DNA binding domain from the transcription activator-like effector

(TALE) protein has a repetitive structure and can be tailored to match many DNA sequences to target a specific gene locus.

Dimerization dependent transcription can be engineered by controlling the interaction of the transcription machinery and a specific gene. VP16 activating domain has been widely used to recruit transcription machinery to a specific gene (102-103). Genes can be transcriptionally silenced from the targeting of a transcriptional repressor and deacetylase (103). Cre recombinase can also be targeted to a specific DNA locus to activate recombinase dependent genes (94, 104)

Inner Membrane Localization

Several systems have used photoinduced dimerization to bring a protein to the membrane to stimulate a cell-signaling cascade. Translocation of active enzymes to the membrane to control cell protrusion is a common application to visualize subcellular spatial control, Figure 1.16.

The C-terminal farnesylation motif from K-Ras called the CAAX box is commonly used for membrane targeting (96). The N-terminus of Lyn is also commonly used to target the membrane (97). The myristoylation sequence at the N-terminus of SOS has been used for membrane recruitment.

The MAPK pathway has been investigated through the membrane localization of the scaffold protein Ste5, the GTP exchange factor SOS, the GTPase Ras and the signaling kinase Raf in different experiments. This MAPK pathway regulates proliferation, differentiation, survival, and apoptosis.

Another pathway that has commonly been targeted is the phophoinositide 3 kinase (PI3K) pathway. This pathway works through the effector proteins AKT, and protein kinase C to control growth, survival, migration, and cell cycle progression. 5-phosphatase was localized to the membrane to control temporally control phosphoinositide metabolism (105).

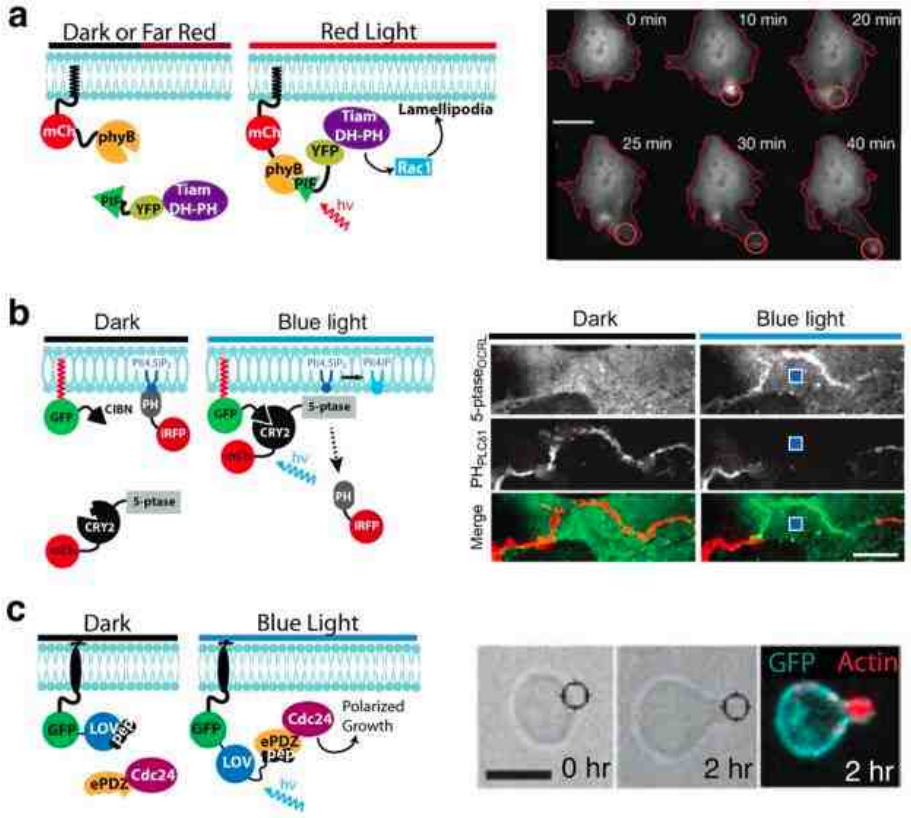

Figure 1.16. Many photodimerizing pairs have been used to control the subcellular activation of signaling cascades. (A) PHY/PIF was used to target Tiam1 to the membrane to activate Rac1 dependent signaling. (B) CRY/CBI was used to target 5-phosphatase to activate phosphoinositide dependent signaling. (C) LOV/PDZ was used to target Cdc24 to the membrane to activate signaling. (106)

Another common pathway employed is the Rho GTPase family to regulate actin dynamics. Often the GTP exchange factors such as Tiam1, intersectin, and Tim are targeted to the membrane to stimulate Rac1, RhoA, or Cdc42 (99). The GTPases Rac1 and Cdc42 have also been targeted to the membrane (97).

Conclusion

Optogenetic control is capable of precise manipulation of neural circuitry in living brains. The technique demonstrates the advantages of using genetics and viral delivery to limit expression to certain cell types in combination with photoactivation. Sub-cellular stimuli can be delivered and responses give information about connectivity and function.

Photoinducible dimerization is one of the optogenetic techniques that can be adapted to control many biological events. This technique can be controlled on the sub-cellular level to spatially sensitive biological events. This technique may be suitable for using as a switch to control sub-cellular activation of protein translation. Photoinducible dimerization may be able to bring the translation machinery into proximity to a specific RNA sequence in a light dependent manner. This may be able to be a tool for investigating the sub-cellular translation of proteins and their roles in development, growth, and functions of cells.

1.3 References

1. Jefferies, H.B.; Fumagalli, S.; Dennis, P.B.; Reinhard, C.; Pearson, R.B.; Thomas, G. Rapamycin suppresses 5'TOP mRNA translation through inhibition of p70s6k. *EMBO J*. **1997**, 16, 3693-704.

2. De Gregorio, E.; Preiss, T.; Hentze, M.W. Translation driven by an eIF4G core domain in vivo. *EMBO J*. **1999**, 18, 4865-74.

3. Kim, D.; Sung, Y.M.; Park, J.; Kim, S.; Kim, J.; Park, J.; Ha, H.; Bae, J.Y.; Kim, S.H; Baek, D. General rules for functional microRNA targeting. *Nature Genetics* **2016**, published online October 24th.

4. Shigeoka, T.; Lu, B.; Holt, C.E. RNA-based mechanisms underlying axon guidance. *J. Cell Biol.* **2013**. 202, 91.

5. Harada, J.J.; Baden, C.S.; Comai, L. Spatially regulated genes expressed during seed germination and postgerminative development are activated during embryogenesis. *Mol. Gen. Genet.* **1988**, 212, 466–473.

6. Lécuyer, E.; Yoshida, H.; Parthasarathy, N.; Alm, C.; Babak, T.; Cerovina, T.; Hughes, T.R.; Tomancak, P.; Krause, H.M. Global analysis of mRNA localization reveals a prominent role in organizing cellular architecture and function. *Cell* **2007**, 131, 174-87.

7. Ku, M.; Melton, D. A. Xwnt-11: A maternally expressed Xenopus wnt gene. *Development* **1993**, 119, 1161–1173.

8. Schroeder, K. E.; Condic, M. L.; Eisenberg, L. M.; Yost, H. J. Spatially Regulated Translation in Embryos: Asymmetric Expression of Maternal Wnt-11 along the Dorsal–Ventral Axis in Xenopus. *Develop. Biol.* **1999**, 214, 288-297.

9. Gavis, E.R.; Lehmann, R. Localization of *nanos* RNA controls embryonic polarity. *Cell* **1992**, 71:301-313.

10. Bergsten, S.E.; Gavis, E.R. Role for mRNA localization in translational activation but not spatial restriction of *nanos* RNA. *Development* **1999**, 126, 659-669

11. Smibert, C.A.; Wilson, J.E.; Kerr, K.; Macdonald, P.M. Smaug protein represses translation of unlocalized *nanos* mRNA in the *Drosophila* embryo. *Genes Dev.* **1996**, 10, 2600-2609

12. Kim-Ha, J.; Kerr, K.; Macdonald, P.M. Translational regulation of *oskar*

mRNA by Bruno, an ovarian RNA-binding protein, is essential. *Cell* **1995**, 81, 403–12.

13. Kim-Ha, J.; Smith, J.L.; Macdonald, P.M. *oskar* mRNA is localized to the posterior pole of the Drosophila oocyte. *Cell* **1991**, 66, 23– 35.

14. Gumy, L.F.; Yeo, G.S.; Tung, Y.C.; Zivraj, K.H.; Willis, D.; Coppola, G.; Lam, B.Y.; Twiss, J.L.; Holt, C.E.; Fawcett, J.W. Transcriptome analysis of embryonic and adult sensory axons reveals changes in mRNA repertoire localization. *RNA* **2011,** 17, 85-98 .

15. Tiruchinapalli, D.M.; Oleynikov, Y.; Kelic, S.; Shenoy, S.M.; Hartley, A.; Stanton, P.K.; Singer, R.H.; Bassell, G.J. Activity-dependent trafficking and dynamic localization of zipcode binding protein 1 and beta-actin mRNA in dendrites and spines of hippocampal neurons. J. Neurosci. **2003**, 23, 3251-3261.

16. Wang, H.; Ardiles, A.O.; Yang, S1.; Tran, T.; Posada-Duque, R.; Valdivia, G.; Baek, M.; Chuang, Y.A.; Palacios, A.G.; Gallagher, M.; Worley, P.; Kirkwood, A. Metabotropic Glutamate Receptors Induce a Form of LTP Controlled by Translation and Arc Signaling in the Hippocampus. *J Neurosci*. **2016**, 36, 1723-9.

17. Willis, D.E.; van Niekerk, E.A.; Sasaki, Y.; Mesngon, M.; Merianda, T.T.; Williams, G.G.; Kendall, M.; Smith, D.S.; Bassell, G.J.; Twiss, J.L. Extracellular stimuli specifically regulate localized levels of individual neuronal mRNAs. *J Cell Biol*. **2007**, 178, 965-80.

18. Piper, M.; Anderson, R.; Dxivedy, A.; Weinl, C.; van Horck, F.; Leung, K.M.; Cogill, E.; Holt, C. Signaling mechanisms underlying Slit2-induced collapse of Xenopus retinal growth cones. *Neuron* **2006**, 49, 215-228.

19. Sonenberg, N. The mRNA 5′ cap-binding protein eIF4E and control of cell growth. Curr. Opin. *Cell Biol.* **1996**, 2, 268-75.

20. Huttelmaier, S.; Zenklusen, D.; Lederer, M.; Dictenberg, J.; Lorenz, M.; Meng, X.; Bassell, G.J.; Condeelis, J.; Singer, R.H. Spatial regulation of beta-actin translation by Src-dependent phosphorylation of ZBP1. *Nature* **2005**, 438, 512-515.

21. Kuersten, S.; Goodwin, E.B. The power of the 3'UTR: translational control and development. *Nature Rev. Genet*. **2003**, 4, 626-637.

22. Richter, J.D.; Sonenberg, N. Regulation of cap-dependent translation by eIF4E inhibitory proteins. *Nature* **2005**, 433, 477-480.

23. Paquin, N.; Ménade, M.; Poirier, G.; Donato, D.; Drouet, E.; Chartrand, P. Local activation of yeast ASH1 mRNA translation through phosphorylation of Khd1p by the casein kinase Yck1p. *Mol. Cell*. **2007**, 26, 795-809.

24. Dahanukar, A.; Walker, J.A.; Wharton, R.P. Smaug, a novel RNA-binding protein that operates a translation switch in Drosophila. *Mol. Cell*. **1999**, 4, 209-218.

25. Lin, A.C.; Holt, C.E. Local translation and directional steering in axons. *EMBO J*. **2007**, 26, 3729-3736.

26. Lawrence, J.C. Jr; Abraham, R.T. PHAS/4E- BPs as regulators of mRNA translation and cell proliferation. *Trends Biochem. Sci.* **1997**, 22, 345–49.

27. Narayanan, U.; Nalavadi, V.; Nakamoto, M.; Thomas, B.; Ceman, S.; Bassel, G.J.; Waren, S.T. S6K1 phosphorylates and regulates fragile X mental retardation protein (FMRP) with the neuronal protein synthesis-dependent mammalian target of rapamycin (mTOR) signaling cascade. *J. Biol. Chem*. **2008**, 283, 18478-18482.

28. Pedersen, S.; Celis, J.E.; Nielsen, J.; Christiansen, J.; Nielsen, F.C. Distinct repression of translation by wortmannin and rapamycin. *Eur. J. Biochem.* **1997**, 247, 449–56.

29. Haghighat, A.; Mader, S.; Pause, A.; Sonenberg, N. Repression of cap-dependent translation by 4E-binding protein 1: competition with p220 for binding to eukaryotic initiation factor-4E. *EMBO J.* **1995**, 14, 5701–9.

30. Campbell, D.S.; Regan, A.G.; Lopez, J.S.; Tannahill, D.; Harris, W.A.; Holt, C.E. Semaphorin 3A elicits stage-dependent collapse, turning, and branching in Xenopus retinal growth cones. *J. Neurosci*. **2001**, 21, 8538-47.

31. Kiebler, M.A.; Bassell, G.J. Neuronal RNA granules: movers and makers. *Neuron* **2006**, 51, 685– 690.

32. Parker, R.; Sheth, U. P bodies and the control of mRNA translation and degradation. *Mol Cell* **2007**, 25, 635– 646.

33. Liu-Yesucevitz, L.; Bilgutay, A.; Zhang, Y.J.; Vanderwyde, T.; Citro, A.; Mehta, T.; Zaarur, N.; McKee, A.; Bowser, R.; Sherman, M.; Petrucelli, L.; Wolozin, B. Tar DNA binding protein-43 (TDP-43) associates with stress granules: analysis of cultured cells and pathological brain tissue. *PLoS One* **2010** 5, 13250.

34. Piazzon, N.; Rage, F.; Schlotter, F.; Moine, H.; Branlant, C.; Massenet, S. In vitro and in cellulo evidences for association of the survival of motor neuron complex with the fragile X mental retardation protein. *J Biol Chem*. **2008**, 283, 5598-610.

35. Knowles, R.B.; Sabry, J.H.; Martone, M.E.; Deerinck, T.J.; Ellisman, M.H.; Bassell, G.J.; Kosik, K.S. Translocation of RNA granules in living neurons. *J Neurosci*. **1996**, 16, 7812–7820.

36. Anderson, P.; Kedersha, N. Stress granules: the Tao of RNA triage. *Trends Biochem. Sci.* **2008** 33, 141–150.

37. Ross, A.F.; Oleynikov, Y.; Kislauskis, E.H.; Taneja, K.L.; Singer, R.H. Characterization of a beta-actin mRNA zipcode-binding protein. *Mol. Cell. Biol.* **1997**, 17, 2158-2165.

38. Bassell, G.J.; Zhang, H.; Byrd, A.L.; Femino, A.M.; Singer, R.H.; Taneja, K.L.; Lifshitz, L.M.; Herman, I.M.; Kosik, K.S. Sorting of beta-actin mRNA and protein to neurites and growth cones in culture. *J. Neurosci.* **1998**, 18, 251-265.

39. Zhang, Y.Q.; Bailey, A.M.; Matthies, H.J.; Renden, R.B.; Smith, M.A.; Speese, S.D.; Rubin, G.M.; Broadie, K. Drosophila fragile X-related gene regulates the MAP1B homolog Futsch to control synaptic structure and function. *Cell*. **2001**, 107, 591-603 .

40. Jin, P.; Zarnescu, D.C.; Ceman, S.; Nakamoto, M.; Mowrey, J.; Jongens, T.A.; Nelson, D.L.; Moses, K.; Warren, S.T. Biochemical and genetic interaction between the fragile X mental retardation protein and the microRNA pathway. *Nat. Neurosci.* **2004**, 7, 113–117.

41. Li, C.; Bassell, C.J.; Sasaki, Y. Fragile X mental retardation protein is involved in protein synthesis-dependent collapse of growth cones induced by semaphoring-3A. *Front. Neural Circuits*. **2009**, 3, 11.

42. Nagaoka, K.; Udagawa, T.; Richter, J.D. CPEB-mediated ZO-1 mRNA localization is required for epithelial tight junction assembly and cell polarity. *Nat Commun*. **2012**, 3, 675.

43. Richter, J.D.; Klann, E. Making synaptic plasticity and memory last: mechanisms of translational regulation. *Genes Dev*. **2009**, 23, 1–11.

44. Hentze, M.W.; Ku¨hn, L.C. Molecular control of vertebrate iron metabolism: mRNA-based regulatory circuits operated by iron, nitric oxide, and oxidative stress. *Proc. Natl. Acad. Sci. USA* **1996**, 93, 8175–82.

45. Cox, T.C.; Bawden, M.J.; Martin, A.; May, B.K. Human erythroid 5-aminolevulinate synthase: promoter analysis and identification of an iron-responsive element in the mRNA. *EMBO J.* **1991**, 10, 1891–902.

46. Schalinske, K.L.; Chen, O.S.; Eisenstein, R.S. Iron differentially stimulates translation of mitochondrial aconitase and ferritin mRNAs in mammalian cells—implications for iron regulatory proteins as regulators of mitochondrial citrate utilization. *J. Biol. Chem.* **1998**, 273, 3740–46.

47. Melefors, O. Translationalregulationin vivo of the *Drosophila melanogaster* mRNA encoding succinate dehydrogenase iron protein via iron responsive elements. *Biochem. Biophys. Res. Commun.* **1996**, 221, 437–41.

48. Gray, N.K.; Hentze, M.W. Iron regulatory protein prevents binding of the 43S translation pre-initiation complex to ferritin and eALAS mRNAs. *EMBO J.* **1994**, 13, 3882–91.

49. Jackson, R.J.; Kaminski, A. Internal initiation of translation in eukaryotes: the picornavirus paradigm and beyond. *RNA* **1995**, 1, 985–1000.

50. Kanamori, Y.; Nakashima, N. A tertiary structure model of the internal ribosome entry site (IRES) for methionine-independent initiation of translation. *RNA* **2001**, 7, 266–274.

51. Vagner, S.; Galy, B.; Pyronnet, S. Irresistible IRES. *EMBO reports*. **2001**, 2, 893-898.

52. Pestova, T.V.; Shatsky, I.N.; Fletcher, S.P.; Jackson, R.J.; Hellen, C.U.T. A prokaryotic-like mode of cytoplasmic eukaryotic ribosome binding to the initiation codon during internal translation initiation of hepatitis C and classical swine fever virus RNAs. *Genes Dev*. **1998**, 12, 67–83

53. Hahm, B.; Kim, Y.K.; Kim, J.H.; Kim, T.Y.; Jang, S.K. Heterogeneous Nuclear Ribonucleoprotein L Interacts with the 3′ Border of the Internal Ribosomal Entry Site of Hepatitis C Virus. *J. Virol*. **1998**, 72, 8782-8788.

54. Holcik, M.; Lefebvre, C.; Yeh, C.; Chow, T.; Korneluk, R.G. A new internal-ribosome-entry-site motif potentiates XIAP-mediated cytoprotection. *Nature Cell Biol.* **1999**, 1, 190–192.

55. Henis-Korenblit, S.; Strumpf, N.L.; Goldstaub, D.; Kimchi, A. A novel form of DAP5 protein accumulates in apoptotic cells as a result of caspase cleavage and internal ribosome entry site-mediated translation. *Mol. Cell. Biol.* **2000**, 20, 496–506.

56. Jang, S.K.; Krau¨sslich, H.G.; Nicklin, M.J.H.; Duke, G.M.; Palmenberg, A.C.; Wimmer, E. A segment of the 5′ non-translated region of encephalomyocarditis virus RNA directs internal entry of ribosomes during in vitro translation. *J. Virol*. **1988**, 62, 2636–43.

57. Vagner, S.; Gensac, M-C.; Maret, A.; Bayard, F.; Amalric, F.; Prats, H.; Prats, A.C. Alternative translation of human fibroblast growth factor 2 mRNA occurs by internal entry of ribosomes. *Mol. Cell. Biol.* **1995**, 15, 35–44.

58. Pestova, T.V.; Shatsky, I.N.; Hellen, C.U.T. Functional dissection of eukaryotic initiation factor 4F: The 4A subunit and the central domain of the 4G subunit are sufficient to mediate internal entry of 43S preinitiation complexes. *Mol. Cell. Biol.* **1996**, 16, 6870–78.

59. Stein, I.; Itin, A.; Einat, P.; Skaliter, R.; Grossman, Z.; Keshet, E. Translation of vascular endothelial growth factor mRNA by internal ribosome entry: implications for translation under hypoxia. *Mol. Cell. Biol.* **1998**, 18, 3112–3119.

60. Fernandez, J.; Yaman, I.; Mishra, R.; Merrick, W .C.; Snider, M.D.; Lamers, W.H.; Hatzoglou, M. Internal ribosome entry site- mediated translation of a mammalian mRNA is regulated by amino acid availability. *J. Biol. Chem.* **2001**, 276, 12285–12291.

61. Morley, S.J. Intracellular signaling pathways regulating initiation factor eIF-4E phosphorylation during the activation of cell growth. *Biochem. Soc. Trans.* **1997**, 25, 503–9.

62. Pinkstaff, J.K.; Chappell, S.A.; Mauro, V.P.; Edelman, G.M.; Krushel, L.A. Internal initiation of translation of five dendritically localized neuronal mRNAs. *Proc. Natl. Acad. Sci. USA* **2001**, 98, 2770-2775.

63. Garber, K.B.; Visootsak, J.; Warren, S.T. Fragile X syndrome. *Eur. J. Hum. Genet.* **2008**, 16, 666–672.

64. Ashley, C.T. Jr.; Wilkinson, K.D.; Reines, D.; Warren, S.T. FMR1 protein: conserved RNP family domains and selective RNA binding. *Science*. **1993**, 262, 563-6.

65. Jiang, C.; Schuman, E.M. Regulation and function of local protein synthesis in neuronal dendrites. *Trends Biochem. Sci.* **2002**, 27, 506 – 513.

66. Klann, E.; Dever, T.E. Biochemical mechanisms for translational regulation in synaptic plasticity. *Nat. Rev. Neurosci*. **2004**, 5, 931–942.

67. Tang, S.J.; Reis, G.; Kang, H.; Gingras, A.C.; Sonenberg, N.; Schuman, E.M. A rapamycin-sensitive signaling pathway contributes to long-term synaptic plasticity in the hippocampus. *Proc. Natl. Acad. Sci. USA* **2002**, 99, 467– 472.

68. Wong, M. Mammalian target of rapamycin (mTOR) pathways in neurological diseases. *Biom. J*. **2013**, 36, 40-50.

69. Beja, O.; Aravind, L.; Koonin, E.V.; Suzuki, M.T.; Hadd, A.; Nguyen, L.P.; Jovanovich, S.B.; Gates, C.M.; Feldman, R.A.; Spudich, J.L.; Spudich, E.N.; DeLong, E.F. Bacterial rhodopsin: evidence for a new type of phototrophy in the sea. *Science* **2000**, 289, 1902–6.

70. Nagel, G.; Szellas, T.; Huhn, W.; Kateriya, S.; Adeishvili, N.; Hegemann, P.; Bamberg, E. Channelrhodopsin-2, a directly light-gated cation-selective membrane channel. *Proc. Natl. Acad. Sci. USA* **2003**, 100, 13940–45.

71. Zhang, F.; Gradinaru, V.; Adamantidis, A.R.; Durand, R.; Airan, R.D.: de Lecea, L.; Deisseroth, K. Optogenetic interrogation of neural circuits: technology for probing mammalian brain structures. *Nat. Protc*. **2010**, 5, 439-456.

72. Gradinaru, V.; Thompson, K.R.; Zhang, F.; Mogri, M.; Kay, K.; Schneider, M.B.; Deisseroth, K. Targeting and readout strategies for fast optical neural control in vitro and in vivo. *J. Neurosci*. **2007**, 27, 14231–38.

73. Boyden, E.S.; Zhang, F.; Bamberg, E.; Nagel, G.; Deisseroth, K.; Millisecond-timescale, genetically targeted optical control of neural activity. *Nat. Neurosci*. **2005**, 8, 1263-1268.

74. Deisseroth, K.; Feng, G.; Majewska, A.K.; Miesenbock, G.; Ting, A.; Schnitzer, M.J. Next-generation optical technologies for illuminating genetically targeted brain circuits. *J. Neurosci*. **2006**, 26, 10380–86.

75. Adamantidis, A.R.; Zhang, F.; Aravanis, A.M.; Deisseroth, K.; de Leccea, L. Neural substrates of awakening probed with optogenetic control of hypocretin neurons. *Nature* **2007**, 450, 420-424.

76. Gradinaru, V.; Morgi, M.; Thompson, K.R.; Henderson, J.M.; Deisseroth, K. Optical deconstruction of parkinsonian neural circuitry. *Science* **2009**, 324, 354-359.

77. Lobo, M.K.; Covington, H.E. 3rd; Chaudhury, D.; Friedman, A.K.; Sun, H.; Damez-Werno, D.; Dietz, D.M.; Zaman, S.; Koo, J.W.; Kennedy, P.J.;

Mouzon, E.; Mogri, M.; Neve, R.L.; Deisseroth, K.; Han, M.H.; Nestler, E.J. Cell type-specific loss of BDNF signaling mimics optogenetic control of cocaine reward. *Science* **2010**, 330, 385-390.

78. Brown, M.T.; Bellone, C.; Mameli, M.; Labouebe, G.; Bocklisch, C.; Balland, B.; Dahan, L.; Luján, R.; Deisseroth, K.; Lüscher, C. Drug-driven AMPA receptor redistribution mimicked by selective dopamine neuron stimulation. *PLoS One* **2010**, 5, 15870.

79. Hira, R.; Honkura, N.; Noguchi, J.; Maruyama, Y.; Augustine, G.J.; Kasai, H.; Matsuzaki, M. Transcranial optogenetic stimulation for functional mapping of the motor cortex. *J. Neurosci. Methods* **2009**, 179, 258–63.

80. Tye, K.; Prakash, R.; Kin, S-Y.; Fenno, L.E.; Grosenick, L.; Zarabi H, Thompson KR, Gradinaru V, Ramakrishnan C, Deisseroth K. Amygdala circuitry mediating reversible and bidirectional control of anxiety. *Nature* **2011,** 471, 358-62.

81. Adams, S. R. ; Kao, J.P.Y.; Tsien, R.Y. Biologically useful chelators that take up calcium(2+) upon illumination. *J. Am. Chem. Soc*. **1989**, 111, 7957–7968.

82. Sobczyk, A.; Scheuss, V.; Svoboda, K. NMDA receptor subunit-dependent [Ca2+] signaling in individual hippocampal dendritic spines. *J Neurosci*. **2005**, 25, 6037-46.

83. Kaplan J.H. Sodium pump-mediated ATP:ADP exchange. The sided effects of sodium and potassium ions. *J. Gen. Physiol*. **1982**, 80, 915-37.

84. Clarke, R.J.; Kane, D.J.; Apell, H.J.; Roudna, M.; Bamberg; E. Kinetics of Na(+)-dependent conformational changes of rabbit kidney Na+,K(+)-ATPase. *Biophys. J*. **1998**, 75, 1340–1353.

85. Shestopalov, I.A.; Sinha, S.; Chen, J.K. Light-controlled gene silencing in zebrafish embryos. *Nat. Chem. Biol*. **2007**, 3, 650-1.

86. Corrie, J.E.T. Photoremovable Protecting Groups Used for the Caging of Biomolecules. Dynamic Studies in Biology. **2005,** WILEY-VCH Verlag GmbH & Co.

87. Choi, J.; Chen, J.; Schreiber, S.L.; Clardy, J. Structure of the FKBP12-rapamycin complex interacting with the binding domain of human FRAP. *Science* **1996**, 273, 239-242.

88. Karginov AV1, Hahn KM. Allosteric activation of kinases: design and application of RapR kinases. *Curr. Protoc. Cell Biol*. **2011**, Unit 14.13.

89. Umeda, N.; Ueno, T.; Pohlmeyer, C.; Nagano, T.; Inoue, T. A photocleavable rapamycin conjugate for spatiotemporal control of small GTPase activity. *J. Am. Chem. Soc.* **2011**, 133, 12-4.

90. Brown, K.A.; Zou, Y.; Shirvanyants, D.; Zhang, J.; Samanta, S.; Mantravadi, P.K.; Dokholyan, N.V.; Deiters, A. Light-cleavable rapamycin dimer as an optical trigger for protein dimerization. *Chem. Commun. (Camb).* **2015**, 51, 5702-5.

91. Miyamoto, T.; DeRose, R.; Suarez, A.; Ueno, T.; Chen, M.; Sun, T.; Wolfgang, M.J.; Mukherjee, C.; Meyers, D.J.; Inoue, T. Rapid and orthogonal logic gating with a gibberellin-induced dimerization system *Nature Chem. Biol*. **2012**, 8, 465–470.

92. Schelkle, K.M.; Griesbaum, T.; Ollech, D.; Becht, S.; Buckup, T.; Hamburger, M.; Wombacher, R. Light-Induced Protein Dimerization by One- and Two-Photon Activation of Gibberellic Acid Derivatives in Living Cells. *Angew Chem. Int. Ed. Engl*. **2015,** 54, 2825-9.

93. Rockwell, N.C.; Su, Y.S.; Lagarias, J.C. Phytochrome structure and signaling mechanisms. *Annu. Rev. Plant Biol*. **2006**, 57, 837-58.

94. Kennedy, M.J. ; Hughes, R.M.; Peteya, L. A.; Schwartz, J.W.; Ehlers, M.D.; Tucker, C.L. Rapid blue-light-mediated induction of protein interactions in living cells. *Nature Methods* **2010**, 7, 973-975.

95. Salomon, M.; Christie, J.M.; Knieb, E.; Lempert, U.; Briggs, W.R. Photochemical and mutational analysis of the FMN-binding domains of the plant blue light receptor, phototropin. *Biochemistry* **2000**, 39, 9401-10.

96. Yazawa, M.; Sadaghiani, A.M.; Hsueh, B.; Dolmetsch, R.E. Induction of protein-protein interactions in live cells using light. *Nat. Biotechnol*. **2009**, 27, 941–45.

97. Strickland, D.; Lin, Y.; Wagner, E.C.; Hope, M.; Zayner, J.; Antoniou, C.; Sosnick, T.R.; Weiss, E.L.; Glotzer, M. TULIPs: Tunable, light-controlled interacting protein tags for cell biology. *Nat. Methods*. **2012**, 9, 379–384.

98. Montgomery, B.L.; Lagarias, J.C. Phytochrome ancestry. Sensors of bilins and light. *Trends Plant Sci.* **2002**, 7, 357-366.

99. Levskaya, A.; Weiner, O.D.;. Lim, W.A.; Voigt, C.A. Spatiotemporal control of cell signaling using a light-switchable protein interaction. *Nature* **2009**, 461, 997-1001.

100. Yang, X.; Jost, A.P.; Weiner, O.D.; Tang, C. A light-inducible organelle-targeting system for dynamically activating and inactivating signaling in budding yeast. *Mol Biol Cell*. **2013**, 24, 2419-30.

101. Ballister, E.R., Aonbangkhen, C., Mayo, A.M., Lampson, M.A., and Chenoweth, D.M. Localized light-induced protein dimerization in living cells using a photocaged dimerizer. *Nat. Commun.* **2014**, 5, 5475

102. Polstein, L.R.; Gersbach, C.A. Light-Inducible Spatiotemporal Control of Gene Activation by Customizable Zinc Finger Transcription Factors. *J. Am. Chem. Soc*. **2012**, 134, 16480-3.

103. Konermann, S.; Brigham, M.D.; Trevino, A.E.; Hsu, P.D.; Heidenreich, M.; Cong, L.; Platt, R.J.; Scott, D.A.; Church, G.M.; Zhang, F. Optical control of mammalian endogenous transcription and epigenetic states. *Nature* **2013***,* 500, 472-6.

104. Jullien, N.; Sampieri, F.; Enjalbert, A.; Herman, J.P. Regulation of Cre recombinase by ligand-induced complementation of inactive fragments. *Nucleic Acids Res*. **2003**, 31, e131.

105. Idevall-Hagren, O.; Dickson, E.J.; Hille, B.; Toomre, D.K.; De Camilli, P. Optogenetic control of phosphoinositide metabolism. *Proc. Natl. Acad. Sci. USA*. **2012**, 109, E2316-23.

106. Pathak,G.P.; Vrana,J.D.; Tucker, C.L. Optogenetic Control of Cell Function Using Engineered Photoreceptors. *Biol. Cell* **2013**, 105, 59–72.

Chapter 2 – Photoactivation of Dimerization

2.1 Introduction

One of the goals of my research is to develop a photocaged chemical dimerizer to mediate light-controlled protein dimerization. For this I will use abscisic acid (ABA) dependent dimerization of the proteins pyrabactin-like regulatory component (PYL) and ABA insensitive (ABI). Based on the crystal structures (1), ABA is completely encapsulated by PYL, Figure 2.1, so any disruption of the three dimensional shape of ABA should prevent binding.

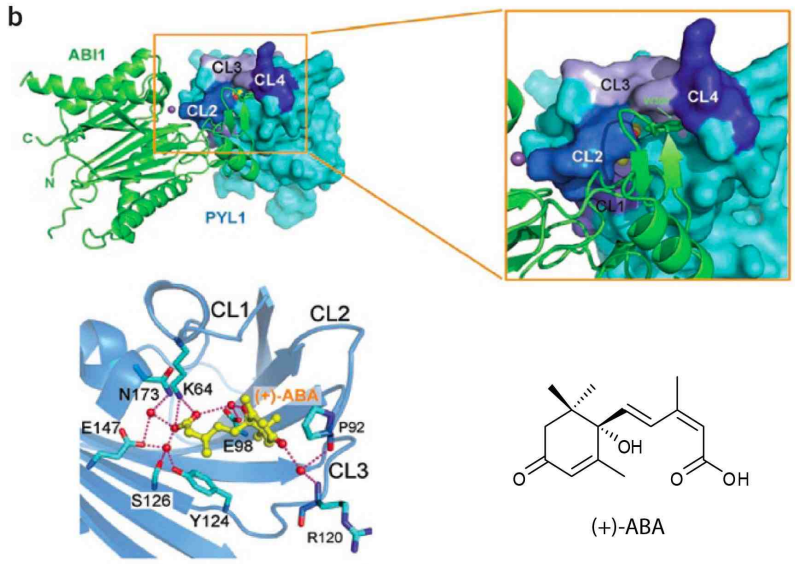

Figure 2.1. ABA is bound by PYL such that it completely encapsulated by the protein. There are many contacts between the carboxylic acid of ABA with residues of PYL. Disruption of these contacts through caging should be able to block ABA binding and therefore dimerization. (1)

The encapsulation of ABA by PYL suggests that any chemical modification to ABA should act as a cage to prevent dimerization of PYL and ABI. The carboxylic acid of the molecule was the easiest functional group to target for caging chemistry. Therefore the design for photo inducible dimerization uses photocaged ABA through attachment at the carboxylic acid to block dimerization in the dark. Photorelease of ABA should be able to induce dimerization of PYL and ABI to provide a light dependent switch for protein proximity, Figure 2.2.

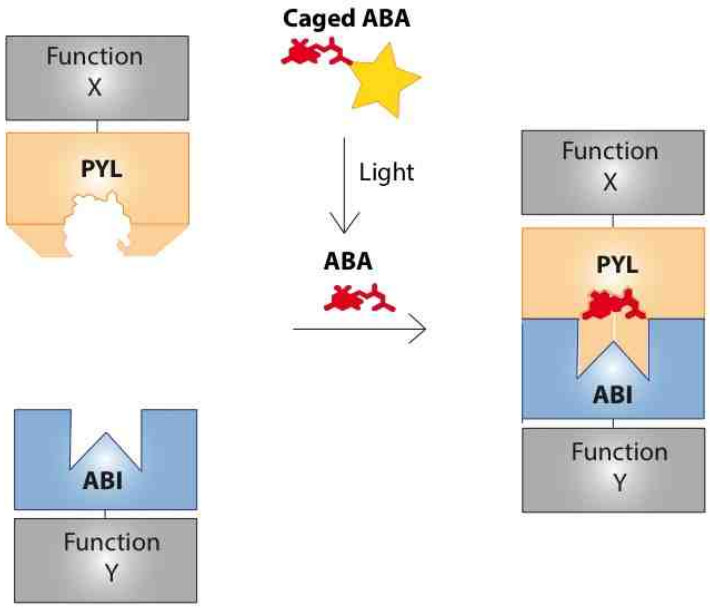

Figure 2.2. Design for photoinducible dimerization of PYL and ABI from release of ABA. Attachment of a photocage on the carboxylic acid of ABA should prevent binding to PYL. Upon irradiation the caged should be released and ABA would be able to bind PYL inducing dimerization with ABI.

To test whether the photocaged version of ABA can be developed by modifying its carboxylic acid group, I decided to cage ABA with commonly used

photocaging groups. *o*-Nitrobenzene groups are one of the most widely used photocaging groups. They can be attached to many functional groups such as alcohols, phenols, carboxylic acids, and phosphates and have been successfully uncaged (2). The photochemical reaction is an intramolecular H-abstraction by the excited nitro group, which then forms an aci-nitro and rearranges into the nitroso derivative, Figure 2.3 (3). Most of the nitrobenzene-derived groups have a maximum absorption below 300nm, which may give low uncaging efficiency with biocompatible wavelengths. A 3,5-dimethoxy substituted nitrobenzene (DMNB) has a longer wavelength of absorption and can be cleaved with 365nm light (1). DMNB caged glutamate shows maximum absorption at 345nm (4).

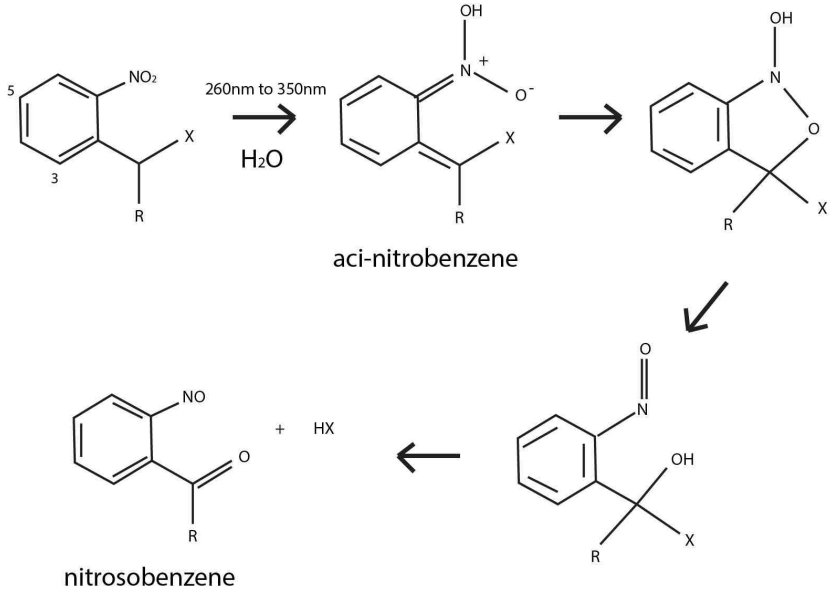

Figure 2.3. Mechanism of nitrobenzene photocleavage. Absorption of a photon causes the rearrangement of the nitro group to form the aci-nitro group. This undergoes further rearrangement to release the protonated small molecule (HX) and the nitrosobenzene product.

Coumarin-4-ylmethyl groups and its derivatives have a slightly longer wavelength, 320nm to 400nm (2), of cleavage than the nitrobenzene. Coumarin

cages can be linked to carboxylic acids and phosphates through ester bonds, and also linked to amines and alcohols. Photoexcitation of the coumarin molecule causes the heterolysis of the C-O bond to form an ion pair, Figure 2.4 (5). Once the ion pair is separated it is trapped in a polar solvent to give the hydroxyl coumarin and the protonated molecule. Substitution on the 6 and 7 positions of the coumarin ring have been found to enhance the solubility and increase the efficiency of photorelease.

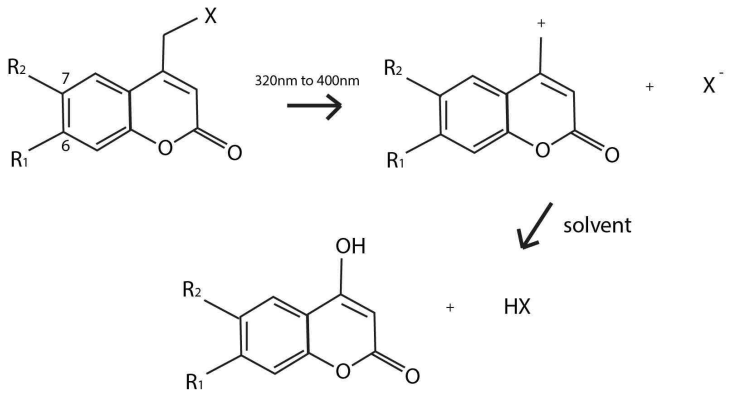

Figure 2.4. Mechanism of coumarin photocleavage. Absorption of a photon causes the cleavage of the bond to the caged molecule (X) creating an ion pair. In solvent this ion pair is converted to an coumarin alcohol and the protonated small molecule (HX).

I want to photocage the small molecule ABA to prevent its ability induce the dimerization in the dark, and be able to activate dimerization with light. To do this I will create photocaged ABA molecules. I want to use photorelease of ABA to induce biological effects that have shown to be controlled by other photodimerizing systems such as transcription, protein translocation, and signal transduction. In addition I wanted to see if the system is capable of spatially controlled activation of signaling, as has been seen with other photodimerizing

systems. If spatial control can be achieved for activation of signaling it is possible that it could be applied to the spatial control of translation as well.

2.2 Results

Photocleavage of Caged ABA

ABA-DMNB and ABA-DEACM were synthesized by conjugating the protecting groups to the carboxylic acid of ABA, Figure 2.5.

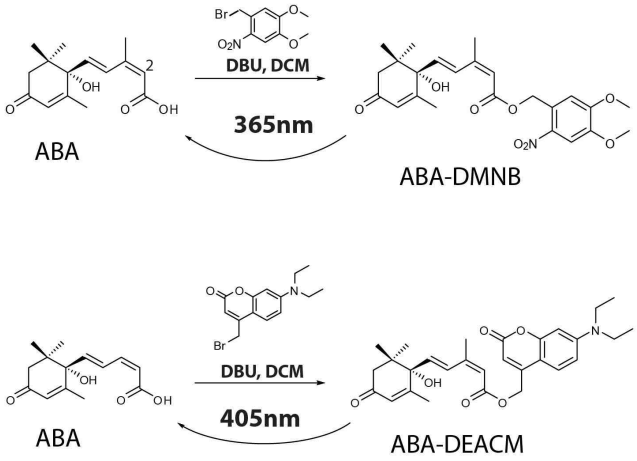

Figure 2.5. ABA is caged with DMNB and DEACM groups to create photoreleased ABA. The reagent 1,8-diazabicyclo[5.4.0]undec-7-ene (DBU) was used to catalyze the reactions in dichloromethane (DCM). DMNB caged ABA should be cleavable with 365nm light, while DEACM caged ABA should be cleavable with 405nm light.

Testing chemical stability of caged ABA: ABA-DMNB and ABA-DEACM at 100μM were incubated in HEPES buffer at 37°C for 24 hours and subsequently analyzed by HPLC. These samples were compared to solutions that had not been incubated for 24 hours. There was a small ABA peak found in the sample of ABA-DEACM that had not been incubated for 24 hours, Figure 2.6. This peak may be due to contamination from the reaction starting material or it

could be a result of spontaneous degradation of the compound. The ABA peak was not seen to increase for either ABA-DEACM or ABA-DMNB after 24 hours.

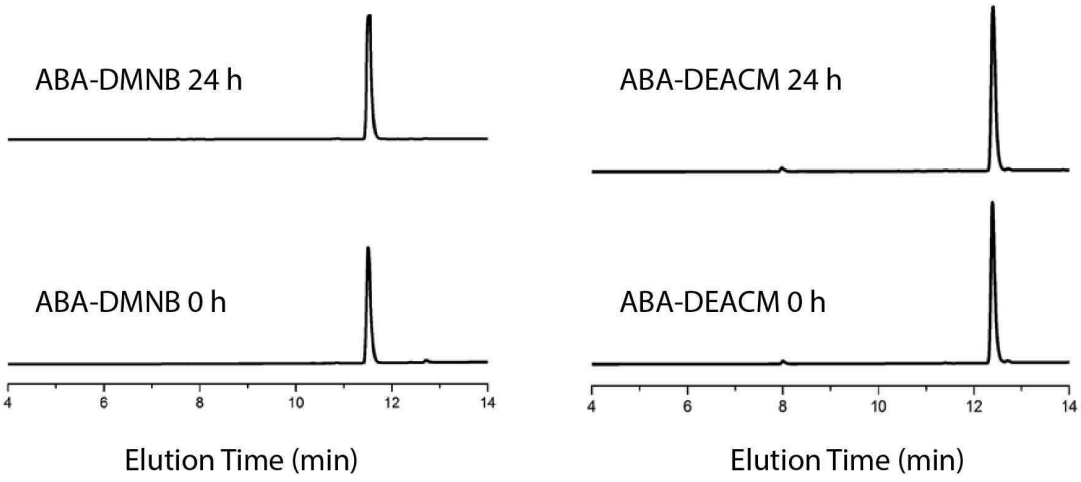

Figure 2.6. HPLC analysis of ABA-DMNB and ABA-DEACM incubated in HEPES buffer for 24 hours at 37°C compared to samples in buffer solution not incubated for 24 hours. There was a small amount of free ABA present in the sample of ABA-DEACM before incubation for 24 hours. The amount of free ABA present did not increase for either compounds after incubation in HEPES buffer for 24 hours at 37°C.

Testing photouncaging of ABA: Solutions of ABA-DMNB and ABA-DEACM were irradiated with either 365nm or 405nm light. The solutions were then analyzed with HPLC and found to have an increased amount of free ABA compared to solutions that were kept in the dark, Figure 2.7. Not only was the 2-*cis* ABA produced as expected, but a 2-*trans* isomer was produced and was more abundant than the 2-*cis* isomer. The reaction from photocleavage of ABA-

DMNB showed more production of the *trans* isomer than the photocleavage of ABA-DEACM.

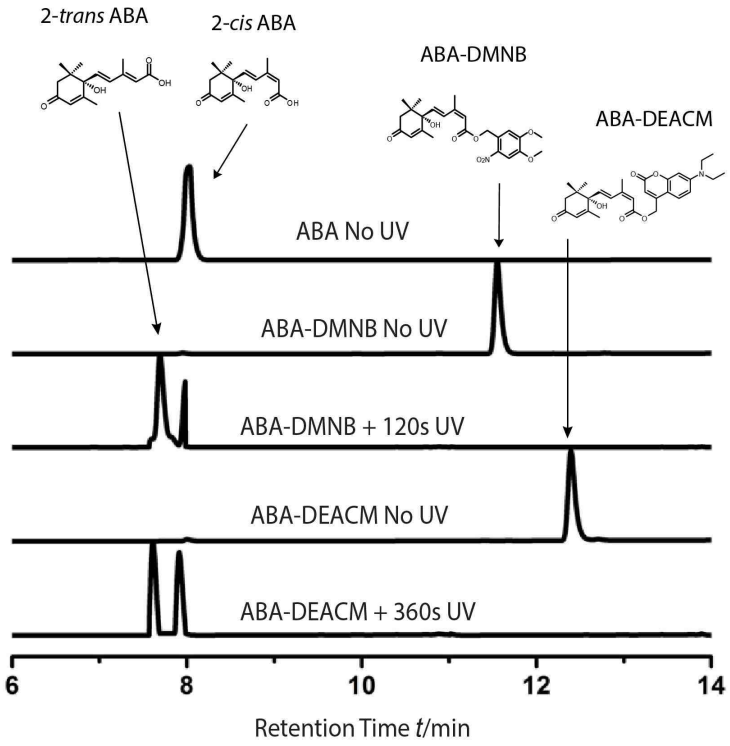

Figure 2.7. HPLC analysis of the products of photocleavage showed a mixture of isomers of ABA. Solutions of ABA-DMNB and ABA-DEACM at a concentration of 100μM were irradiated with 365nm light and 405nm light respectively. The photocleavage products showed the regeneration of free 2-*cis* ABA, but in addition produced 2-*trans* ABA. The photocleavage reactions from ABA-DMNB and ABA-DEACM showed different ratios of the *cis* and *trans* isomers produced.

Photocleavage was quantified by integration of the HPLC peaks to give the percentage of caged ABA compared to free ABA in solution, Figure 2.8. ABA-DMNB could be nearly completely cleaved by irradiation for three minutes with 365nm light at the tested concentration, while the same irradiation conditions uncaged only 25% of the ABA-DEACM at the tested concentration. ABA-

DEACM was irradiated for six minutes with 405nm light and was nearly completely cleaved. ABA-DMNB that was irradiated with 405nm light produced a substantial amount of free ABA.

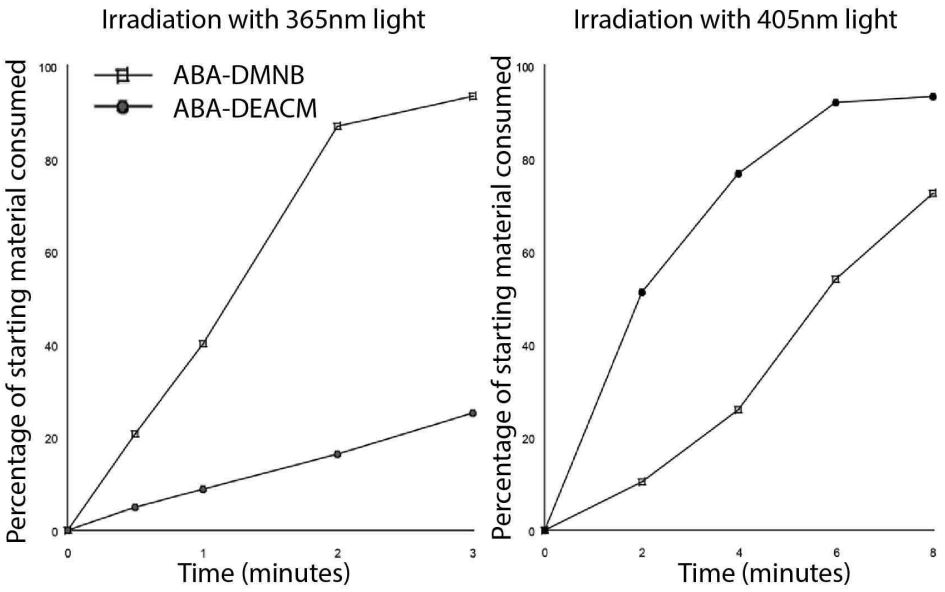

Figure 2.8. Photocleavage of ABA-DMNB and ABA-DEACM with 365nm and 405nm light. Irradiation of the caged ABA with 365nm light preferentially cleaved ABA-DMNB, but also resulted in some cleavage of ABA-DECM as well (left). Irradiation of the molecules with 405nm light resulted in slightly greater cleavage of ABA-DEACM, but still showed significant cleavage of ABA-DMNB.

The photouncaging of ABA-DMNB is more efficient than that of ABA-DEACM when using 365nm light. ABA-DMNB was nearly completely uncaged by irradiation with 365nm light within 3 minutes, but ABA-DEACM was uncaged just over twenty percent. Using 405nm light uncaged over half the starting material of both ABA-DMNB and ABA-EACM within 6 minutes.

Testing isomerization of ABA: Free ABA was irradiated with different wavelengths of light for 4 minutes to see how much isomerization occurs from light, but without the photocleavage reaction. Formation of *trans* ABA was seen from irradiation with UV light, but at much lower levels than those seen when irradiating caged ABA under the same conditions, Figure 2.9. Isomerization was not seen when ABA was irradiated with blue or green light.

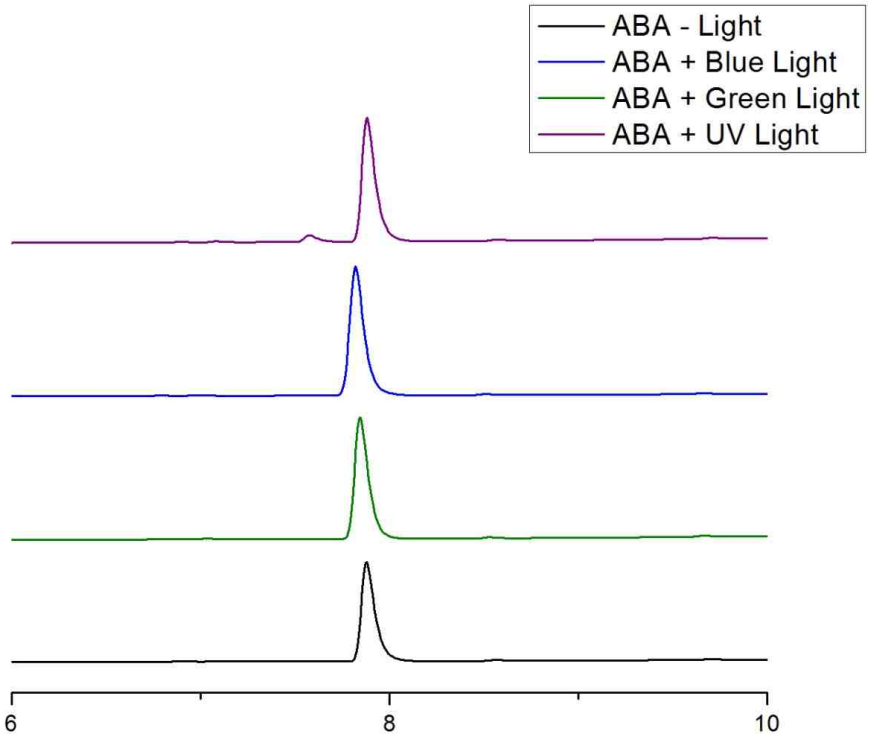

Figure 2.9. ABA samples at 100μM were irradiated with different wavelengths of light for 4 minute. The samples were analyzed with HPLC to see which wavelength of light are able to induce isomerization of ABA. Samples were irradiated for 4 minutes with each channel of the fluorescent microscope. For UV light the DAPI filter was used that emits 365nm light; for blue light the GFP filter was used that emits 455nm to 495nm light and for green light the Rhodamine filter was used that emits 534nm to 558nm. Only irradiation with UV light was able to isomerize

2-*cis* ABA to create 2-*trans* ABA, and in much lower amounts seen compared to the photocleavage reactions of ABA-DMNB and ABA-DEACM.

Photoinducible Transcription

An ABA-inducible transcription assay was used to analyze the photorelease of ABA in cells. Cells expressing VP16-PYL and GAL4BD-ABI were used to activate the transcription of reporter genes, luciferase or GFP, downstream of the GAL4 upstream activating sequence in response to ABA, Figure 2.10.

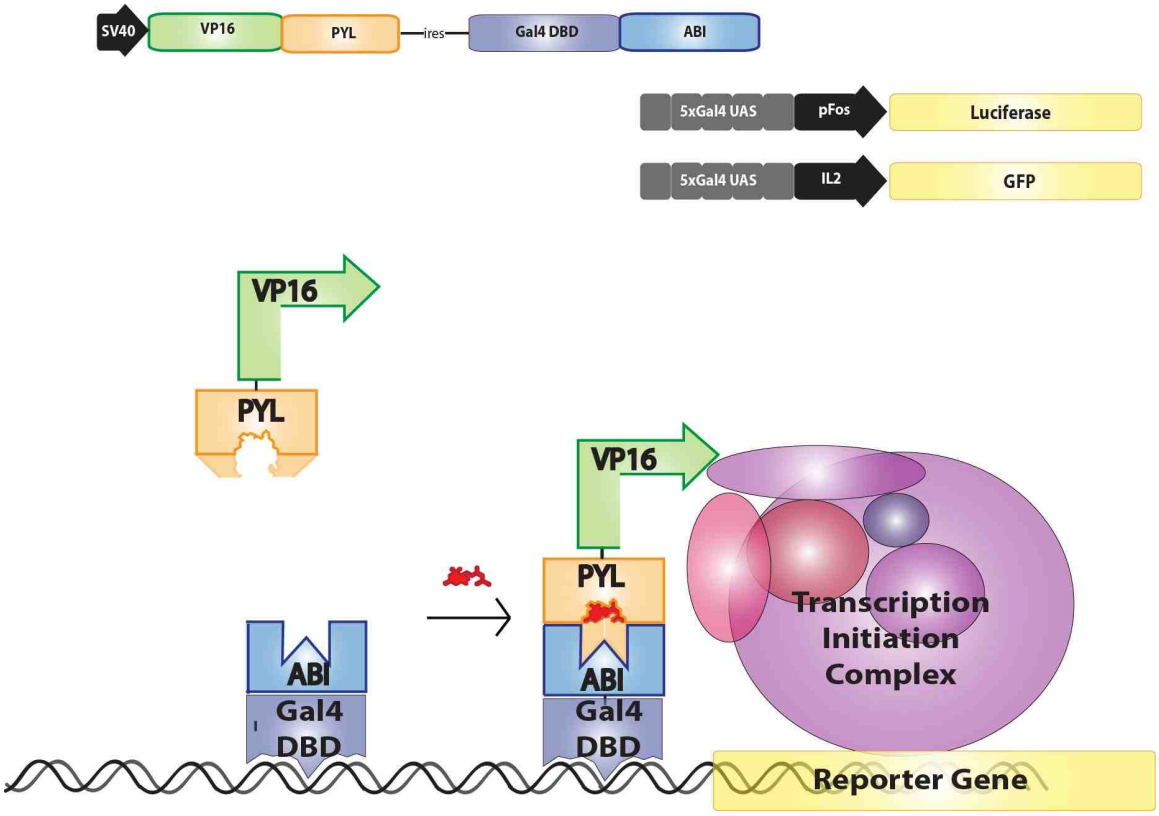

Figure 2.10. Initiation of transcription due to chemically induced dimerization. VP16 transcription activating domain is fused to PYL and ABI is fused to the Gal4 DNA binding domain (DBD). ABA induced dimerization causes the localization of VP16 to the Gal4 upstream activating sequence

that binds GAL4DBD. This recruits the transcription initiation complex to a reporter gene downstream from this sequence.

The 2-*cis* form of ABA is shown to stimulate transcription of reporter genes (6), but *trans* ABA has been shown to have decreased biological activity (7). I wanted to test the abilities of the two different isomers to induce dimerization dependent transcription because they are both produced in the photocleavage reaction.

Cis and *trans* ABA were created through the photouncaging of ABA-DMNB and isolated with HPLC fraction collection. The isolated compounds were added to cells transfected with transcription inducing constructs at a concentration of 10μM and incubated for 24 hours. The *cis* ABA is much more effective for inducing transcription, Figure 2.11. When 10μM of each isomer was added to the cell culture it gave luciferase expression greater than that seen with only 10μM *cis* ABA. This indicates that even though the *trans* isomer is not effective at inducing dimerization, it will not prevent the *cis* isomer from doing so.

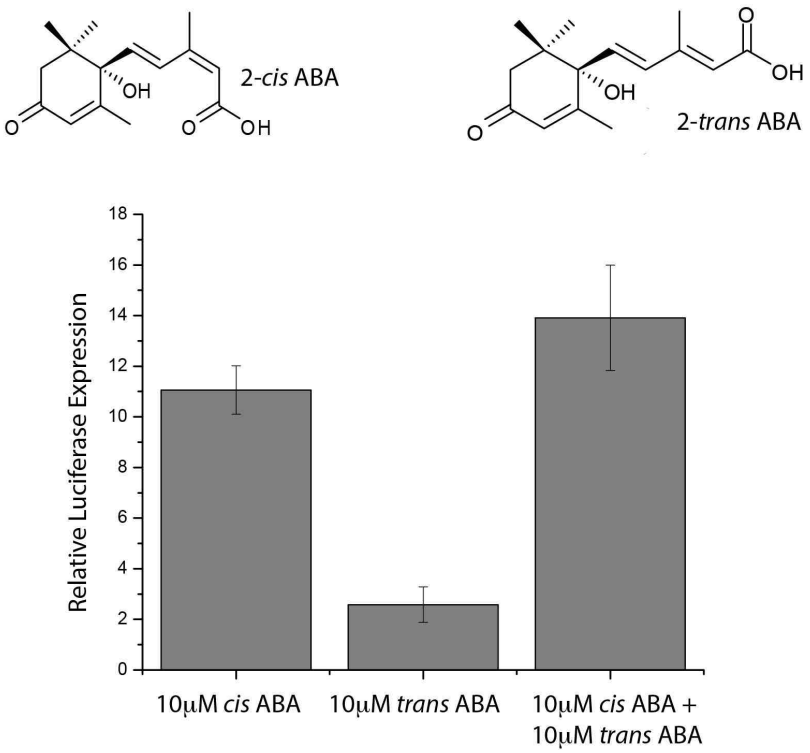

Figure 2.11. CHO cells were transfected with constructs for ABA inducible transcription of luciferase. Cells were given either 2-*cis* ABA or 2-*trans* ABA at a concentration of 10μM and incubated for 24 hours. Luciferase expression was much lower in cells incubated with 2-*trans* ABA compared to 2-*cis* ABA. This indicates that the *trans* isomer is incapable of inducing dimerization.

Testing biological stability of caged ABA: There are endogenous esterase enzymes that exist in cells that could act to cleave the linkage between ABA and the protecting group. Therefore caged ABA at a concentration of 10μM was added to cells that were transfected with transcription inducing constructs to test the stability of the caged molecule in a biological system. There was little increase in the expression of the luciferase reporter gene even after incubation with the caged ABA for up to 24 hours in the absence of light, Figure 2.12. This

shows that the cages are stable in cell culture and can be used for hours in an experimental setting with minimal amounts of transcription induction. This indicates that the DMNB and DEACM cages are capable of preventing dimerization in the dark state.

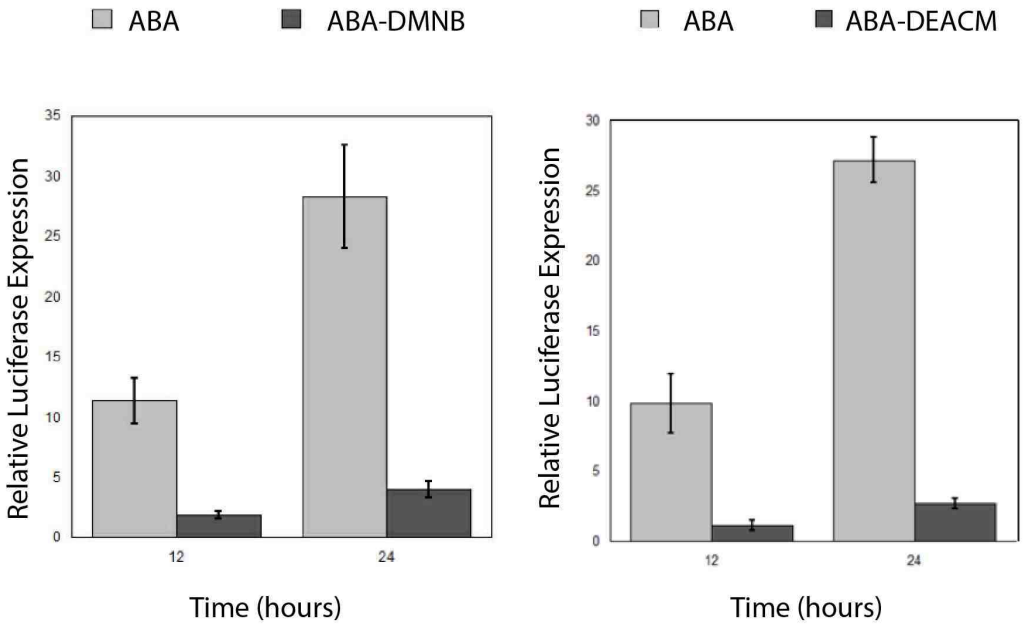

Figure 2.12. The stability of ABA-DMNB and ABA-DEACM in cell culture for up to 24 hours was tested. CHO cells were transfected with constructs for ABA inducible transcription of luciferase. Cells were incubated with ABA or caged ABA at a concentration of 10μM and kept in the dark for either 12 or 24 hours. Cells incubated with either ABA-DMNB (left) or ABA-DEACM (right) showed much lower luciferase expression than that of cells incubated with ABA. This suggests that the cages are capable of blocking the dimerization of PYL and ABI to prevent ABA induced transcription.

Testing photocleavage products for transcription induction: The pre-irradiated solution of ABA-DMNB was added to cells containing the transcription inducing constructs with the GFP reporter. Cells showed induction of GFP from incubation with the solution of irradiated ABA-DMNB, while ABA-DMNB that was not irradiated did not induce GFP expression, Figure 2.13. This indicates that the photocleavage products contain active ABA and are able to induce dimerization dependent transcription.

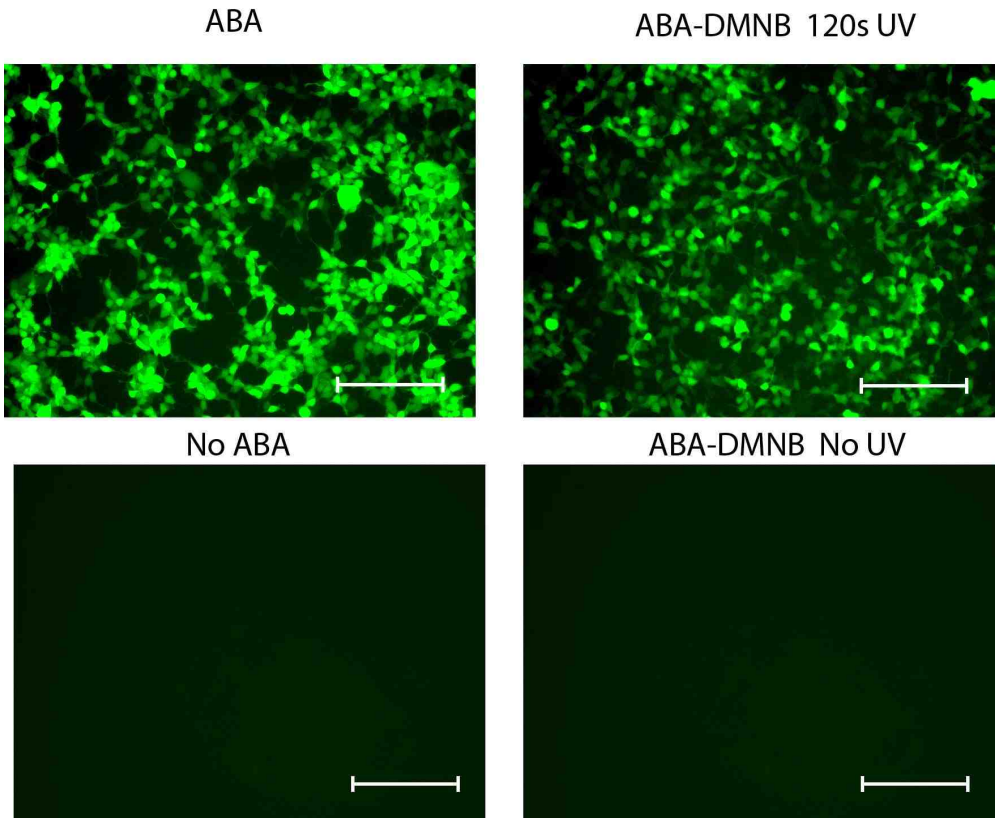

Figure 2.13. ABA-DMNB at 1mM was irradiated for 3 minutes. Products of photocleavage were diluted to 10μM and added to 293-GFP cells containing ABA inducible GFP constructs. Cells that received ABA or photoirradiated ABA-DMNB showed increased GFP expression compared to cells that were not given ABA or were given ABA-DMNB at 10μM that was not irradiated. Scale bar 100μm.

Testing photoinduced transcription: Caged ABA at a concentration of 10μM was added to cell culture transfected with luciferase inducing constructs. The cells were irradiated with UV light to analyze the ability of photorelease of ABA *in situ*. There was an increase of luciferase expression that was similar to the increase seen from the addition of free ABA, Figure 2.14. The level of response of transcription activation can be controlled by the dosage of ABA or photoreleased ABA over a wide range of concentration. This system could be used to precisely control the amount of transcription activated by photocleavage. In addition it indicates that the amount of dimerization can be controlled as well, which could be used to affect the intensity of the desired biological response.

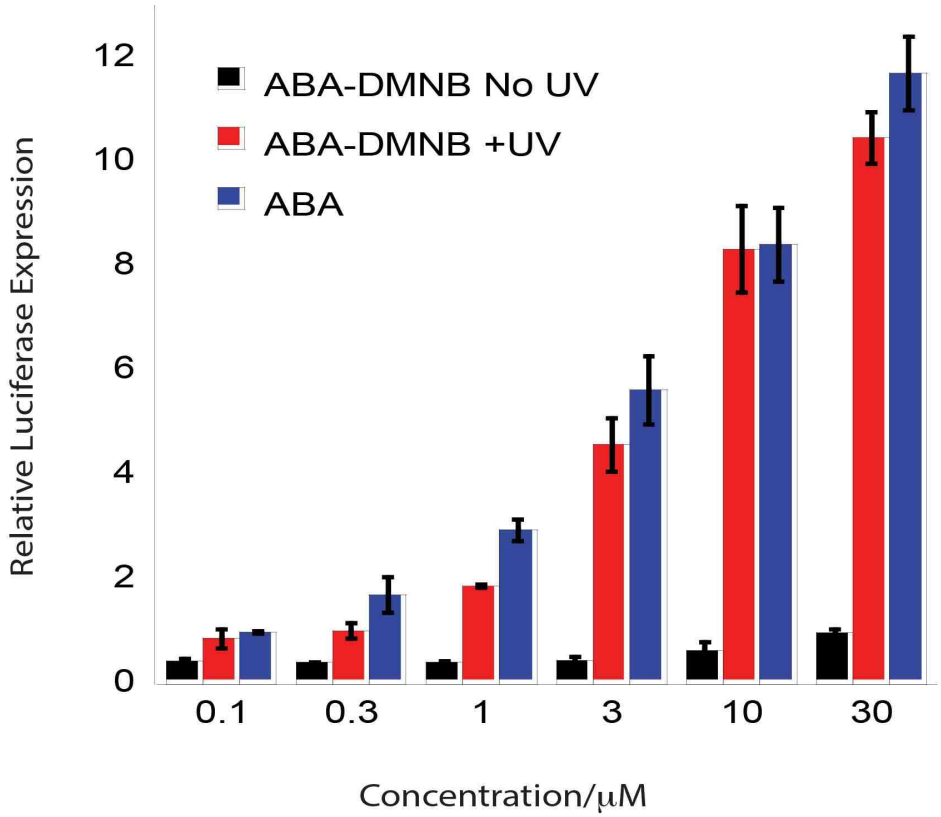

Figure 2.14. CHO cells were transfected with constructs for ABA inducible transcription of luciferase. Cells were incubated with ABA or ABA-DMNB at concentrations ranging from 100nM to 30μM. Half of the cells incubated with ABA-DMNB were irradiated with 365nm light for 2 minutes and half were kept in the dark. The cells that had been incubated with ABA-DMNB and irradiated (red) show similar luciferase expression to the cells incubated with ABA (blue), and greater than those incubated with ABA-DMNB and kept in the dark (black).

Photoinduced Protein Translocation

In order to be able to watch the photoinduced protein dimerization in real time I used it to control translocation of a fluorescent protein. I wanted to visualize the effects of photoreleased ABA upon translocation of GFP. For this I used a GFP-PYL construct that is not localized to any given cellular region on its own. I used ABI that was linked to a nuclear export sequence (NES) to be able to translocate the GFP-PYL out of the nucleus upon production of free ABA, Figure 2.15.

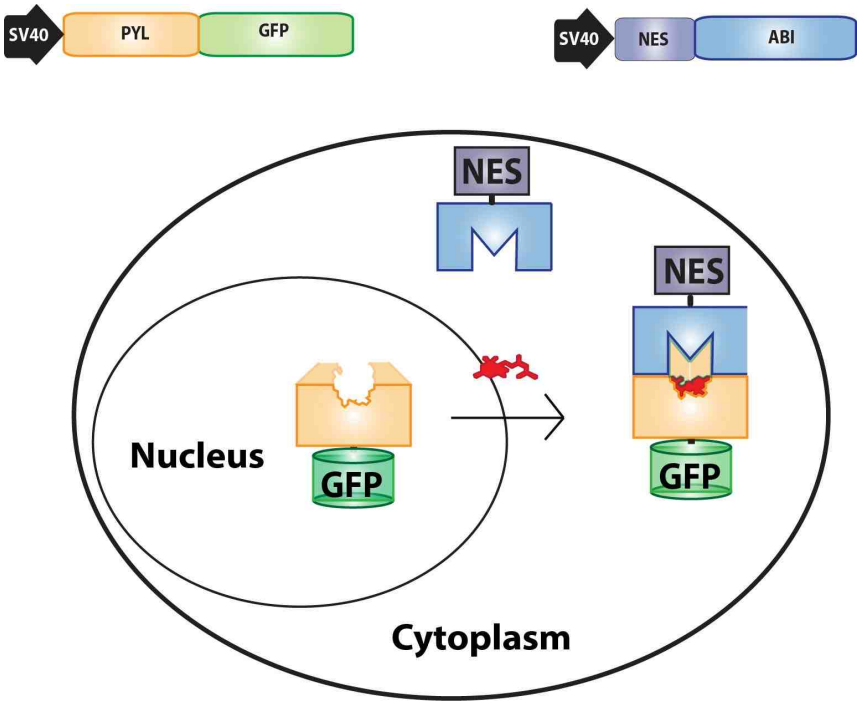

Figure 2.15. GFP-PYL dimerizes in response to ABA, which causes loss of GFP fluorescence in the nucleus.

Testing photoinduced translocation: Cells were given caged ABA at 10μM immediately prior to experiment and either irradiated for 2 min or kept in the dark, and were fixed after 15 minutes. Photouncaging of ABA caused an increased amount of cells to display nuclear export of GFP compared to caged ABA that was kept in the dark, Figure 2.16. There are slightly elevated levels of cells showing nuclear export when they are incubated with ABA-DEACM without UV compared to cells that were given no drug, Figure 2.16. This may be due to small amount of fee ABA present in the ABA-DEACM sample.

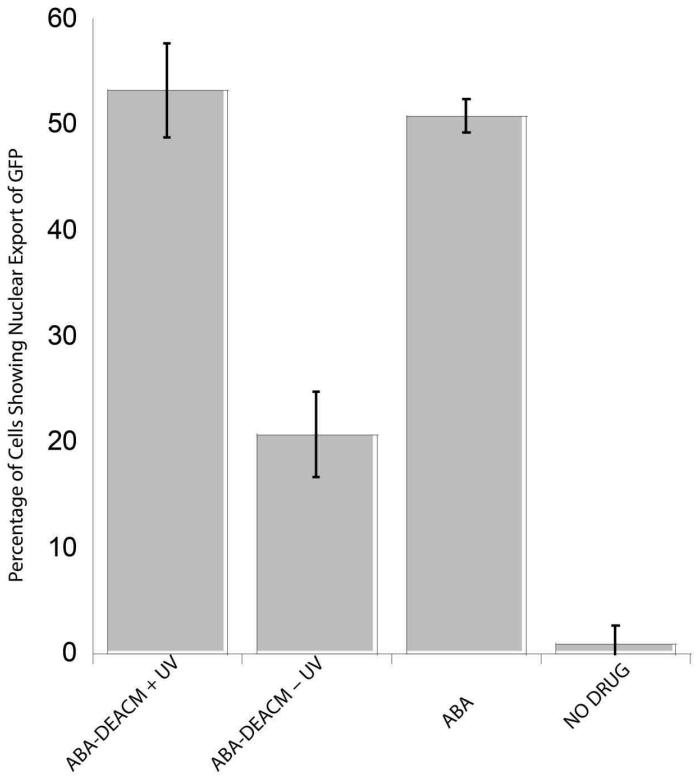

Figure 2.16. CHO cells were transfected with PYL-GFP and NES-ABI. The cells were given ABA or ABA-DEACMat 10μM. Half of the cells containing ABA-DEACM were irradiated with 405nm light and the other half was kept in the dark. Cells were incubated for 1 hour after treatment before they were fixed. The number of cells showing nuclear export of GFP was counted to get the overall percentage of the cell population showing nuclear export fo GFP. Cells that were given ABA or ABA-DEACM and irradiated showed the highest amount of cells displaying nuclear export of GFP. Cells that were incubated with ABA-DEACM and kept in the dark showed slightly elevated amounts of cells displaying nuclear export compared to cells that received no drug.

Testing reversibility of translocation: The reversibility of the dimerization was analyzed by tracking the nuclear exported GFP, Figure 2.17. Cells were transfected with NES-ABI and PYL-GFP and incubated with ABA-DMNB were irradiated and allowed to sit for 15 minutes like before, but next the

media was removed and replaced with fresh media and incubated at 37°C for 5 minutes. This washing with fresh media was repeated three times before cells were fixed. There was a decrease in the amount of cells showing nuclear export of GFP compared to those that were not washed, Figure 2.17. This indicates that lowering the concentration of ABA by replacing with fresh media was able to reverse dimerization dependent protein translocation. The reversible nature of the dimerization based upon the presence of ABA allows the system to be turned off with the removal of ABA. This could allow more precisely controlled activation of any dimerization dependent biological effects.

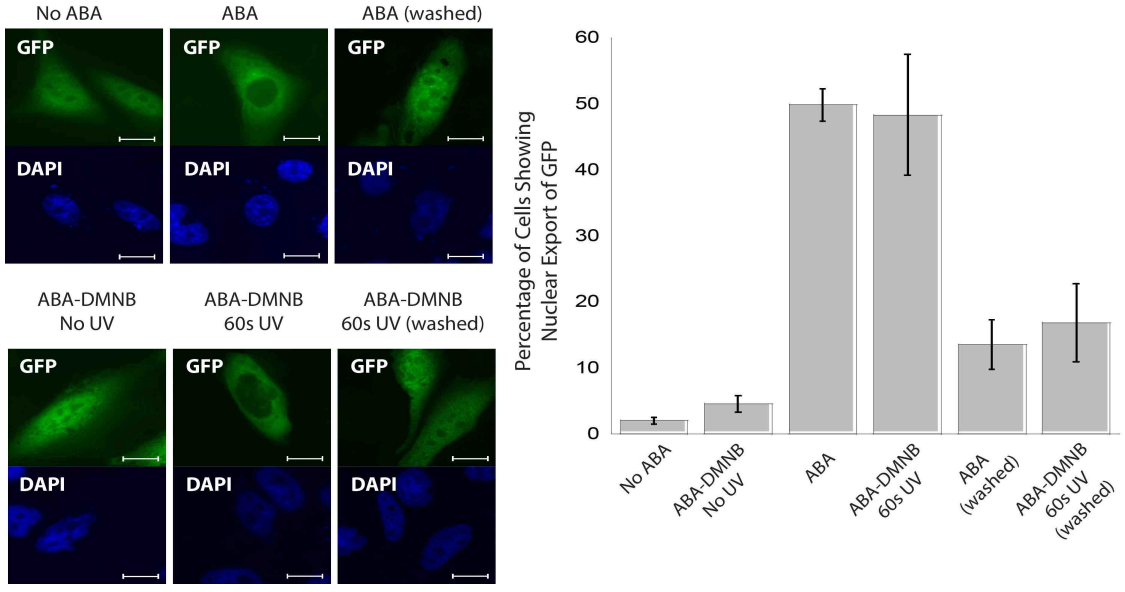

Figure 2.17. CHO cells were transfected with PYL-GFP and NES-ABI and given either ABA or ABA-DMNB at a concentration of 10μM. Cells that were given ABA-DMNB were either kept in the dark or irradiated with 365nm light for 2 minutes. After 15 minutes half the samples that have been given ABA or ABA-DMNB and UV were washed three times with fresh media to remove any ABA. The cells were then fixed and stained with DAPI for imaging (left). Scale bar 10μm. The

amount of cells showing visible nuclear export of GFP was counted to calculate the percentages of cells with nuclear export of GFP for each condition. Cells that were given ABA or ABA-DMNB and UV showed increased numbers of cells showing nuclear export of GFP compared to those with ABA-DMNB and no UV or without any drug at all. Cells that were washed showed decreased amounts of nuclear export of GFP. This indicates that dimerization is reversible upon removal of free ABA.

.

Testing real-time photoinduced translocation: The movement of GFP-PYL in response to photorelease of ABA can be monitored by live cell microscopy. CHO cells transfected with NES-ABI and PYL-GFP were irradiated with the 405nm laser of a confocal microscope and images were taken every 20 seconds for 20 minutes to track the GFP. A decrease of fluorescence intensity was seen in the nucleus compared to the cytoplasm, Figure 2.18, of cells incubated with ABA-DEACM and irradiated compared to those with ABA-DEACM that were not irradiated or those that were irradiated but were not incubated with ABA-DEACM. This indicates that the decrease in fluorescence intensity in the nucleus is not due to photobleaching because it is dependent upon the presence of ABA-DEACM.

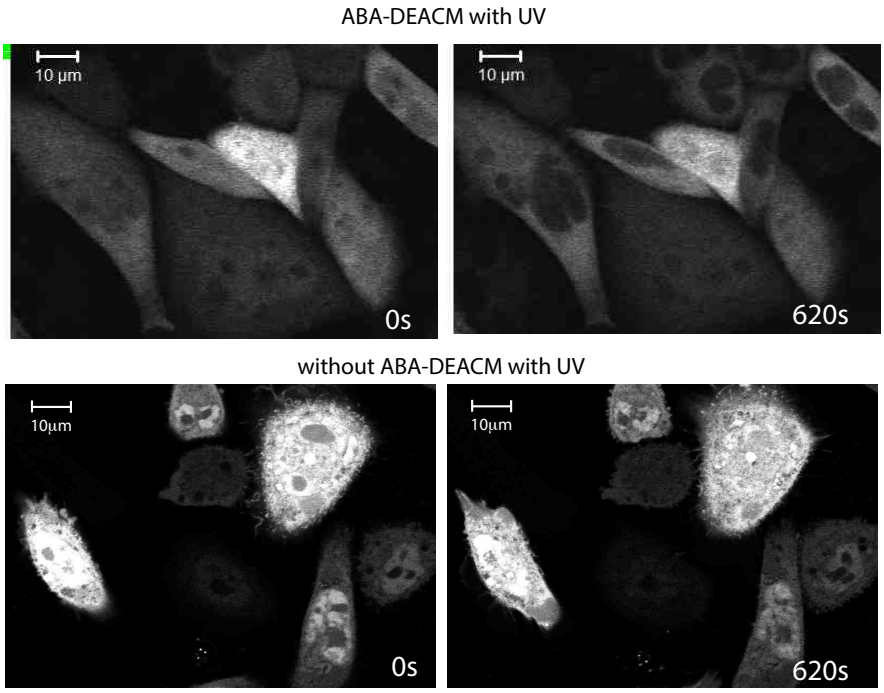

Figure 2.18. CHO cells were transfected with PYL_GFP and NES-ABI and given ABA-DEACM at a concentration of 10µM. Cells were irradiated with the 405nm laser of a confocal microscope and compared to cells that were not irradiated. Cells were imaged every 20 seconds to track the translocation of PYL-GFP in real time. Cells that were irradiated showed a decrease in the flourescence intensity of GFP in the nucleus compared to cells that were not irradiated.

The amount of translocation was quantitated using the ratio of fluorescence intensity in the nucleus divided by the fluorescence intensity in the cytoplasm, Figure 2.19. This showed a difference in the fluorescence intensity in the nucleus within minutes of irradiation. This indicates that the photorelease of ABA is able to rapidly control the translocation of a protein through dimerization dependent anchoring of one of the ABI and PYL pair.

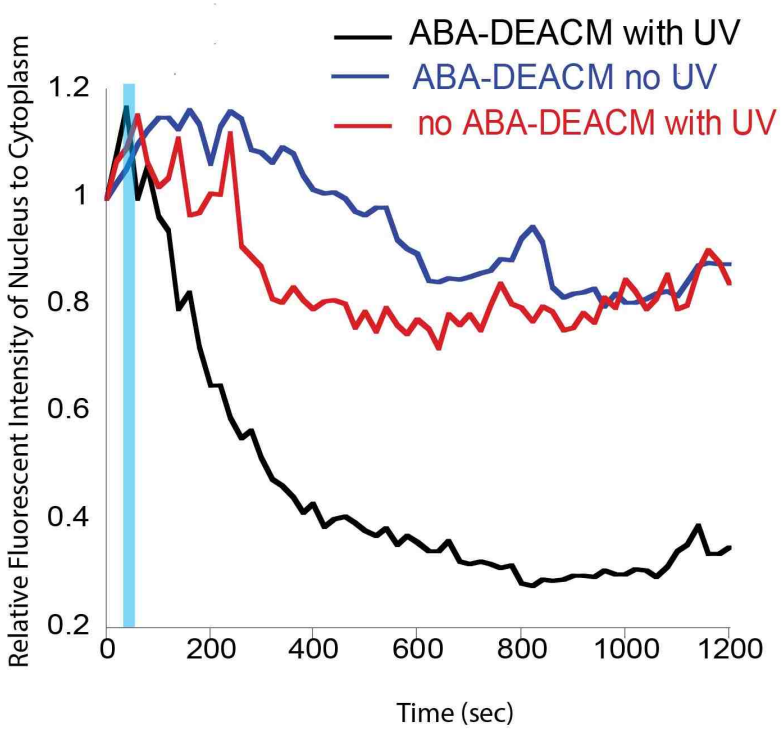

Figure 2.19. The fluorescent intensity of the nucleus compared to the cytomplasm was calculated from live cell images. Cells with 10μM ABA-DEACM showed a decrease in the relative fluorescent intensity in the nucleus after irradiation (blue bar) compared to cells that received only ABA-DEACM or irradiation, but not both.

Photoinduced Signaling Transduction

I wanted to see if the area of biological response could be controlled within the region of illumination. For this we used dimerization dependent induction of signalling cascade to visualize the rapid activation of biological events. A membrane targeting sequence for myrisylation was fused to ABI to give myr-ABI. A GTP exchange factor for Rac1 activation, Tiam1, was fused to PYL-GFP. ABA

inducible dimerization was used to target a cytoplasmic Tiam1 to the membrane to activate a signaling cascade, Figure 2.20. The localization of Tiam1 to the membrane results in the formation of lamelopodia and ruffles on the membrane of the cell, Figure 2.21.

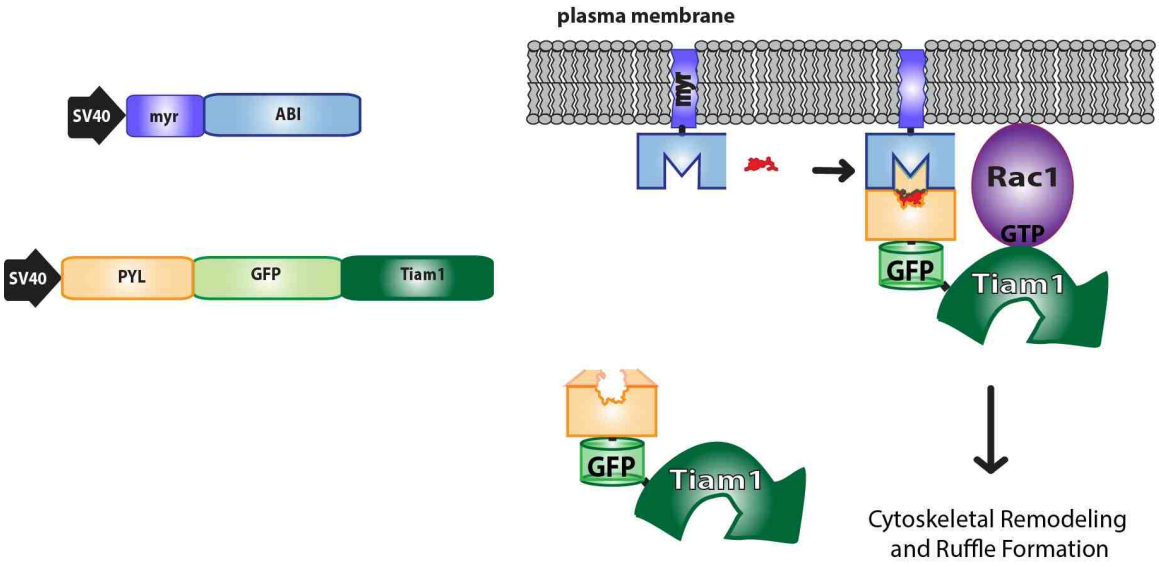

Figure 2.20. The GTP exchange factor Tiam1 is localized to the membrane upon addition of ABA. Tiam1 causes the activation of Rac1 signaling, which is seen by the formation of membrane ruffling.

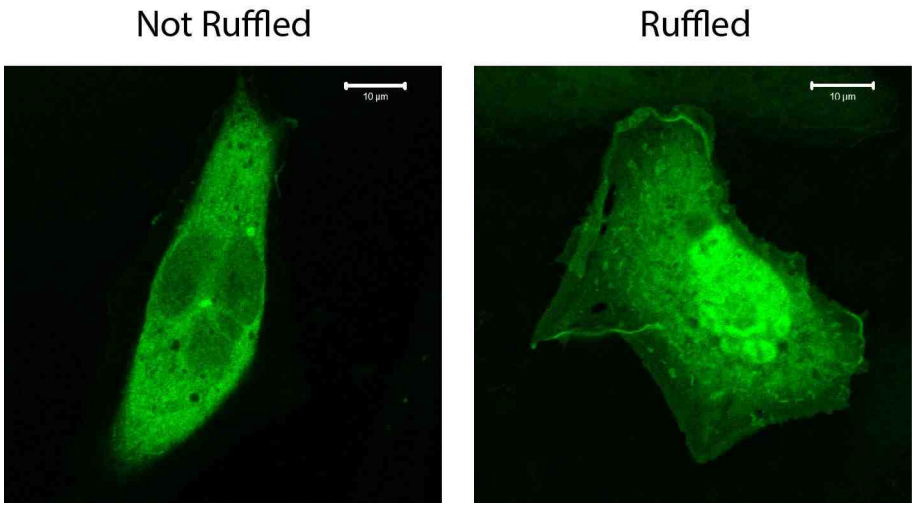

Figure 2.21. Cells without membrane localized PYL-GFP-Tiam1 show a smooth shape (left), whereas cells with membrane localized PYL-GFP-Tiam1 show a ruffled phenotype (right).

Cells expressing PYL-GFP-Tiam1 and myr-ABI that had no ABA added still showed some cells having ruffles. Adding ABA at a concntration of 10μM to the cell culture for one hour caused GFP localization at the membrane and increased numbers of cells showing ruffles, Figure 2.22. Incubating the cells with caged ABA at 10μM or no drug showed lower percentages of cells displaying ruffles compared to cells incubated with caged ABA at 10μM and irradiated showed levels similar to those seen with free ABA at 10μM after 24 hours.

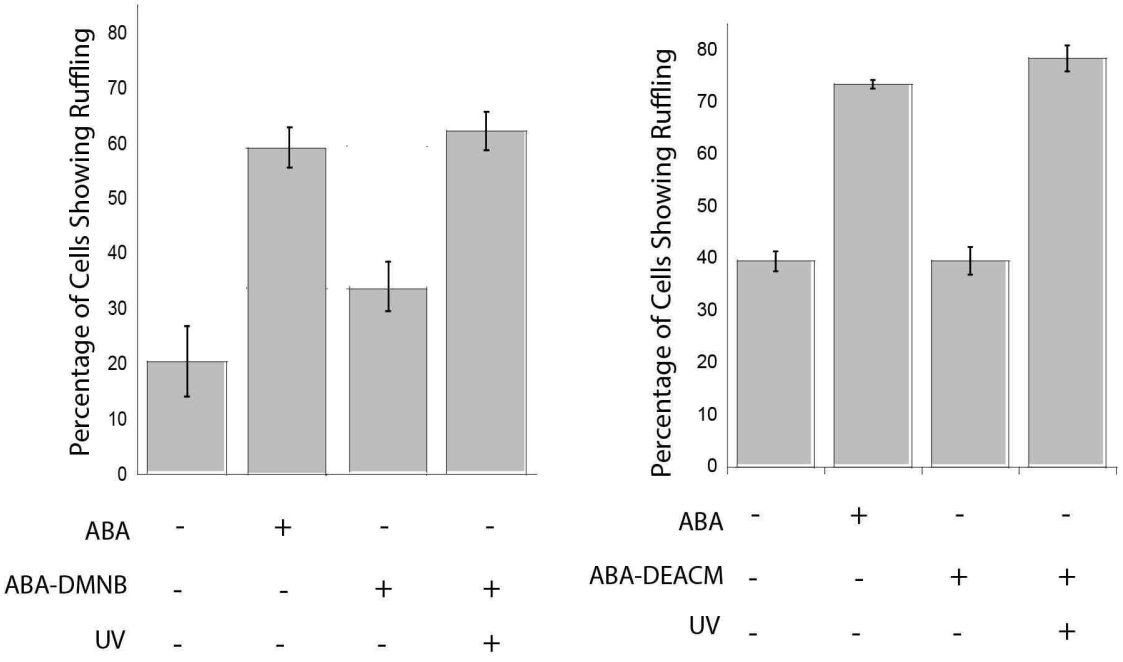

Figure 2.22. CHO cells were transfected with PYL-GFP-Tiam1 and myr-ABI and given ABA or caged ABA, with or with light. Cells were fixed one hour after the drug and irradiation were given. Cells were counted to calculate the percentage of cells showing membrane ruffles after photocleavage of ABA-DMNB and ABA-DEACM. The percentage of cells displaying ruffles increases when the cells are given ABA or caged ABA and light compared to cells that did not receive ABA or caged ABA and light. Photoreleased ABA is capable of increasing the amount of Tiam1 signaling.

Testing real-time photoinduced signaling: This system of photoinducible signal transduction was used in conjunction with live cell microscopy to watch the formation of ruffles in real time. Cultures transfected with myr-AIB and PYL-GFP-Tiam1 and incubated with ABA-DEACM were irradiated over the whole cell and showed formation of ruffles within minutes, Figure 2.23, 2.24. Cells that were incubated with ABA-DEACM but were not irradiated did not show formation of ruffles, Figure 2.24. The system can be used for light dependent control over biological events.

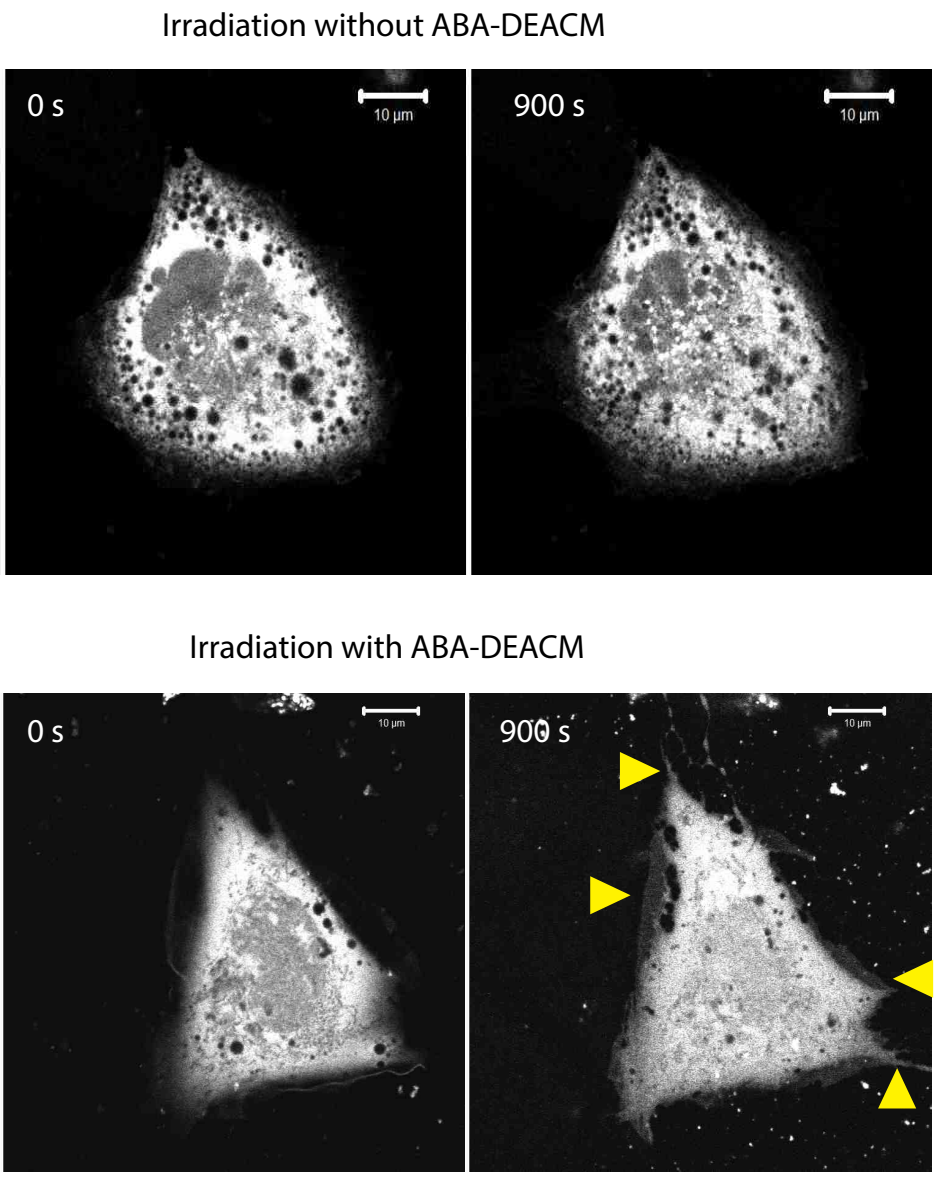

Figure 2.23. CHO cells were tranfected with PYL-GFP-Tiam1 and myr-ABI and either given ABA-DEACM at a concentration of 10µM or given no drug. Cells were irradiated with the 405nm laser of a confocal microscope and images were taken every 20 seconds for 20 minutes. Cells that were irradiated without ABA- DEACM did not show any changes in cytoskeletal structure. Cells that were incubated with ABA-DEACM showed morphological changes after irradiation. Scale bars 10µm.

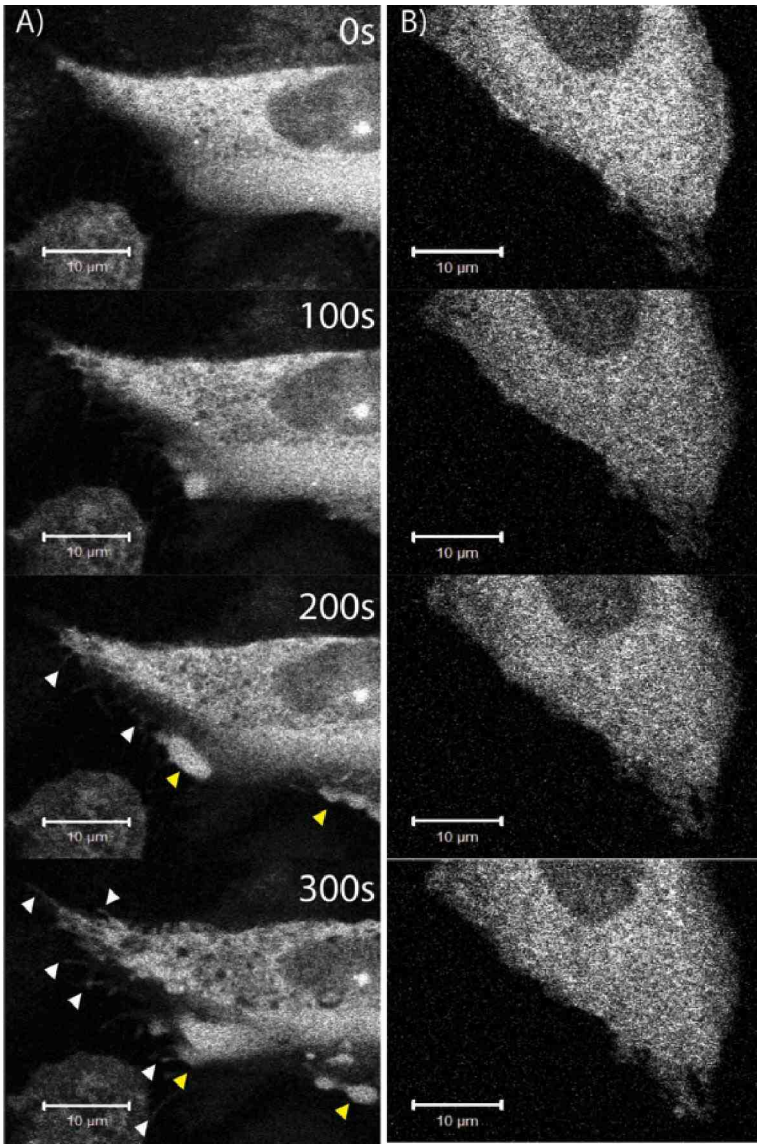

Figure 2.24. CHO cells were transfected with PYL-GFP-Tiam1 and myr-ABI and given ABA-DEACM at a concentration of 10µM. Images were taken every 20 seconds for 20 minutes. Cells that were incubated with ABA-DEACM and irradiated with 405nm light showed cytoskeletal remodeling, left. Cells incubated with ABA-DEACM but not irradiated did not show any cytoskeletal remodeling, right.

Testing sub-cellular induction of signaling: I wanted to test this system's ability to induce biological responses on the subcellular level. A small region was selected at one end of a cell and irradiated. Subcellular irradiation did

induce signalling transduction but this effect was not confined to the region of irradiation, Figure 2.25. This could be due to the rapid diffusion of free ABA to the other regions of the cell that were not irradiated.

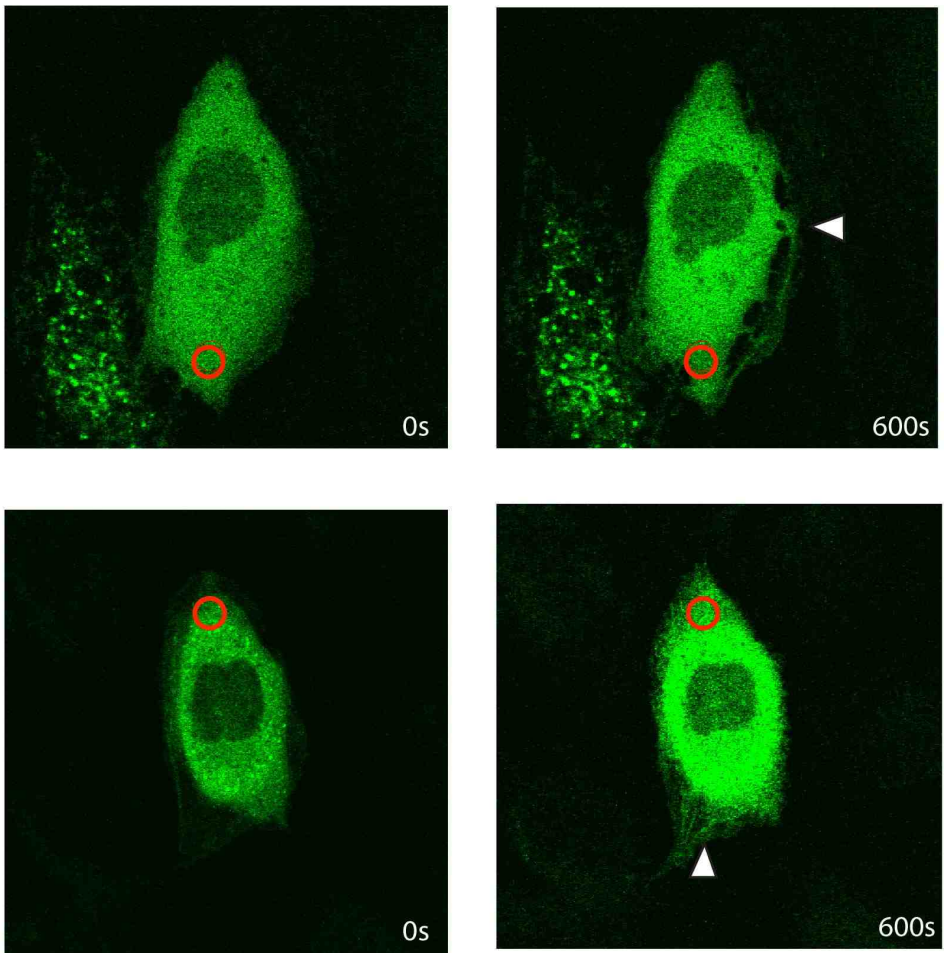

Figure 2.25. CHO cells were transfected with PYL-GFP-Tiam1 and myr-ABI and given ABA-DEACM at a concentration of 10μM. Cells were irradiated in a small region of the field (red circle) and images were taken every 20 seconds for 20 minutes. Irradiation of a sub-cellular region did not produce sub-cellular activation of Ruffle formation, and often caused ruffling in areas of the cells distant from the region of irradiation (white arrow).

It was seen in previous experiments (8) that regions of the cell that showed cytoskeletal protrustions had more intense responses to membrane localized Tiam1. Therefore the diffusion of ABA throughout the cell after photocleavage could cause the prefered activation of remodeling at these location, independent of the location of illumination.

2.3 Conclusion and Discussion

ABA inducible dimerization can be blocked with nitrobenzene or coumarin derived cages linked to the carboxylic acid of ABA. A photocleavable cage allowed the use of light to release ABA to induce dimerization and control designed biological effects. The system shows little dimerization when caged ABAs are kept in the dark and high levels of dimerization after irradiation.

Photoactivation of ABA induced dimerization is capable of controlling transcription of a reporter gene and translocation of signaling proteins. The system gives temporal control to signaling events that can be seen within minutes after irradiation. Subcellular spatial control has not been achieved, possibly because of the rapid diffusion of ABA after irradiation.

It may be possible to achieve sub-cellular control of ABA dependent dimerization if strategies are borrowed from other researchers. The cage could be conjugated to a large group that could function to sequester the molecule outside of the cell. This could allow the activation of a small area near the membrane as it has done for others.

I have expanded the use of ABA inducible dimerization to be photoinducible. This means that any further biological processes engineered to be ABA dependent could be put under optical control as well. This allows the combination of more inputs and outputs for the dimerization of PYL and ABI.

2.4 Methods

Materials

Restriction enzymes and polymerases were purchased from NEB. Cell culture plates and tubes are from Grenier-Bio One. Cell culture reagents such as media, trypsin, and PBS were purchase from Gibco. Chemicals were purchased from Sigma unless otherwise noted.

Caged ABA Synthesis

Chemicals and instruments:

Bulk solvents were obtained from EMD. (+)-Abscisic acid was obtained from Gold Biotechnology. 4,5-Dimethoxy-2-nitrobenzylbromide was obtained from Sigma-Aldrich. These compounds were used directly without further purification. Other chemicals are commercially available. NMR spectra were recorded on a Bruker instrument (300 MHz). Mass and NMR spectra for new compounds were recorded at the Mass Spectrometry and NMR Facilities, Department of Chemistry and Chemical Biology, University of New Mexico.

Synthesis of ABA-DMNB

4,5-Dimethoxy-2-nitrobenzyl bromide (DMNB; 303.6 mg, 1.2 mmol) was added to a CH_2Cl_2 solution of abscisic acid (ABA; 264 mg, 1 mmol) and 1,8-diazabicyclo[5.4.0]undec-7-ene (DBU; 168 mg, 1.2 mmol) at room temperature. After 2h, the solution was concentrated under vacuum. A pale yellow powder was

obtained after purification by silica gel column chromatography using hexane/ethyl acetate (v/v= 1: 1) as an eluting solvent (Rf= 0.5). Yield: 94 %. 1H NMR (300 MHz, $CDCl_3$): 7.89-7.84 (d, J= 15.9 Hz, 1H), 7.70 (s, 1H), 7.00 (s, 1H), 6.20- 6.15 (d, J= 15.9 Hz, 1H), 5.90 (s, 1H), 5.82 (s, 1H), 5.53 (s, 2H), 3.96 (s, 3H), 3.94 (s, 3H), 2.48-2.25 (dd, J= 17.1, 54 Hz, 2H), 2.06 (s, 1H), 2.02 (s, 3H), 1.88 (s, 3H), 1.63 (s, 1H), 1.08 (s, 3H), 0.99 (s, 3H). 13C NMR (100.6 MHz, $CDCl_3$): 197.72, 165.31, 162.45, 153.59, 150.87, 148.38, 140.17, 137.18, 128.01, 127.30, 127.13, 117.64, 110.83, 108.38, 79.72, 62.91, 56.53, 49.87, 41.60, 24.45, 23.16, 21.41, 18.94. TOF-HRMS (m/z) found (calcd.) for $C_{24}H_{29}NO_8$ (M): [M+Na]+, 482.1790 (482.1791).

Synthesis of ABA-DEACM

A CH_2Cl_2 solution of abscisic acid (ABA; 264 mg, 1 mmol), EDC (230 mg, 1.2 mmol) and DMAP (catalytic amount) was stirred 10 min at room temperature, to which compound 3 (299 mg, 1.2 mmol) was added. Compound 3 was synthesized according to the literature.[1] The reaction was then stirred overnight at room temperature. The organic solution was washed three times with sodium bicarbonate (saturated aqueous solution), dried over sodium sulfate and concentrated under vacuum. A yellow powder was obtained after purification by silica gel column chromatography using hexane/ethyl acetate (v/v= 1: 1) as an eluting solvent (Rf= 0.47). Yield: 82 %. 1H NMR (300 MHz, $CDCl_3$): 7.93-7.88 (d, J= 15.9 Hz, 1H), 7.30-7.27 (d, J= 9 Hz, 1H), 6.60- 6.56 (d, J= 11.4 Hz, 1H), 6.51 (s, 1H), 6.23-6.18 (d, J= 15.9 Hz, 1H), 6.21 (s, 1H), 5.93 (s, 1H), 5.85 (s, 1H),

5.26 (s, 2H), 3.44-3.37 (q, J= 21.3 Hz, 4H), 2.51-2.27 (dd, J= 17.1, 57 Hz, 2H), 2.05 (s, 3H), 1.92 (s, 3H), 1.75 (s, 1H), 1.23-1.18 (t, J= 14.1 Hz, 6H), 1.11 (s, 3H), 1.02 (s, 3H). 13C NMR (100.6 MHz, CDCl3): 197.77, 165.18, 162.48, 162.25, 156.36, 151.25, 150.78, 149.85, 137.32, 128.18, 127.20, 124.46, 117.49, 108.83, 106.39, 106.16, 97.97, 79.81, 61.12, 49.92, 44.89, 44.66, 24.50, 23.17, 21.49, 12.56. TOF-HRMS (m/z) found (calcd.) for $C_{29}H_{35}NO_6$ (M): [M+Na]+, 516.2360 (516.2362).

HPLC Analysis

Reversed-phase HPLC was performed on a Dionex Acclaim 120 (4.6 x 100mm) C18 column using an UltiMate 3000 pump system that included Variable Wavelength Detector 3100, Degasser 1210, and Autosampler SPS 3000. A mixture of water and acetonitrile containing 0.1% TFA was used as the eluent. Absorbance at 250 nm was used to monitor the elution of the molecules. The method used an increase in acetonitrile from 5% to 95% over 15 min to elute the molecules at a flow rate of 0.7 mL/min. The peaks for the molecules were integrated using Chromeleon software. The molar absorptivity of both free and caged ABA at 250 nm was measured, which was used to calculate the concentration of each species from the intensity of absorbance at 250 nm. The relative concentration of each compound was used to calculate the percent concentration of free ABA relative to the concentration of total ABA species (both caged and uncaged).

Cell Culture and Transfection

CHO cells and 293T EGFP reporter cells (provided by Dr. Gerald R. Crabtree) were cultured in Dulbecco's modified Eagle's medium (DMEM) (Gibco) with 10% FBS (Atlanta Biologicals), 1x GlutaMAX (Gibco), and 1x penicillin/streptomycin (Pen/Strep; Gibco). Cells (15,000 to 50,000) were plated in wells of a 24- or 8-well plate for 24 h before transfection. DNA constructs (0.1 μg to 0.5 μg) were added to 50x (v/w) Opti-MEM (Gibco) and then 3x (v/w) PEI (Polysciences) was mixed with the DNA. The mixture was incubated for 20 min at the room temperature before adding it to cell cultures. The cells were grown for 1 day after transfection before experiments were performed.

DNA Plasmids Construction

The construction of the 5FL, 5IG, SV-VPiGA, NES-ABI, GFP-PYL, myr-ABI plasmids has been described previously (6). PYL-EGFP-Tiam1 construct was derived from pSV40-VP16-PYL-IRES-Gal4DBD-ABI by inserting codon optimized PYL fragment (PCR amplified by primers CCGACAGAATTCGCCACCATGACCCAGGACGAGTTTACCCAG and CCGACAGGCGCGCCGCTGCCGCCGTTCATAGCCTCAGTAATGCT) using EcoRI and AscI sites, Tiam1-SG linker fragment (amplified by primers GCTATGAACGGCGCGCCA-AGTGCTGGTGGTAGTGCTGGT and CTAGAGTCGCGGCCGCTCAG-ATCTCAGTGTTC-AGTTTC) using AscI and NotI sites, and EGFP-SG-linker fragment (amplified by primers CCGACAGGCGCGCCAG-

GTGGATCTGGAGGTTCAGGTGGATCTGGAGGTGTGAGCAAGGGCGAGGAG CTG and CCGACAGGCGCGCCCTTGTACAGCTCGTCCAT-GCC using AscI site.

Photoirradiation

Irradiation at 365 nm was performed using an Axio Observer (Zeiss) microscope with an HBO103 W/2 mercury arc lamp. Irradiation was performed using the DAPI filter set with peak excitation at 365 nm (power density 23 mW/cm2) and spectral width of 50 nm. No objective lens was used for whole-well irradiation, which created an area of illumination that nearly completely covers one well of a 24-well plate. Light was transmitted through the bottom of the well of polystyrene plate. Irradiation at 405 nm was performed using an Adjustable Focus Violet Purple Laser Pointer (LazerPoint SKU 0733579) with excitation wavelength of 405 nm and 1000 mW intensity positioned 8 cm above the bottom of either a 96- or 24-well plate and irradiated through the polystyrene lid. All samples for HPLC analysis were irradiated in DMSO to prevent evaporation of solvent and changes in sample concentration. Irradiation of cell cultures was in 24-well plates containing 500 µL of culture media.

Luciferase Assay

Cells from 24-well plates were washed with PBS and lysed with 100 µL of Reporter Lysis Buffer (Promega) by incubating and gently shaken at room

temperature for 10 min after a freeze/thaw cycle. Cell lysates were centrifuged at 15,000 rpm in an Eppendorf Centrifuge 5424 and 25 µL of lysate was used for luciferase assay. 100 µL of luciferase assay reagent (5 mg luciferin (GoldBio) and 7 mg coenzyme A (Sigma) in 33 mL of luciferase assay buffer [20 mM tricine, 1.07 mM (MgCO3)4Mg(OH)2•5H2O, 2.67 mM MgSO4, 0.1 mM EDTA, 33.3 mM dithiothreitol, and 0.53 mM ATP in water) was added to lysates. Luciferase assay reagent was added through the auto-injector of GLOMAX-Multi Detection System (Promega), and the signal was detected by the instrument with a 1.5 s delay and 0.5 s integration time. All experiments were conducted in triplicate.

Slide Preparation

Cells were grown on glass coverslips in 24-well plates. The coverslips were washed with phosphate-buffered saline (PBS) and fixed with 300 µL of 4% paraformaldehyde (PFA, prepared in PBS) at room temperature for 20 min. The cells were then washed twice with PBS and incubated with 1x DAPI in the dark at the room temperature for 5 min. After a final wash with PBS, the coverslips were mounted on a glass slide with Vectashield (VWR) mounting media and allowed to stand for 2 h in the dark before imaging.

Fluorescence Microscopy Imaging

Slides were imaged with Axio Observer (Zeiss) microscope or with Zeiss LSM 510 Meta confocal mounted on an AxioObserver inverted microsope using the 63x oil objective. Images were taken with DAPI and GFP channels.

Live Cell Confocal Microscopy Irradiation and Imaging

EGFP fluorescence of CHO cells was detected with a Zeiss LSM 510 Meta confocal mounted on an AxioObserver inverted microscope. The ABA-DEACM was uncaged using the 405 nm UV laser (25 mW) set to 25% power for around 3 sec. To image, fluorescence was excited with the 488 nm line of an argon laser (30 mW) with laser power attenuated to 50%. EGFP emission was collected with a FITC filter. Live cells were plated in 8-well coverslip-bottom culture chambers in 200 µL media and maintained at 37 °C with an objective lens heater (Bioptics). Culture medium was exchanged to OptiMEM (Gibco) with caged ABA, or no drug prior to imaging. Images were acquired every 10 to 20 sec in different experiments with a 63x/ 1.2 NA water objective.

Statistical Analysis of Cell Population

Cells were categorized as displaying nuclear export of EGFP when the fluorescent intensity of the nucleus was less than 60% of the intensity of the cytoplasm. Cells were categorized as Ruffled when they displayed broad extensions identifiable as lemellopodia or fillopodia from the GFP fluorescence

from membrane localized EGFP-PYL-Tiam1. Cells were counted from three separate experiments with N > 50 for each experiment.

Image Analysis of Fluorescence Intensity in Nuclear Export Experiments: Images generated were analyzed for fluorescent intensity using Slide Book v.6 software. Equal sized regions of interest were analyzed from the cytoplasm and the nucleus to compare fluorescent intensity of EGFP in three cells for each condition from images taken every 20 sec for duration of 20 min.

2.5 References

1. Yin, P.; Fan, H.; Hao, Q.; Yuan, X.; Wu, D.; Pang, Y.; Yan, C.; Li, W.; Wang, J.; Yan, N. Structural insights into the mechanism of abscisic acid signaling by PYL proteins. *Nat. Struct. Mol. Biol*. **2009**, 16, 1230-6.

2. Corrie, J.E.T. Photoremovable Protecting Groups Used for the Caging of Biomolecules. Dynamic Studies in Biology. **2005,** WILEY-VCH Verlag GmbH & Co.

3. Morrison, H.A. The chemistry of the Nitro and Nitroso Groups. Ed. Henry Feuer, John Wiley and Sons, *New York*, **1970**.

4. Fedoryak, O.D.; Sul, J.Y.; Haydonb, P.G; Ellis-Davies, G.C.R. Synthesis of a caged glutamate for efficient one- and two-photon photorelease on living cells. *Chem. Commun*. **2005**, 3664-3666.

5. Schade, B.; Hagen, V.; Schmidt, R.; Herbrich, R.; Krause, E.; Eckardt, T.; Bendig, J. Deactivation Behavior and Excited-State Properties of (Coumarin-4-yl)methyl Derivatives. 1. Photocleavage of (7-Methoxycoumarin-4-yl)methyl-Caged Acids with Fluorescence Enhancement *J. Org. Chem.* **1999**, 64, 9109–9117.

6. Liang, F.S.; Ho, W.Q.; Crabtree, G.R. Engineering the ABA plant stress pathway for regulation of induced proximity. *Sci Signal.* **2011**, 4, 164.

7. Milborrow, B. V. The Chemistry and Physiology of Abscisic Acid *Ann. Rev. Plant Physiol.* **1974**, 25, 259-307.

8. Umeda, N.; Ueno, T.; Pohlmeyer, C.; Nagano, T.; Inoue, T. A photocleavable rapamycin conjugate for spatiotemporal control of small GTPase activity. *J. Am. Chem. Soc.* **2011**, 133, 12-4.

Chapter 3 – Chemically Inducible Translation

3.1 Introduction

I want to use ABA based dimerization to initiate the translation of a specific reporter gene. To do this I want to use the dimerization event to bring the translation initiation complex into proximity of a specific mRNA. I will fuse an RNA binding protein fused to one of the dimerizing proteins and a translation initiation factor to the other dimerizing protein. This should allow the recruitment of the ribosome to an mRNA only when ABA is present.

Protein components of the translation initiation complex have been fused to RNA binding proteins to target their function directly to the mRNA. This has been used to separate the RNA binding domains from the translation regulation domains. The C-terminus of eIF4G was fused to RNA binding domains to target translational machinery to reporter genes (1). Truncated versions of eIF4G that had any parts of the eIF4A binding sites removed were less effective at inducing translation, Figure 3.1 (1). This indicates that the C-terminus of eIF4G would be the best candidate for recruiting the translation initiation complex. Expression of any of the proteins containing the RNA binding domain without eIF4G had no effect on the level of reporter mRNAs indicating that the increase in translation is specific to the sequence of the RNA and the corresponding RBP-eIF4G fusion protein (1).

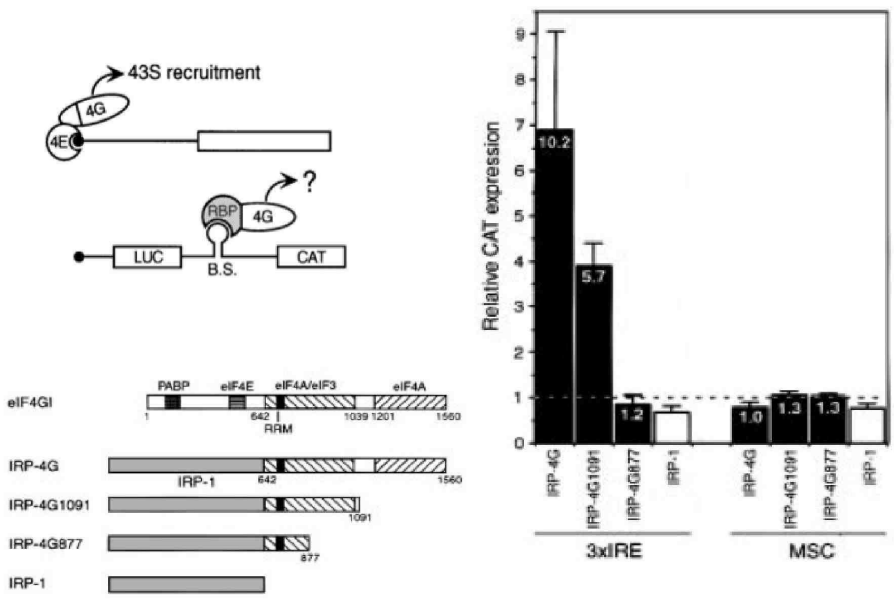

Figure 3.1. The section of eIF4G that is most effective at inducing translation is from amino acid 642 to 1560. Truncated versions were less effective. (1)

The RNA stem loop and RNA binding domain pair are interchangeable for tethering the function of eIF4G, and it was shown that multiple pairs of RNA stem loops and RNA binding proteins could both be used to elicit translation of the downstream gene (1). Although any stem loop/protein pair can induce translation there could be drawbacks to using the iron-responsive protein in that the iron-responsive element is found in the 5' and 3' UTR of quite a few mRNAs (2).

λN, a protein from the Lambda bacteriophage, is an antiterminator that binds regions within the viral genome to allow the read through of termination sites and promote transcription of downstream genes (3). In these sites there is a 15 nucleotide palindromic sequence, BoxB, capable of folding into a hairpin

loop, and it is this RNA structure that binds the λN protein (4). Only the first 22 amino acids of λN are required for binding (5). In addition to binding the loop sequence the protein binds asymmetrically to only the 5' arm of the BoxB stem (6).

MS2 coat protein (MCP) is a common protein used to target mRNA binding. MCP is responsible for forming the capsid of the MS2 virus. This protein also regulates the translation of a viral replicase gene that contains an MS2 stem loop in the 5'UTR (7). Fusion proteins between MCP and GFP have been used to track the location of transcripts containing the MS2 stem loop (8).

There is an equilibrium between the dimer of MCP that binds the stem loop and oligomerization that forms the viral capsid. When capsids are formed MCP is unable to bind the mRNA and repress translation (9). There is a flexible 15 amino acid loop between the F and G β-strands of the monomer that is involved in the contacts important for the formation of the capsid. Deletion of the FG loop causes the protein to not be able to form capsids (10). A mutation of valine 29 to isoleucine created a protein that was able to repress translation better than the wild type protein, but was still able to assemble into capsids (11). It was later shown that the V29I mutant binds more tightly to wild type and mutant stem loops (12).

MCP dimerizes and creates a large β-sheet composed of 5 β-strands from each protein, and binds the MS2 loop with this surface. The C-terminus of one monomer is in close in proximity to the N-terminus of the other monomer (13). The production of MCP as a fused dimer with an amino acid linker is able to bind

the MS2 sequence and suppress translation (14). The duplicated protein has the same binding affinity as the wild-type protein (14).

The design of the intercistronic region of the reporter mRNA is important for inducing translation. The spacing between the first gene and the stem loops influences the amount that the second gene can be translated. Having only 70 base pairs gives nearly three-fold increase in translation, while having 136 base pairs increases that to four-fold (1). The distance between the stem loops and the second gene is also important. Decreasing that distance from 46 base pairs to 13 showed a negative effect upon the translation of the second gene (1). The spacing used in previous experiments may or may not be optimal for our system because of the increased distance between the RNA binding domain and eIF4G because of the addition of the dimerizing protein pair.

The identities of the nucleotides in the MS2 loop are most important for binding to the coat protein. There is an unpaired adenosine two base pairs upstream from the loop that is also important for binding (15). There also should be at least three paired nucleotides below the bulge for optimal structure (9). An MS2 stem loop that has a mutation of a C at the -5 position binds the coat protein 150 better than the wild type loop sequence (16). A factor that has a large influence on the amount of translation of the downstream gene is the number of stem loops present. Increasing the number of RNA stem loops, from 1 to 3, in the reporter construct has a two-fold increase in translation, Figure 3.2A (1).

The first gene of the reporter construct did not show any change in expression from the translation of the downstream gene. Translation of the

downstream gene is not affected by the repression of cap-dependent translation from a large stem loop in the 5'UTR. The induction of translation of the downstream gene is 10-15% as efficient as the hepatitis C viral IRES, Figure 3.2B, and is about 5% as efficient as cap-dependent translation. The background translation of the second gene without induction is about 0.7% that of the upstream gene (1).

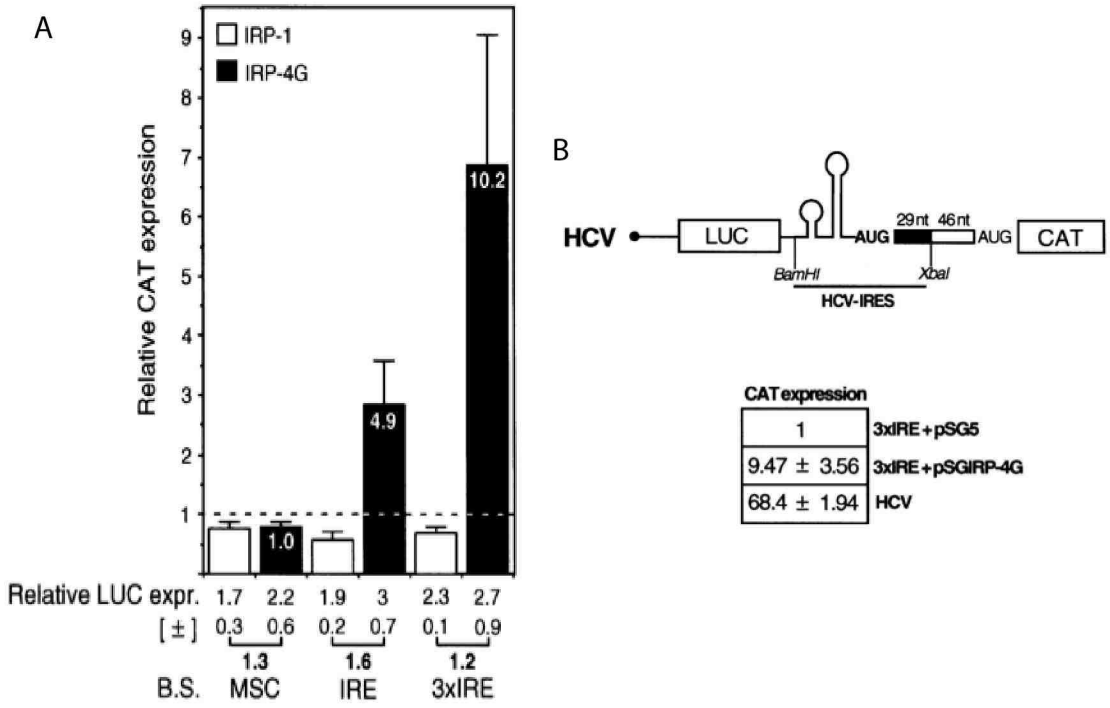

Figure 3.2. (A) An increasing number of stem loops in the reporter construct causes and increase in translation of downstream genes. (B) The HCV IRES was found to be more effective for inducing translation than RBP based targeting of eIF4G. (1)

I want to use ABA inducible dimerization as a switch to control the translation of a gene downstream of an RNA stem loop. I want to do this by using the dimerization to control the proximity of eIF4G to RNA binding protein that targets the mRNA with corresponding RNA stem loop, Figure 3.3. To make

the system I will fuse one of the PYL and ABI dimerizing pair to either the RNA binding protein or eIF4G. These proteins can be expressed constantly, but should not elicit a response until ABA is present.

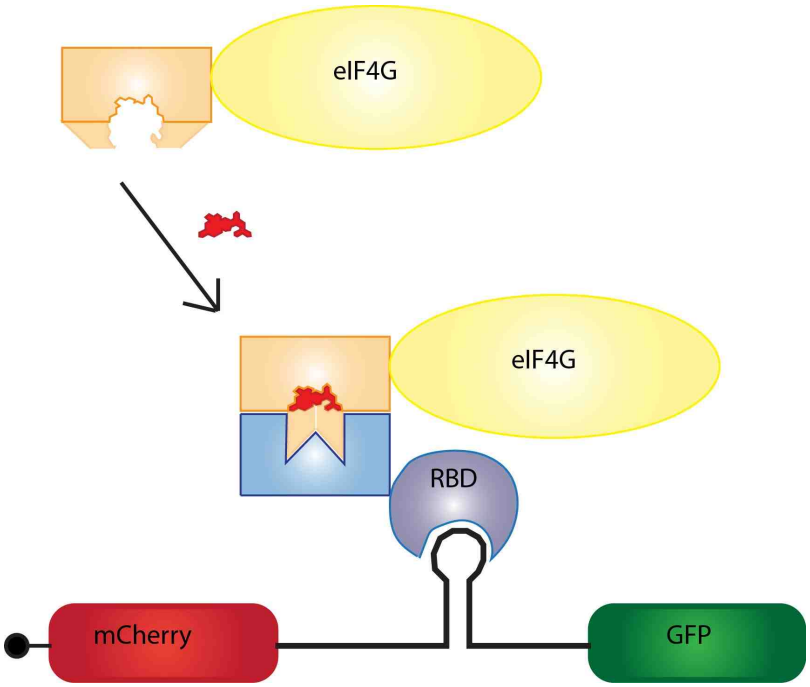

Figure 3.3 . Strategy for engineering ABA inducible translation. The translation of GFP occurs when eIF4G is recruited to the RNA sequence upstream from it. An RNA binding protein is used to target a specific sequence and bring eIF4G into proximity upon dimerization of PYL and ABI.

Using a chemical activator allows fast control of dimerization and could allow greater precision of translation compared to direct fusion proteins. In addition it could be possible to combine this with the photorelease of ABA in order to spatially control the activation of translation of a specific protein. This could be used to produce a biologically relevant protein sub-cellularly to investigate its role neural growth and function.

3.2 Results

I am going to use a system that employs a reporter construct expressing fluorescent proteins. Similar to previous work I will put one gene under normal cap-dependent translation and the other will be downstream of an RNA stem loop that can bind an RBP to target the localization of eIF4G. In this way I can use the fluorescence intensity of each of the reporter proteins as measure of the relative amounts of cap-dependent and cap-independent translation.

Optimizing the Reporter Construct

RNA binding domains from viruses were used to target RNA sequences because they are not used in normal cellular contexts. The RNA binding domains were fused to the C-terminal region of eIF4G containing amino acids 642-1560 with a flexible linker in between. I created direct fusion proteins that have one or two copies of MCP, as well as one that contained two copies of the λN protein, Figure 3.4.

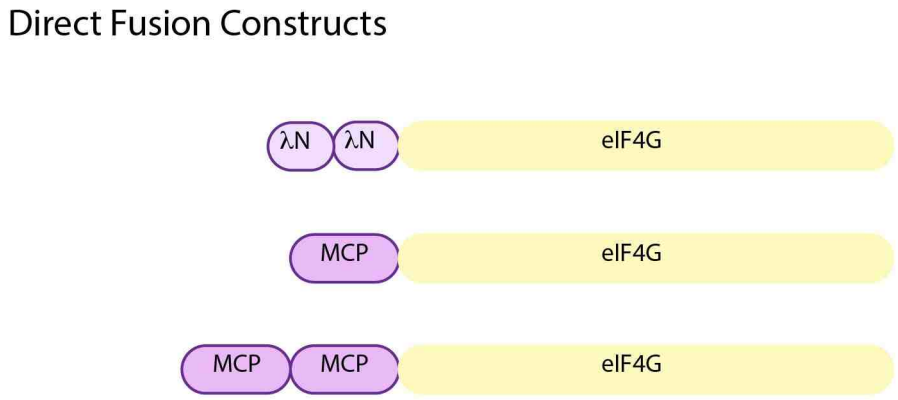

Figure 3.4. The RNA binding proteins MCP and λN were fused to C-terminal domain of eIF4G containing amino acids 642-1560. The MCP protein was fused to eIF4G as both a monomer (MCP-eIF4G) and a dimer (2xMCP-eIF4G). The λN protein was used as a dimer but is the only one so is called λN-eIF4G.

The reporter constructs have an mCherry gene that is translated through normal cap-dependent processes as a control for expression levels of the reporter construct. Downstream of this gene is a 70 nucleotide spacer before the stem loops and then a 40 nucleotide spacer after the stem loops and before the inducible GFP gene. I created several versions of the reporter construct that contained either one or three copies of the MS2 stem loop, Figure 3.5. These constructs were named mCherry-$MS2_1$-GFP (CM1G) and mCherry-$MS2_3$-GFP (CM3G).

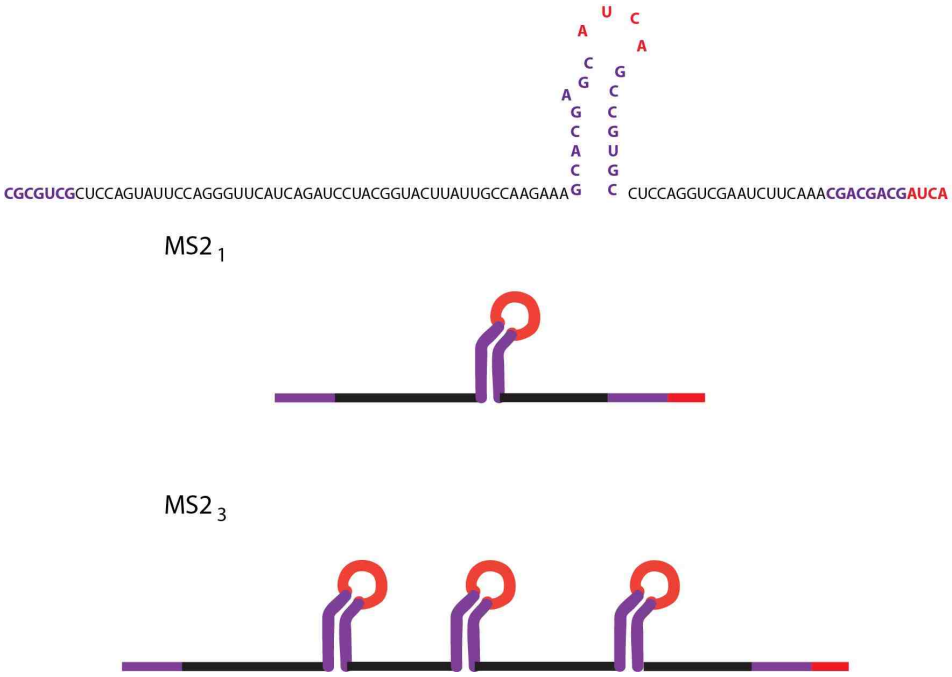

Figure 3.5. The MS2 insert from pCR4-24XMS2SL is shown restricted with MluI. The enzyme cuts in the middle of an stem loop such that ligation of two fragments rejoins the two halves of the MS2 sequence. Therefore there are MS2 reporter constructs with one ($MS2_1$) and three ($MS2_3$) stem loops.

I made a reporter construct with the BoxB sequence instead of the MS2 sequence to test the specificity of the RNA binding domains for their respective reporters, Figure 3.6. The λN protein should not be able to bind the MS2 stem loop and vise versa.

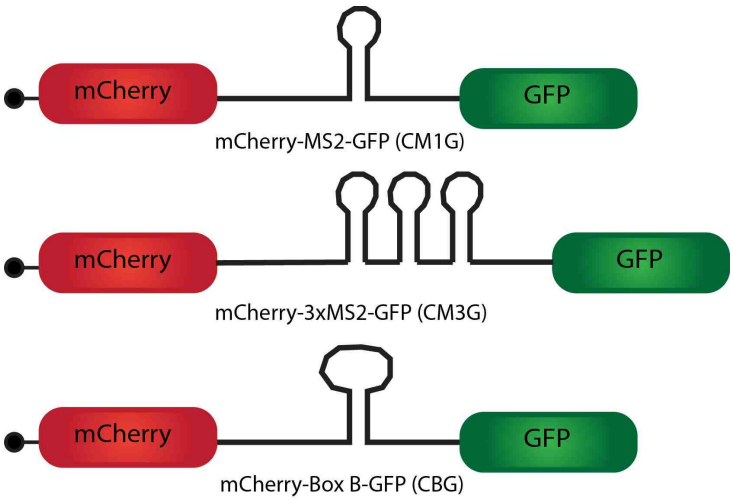

Figure 3.6. Reporter constructs contained MS2 or BoxB stem loops downstream of the mCherry coding sequence and upstream of the GFP coding sequence. These were used to compare the fluorescence of mCherry compared to GFP for each condition.

I wanted to make a BoxB construct with two stem loops in order to bind the two λN proteins fused to eIF4G. I wanted to create these so that I could compare the use of multiple RNA-protein contacts to increase the interaction. I initially ordered a double stranded DNA fragment (IDT) containing two copies of the BoxB stem loop, but with one stem sequence changed to avoid repetitive sequences to facilitate synthesis of the DNA. Because the λN protein binds the stem as well as the loop this would essentially only make one function copy of BoxB and therefore this construct was named mCherry-$BoxB_1$-GFP (CB1G). I made another BoxB reporter containing two stem loops using short oligonucleotides of the BoxB sequence, Figure 3.7, and this construct was named mCherry-$BoxB_2$-GFP (CB2G).

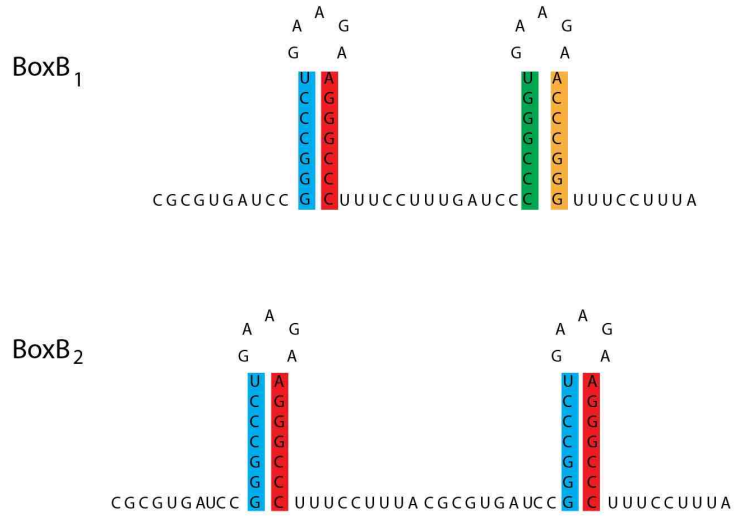

Figure 3.7. BoxB stem loops were designed to not have similarity in the stem sequence so that it doesn't form other secondary structures. The λN protein binds the 5' region of the stem, and hence the second BoxB stem loop (green/yellow) may not bind λN. Therefore the reporter construct with this sequence is mCherry-$BoxB_1$-GFP (top). Two copies of a DNA fragment containing the BoxB stem loop (blue/red) were inserted into a reporter plasmid to give mCherry-$BoxB_2$-GFP (bottom).

Testing the BoxB reporters: B35 cells were transfected with the either one of BoxB reporter constructs and the λN-eIF4G construct and grown for 24 hours. The mCherry-$BoxB_2$-GFP construct showed almost no ability to induce the translation of GFP in the presence of λN-eIF4G, Figure 3.8. This may be due to the formation of larger RNA structures involving pairing between the two copies of the BoxB sequences. It may be that the 5' side of the first stem of the first sequence (blue in Figure 3.5) would bind the 3' side of the stem of the second sequence (red in Figure 3.5) creating a RNA structure that would not resemble the three dimensional structure necessary to bind λN.

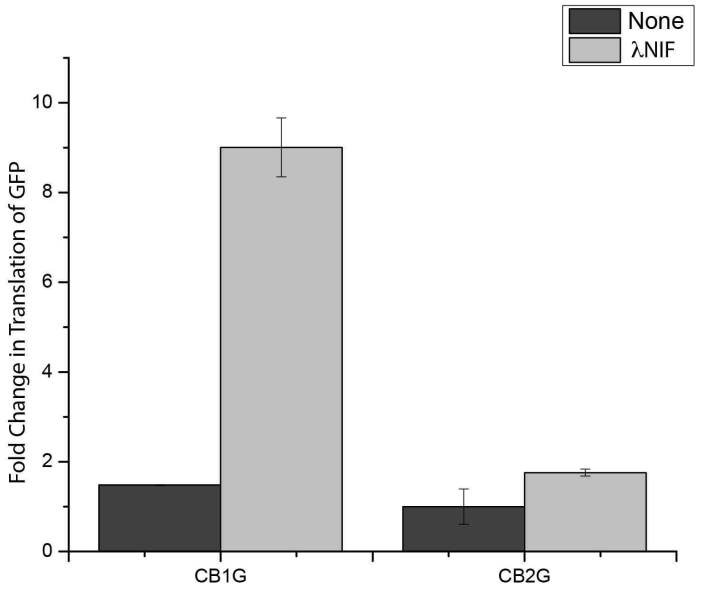

Figure 3.8. B35 cells were transfected with the BoxB reporter constructs mCherry-BoxB_1-GFP (CB1G) and mCherry-BoxB_2-GFP (CB2G). These cells were either transfected with λN-eIF4G (λNIF) or no inducer. Cells with λNIF and CB1G showed increased translation of GFP compared to cells with λNIF and CB2G. This may be due to the formation of a different secondary structure of the BoxB stem loops when there are two exact copies.

Testing the reporter specificity: B35 cells were transfected with one of the eIF4G fusion proteins and one of the reporter constructs. All of the eIF4G fusion constructs were tested against all of the reporter constructs to see if the binding was specific to the corresponding stem loop and protein, Figure 3.9. The relative induction of translation was calculated by getting the ratio of the fluorescence of GFP over mCherry for each condition. The relative induction of each condition was normalized by dividing by the relative induction of translation of a negative control to get the fold change in translation of GFP. This was

normalized to the relative induction of translation for the negative control with the lowest background, in this case CB1G, Figure 3.9.

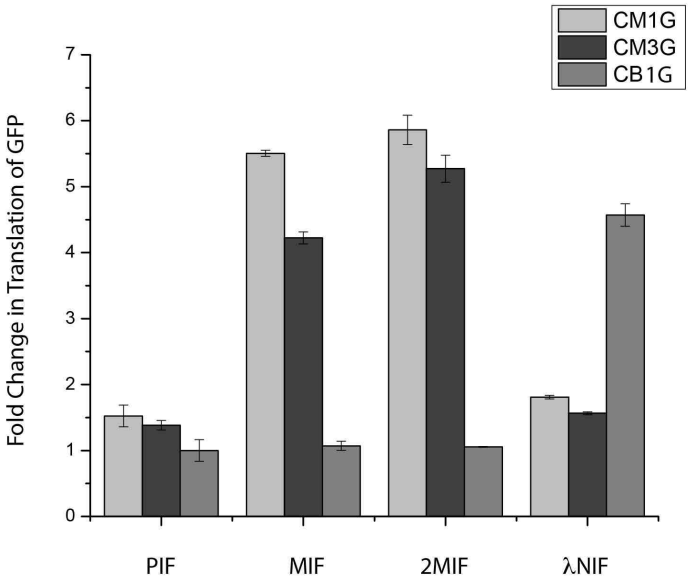

Figure 3.9. Flow cytometry analysis shows the amount translation induction from different combinations of reporter constructs and eIF4G fusion proteins. There was an increase in translation of GFP when MCP-eIF4G (MIF) or 2xMCP-eIF4G (2MIF) were cotransfected with either mCherry-$MS2_1$-GFP (CM1G) or mCherry-$MS2_3$-GFP (CM3G) compared to background levels. An increase was also increase of translation when λN-eIF4G (λIF) is cotransfected with mCherry-$BoxB_1$–GFP (CB1G). Translation of GFP occurs only when the eIF4G fusion protein is present with the corresponding stem loop reporter. There are low levels of translation of GFP when an eIF4G fusion protein is present that does not bind the reporter sequence showing that GFP translation is not a result of overexpression of eIF4G.

The expression of GFP from the CM1G reporter construct was slightly higher than that of the CM3G reporter construct. This may be due to a decreased ability to block the ribosome from scanning through the intercistronic

distance. The presence of the additional MS2 stem loops creates more of a barrier to the ribosome to decrease background translation of GFP. The expression of GFP greatly increases when MS2 containing reporter constructs are expressed with MCP-eIF4G fusion proteins, while the expression of GFP also increases when the BoxB1 reporter construct is expressed with the 2xλN-eIF4G fusion protein. Importantly, there is little expression of GFP when MS2 reporter constructs are used with the λN-eIF4G fusion protein or when the BoxB1 reporter construct is used with the MCP-eIF4G fusion proteins. This shows that the translation is dependent upon the RNA binding protein's specific interactions with the corresponding RNA stem loop sequence and can be specifically targeted.

There are slightly higher fold change in translation of GFP when either of the MCP fusion proteins are used with CM1G compared to CM3G, this may be due to the slightly higher background expression of the GFP gene when there is just one stem loop. Therefore some of the GFP signal is from the carry over of the ribsome from mCherry and is not specific to the localization of the MCP-eIF4G fusion proteins to the stem loops.

Testing the MS2 reporters: In another experiment the MCP direct fusion proteins were co-transfected with the reporter constructs either containing one MS2 stem loop or three MS2 stem loops. This time each data set, either CM1G or CM3G, was normalized separately to its background levels of GFP. The relative induction of MIF's with CM1G was divided by the relative induction of PIF with CM1G, and the relative induction of MIF's with CM3G was divided by the relative induction of PIF with CM3G, In this way I could see which reporter

construct and inducer construct pair gave the greatest change in translation induction, Figure 3.10. It was shown that the constitutive dimer of MCP fused to eIF4G was able to induce slightly more translation of GFP compared to the monomer. The CM3G reporter construct had a greater fold change in translation compared to CM1G when normalized in this manner compared to normalization of all of the reporter constructs to the lowest negative control.

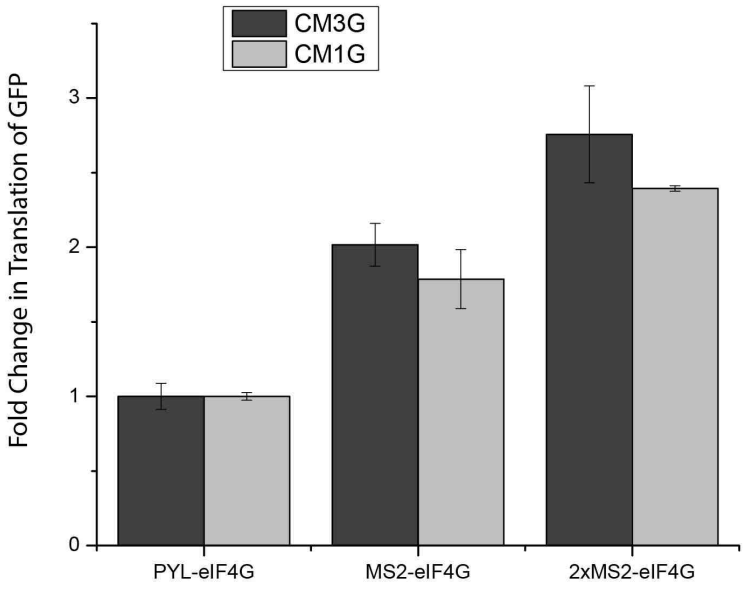

Figure 3.10. Whole well analysis was used to measure the amount translation induced for each MS2 reporter construct. Each construct was normalized by its own value for the negative control with PYL-eIF4G. In this way one can see the amount of change in translation for each construct from localization of MCP-eIF4G proteins. It was shown that mCherry-$MS2_3$-GFP (CM3G) has the highest amount of change in the translation of GFP compared to its background levels.

Testing the effects of installing a repressor loop: I also created a reporter construct with an additional stem loop that is 24 nucleotides in length and has been shown to decrease cap-dependent translation by over 96% (1), Figure 3.11. I wanted to see if the system could be optimized by further suppression of the basal translation of the second gene. The repressor loop was installed downstream of the mCherry sequence and directly upstream from the MS2 fragment, which puts it over 70 nucleotides from the first MS2 stem loop.

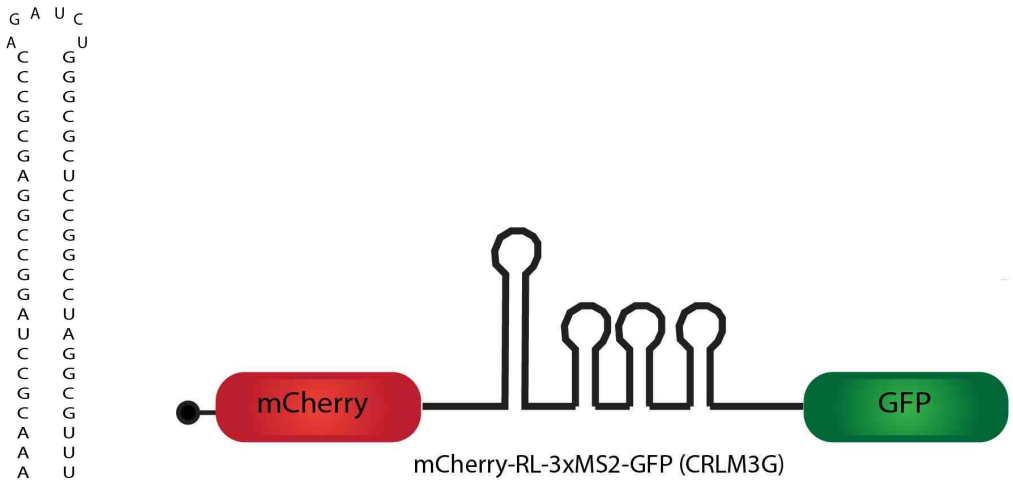

Figure 3.11. The 24 base pair repressor loop was inserted directly upstream of the MS2 insert to decrease ambient translation of GFP.

Cells were transfected with either the mChery-MS2$_3$-GFP (CM3G) or the repressor loop reporter mCherry-RL-MS2$_3$-GFP (CRLM3G) in addition to the direct fusion inducer 2xMCP-eIF4G or one of the split constructs PYL-eIF4G or

2-MCP-ABI. When whole well fluorescence was analyzed it showed nearly the same levels of background expression of GFP, Figure 3.12. The repressor loop reporter construct also showed lower levels of GFP expression when induced with 2xMCP-eIF4G. The decrease fold change of translation using the repressor loop construct may be due to placement of the eIF4G upon binding. Upon binding the MS2 stem loop, the MCP-eIF4G protein could be oriented upstream or downstream. If the eIF4G is positioned upstream from the repressor loop, that loop will block the advancement and scanning of the ribosome. This could be the reason for the decrease in translation activation of the repressor loop construct.

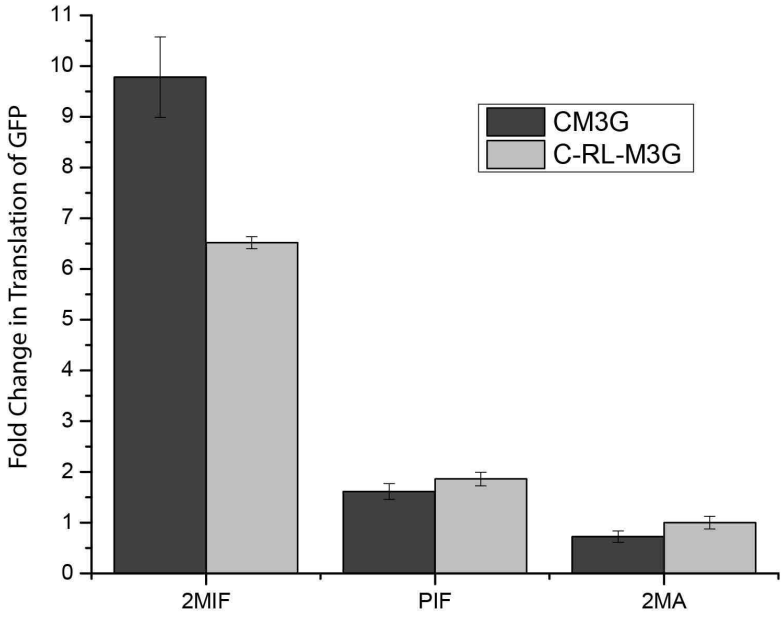

Figure 3.12. Flow cytometry analysis of B35 cells transfected with either the mChery-$MS2_3$-GFP (CM3G) or the repressor loop reporter mCherry-RL-$MS2_3$-GFP (CRLM3G) shows that the repressor loop constructs shows similar levels of background when cotransfected with PYL-eIF4G (PIF) or 2xMCP-ABI compared to the construct without the repressor loop. The repressor

loop construct does show lower levels of GFP expression when induced with 2xMCP-eIF4G (2MIF).

Optimizing ABA Inducible Translation

Next I wanted to employ chemically induced dimerization as a switch to localize eIF4G to the mRNA upon addition of the activator. Therefore I created MCP-ABI fusion proteins and used them in conjunction with PYL-eIF4G to create an ABA inducible translation system. I made both the MCP monomer and dimer fused to ABI for targeting the mRNA in ABA induced translation, Figure 3.13.

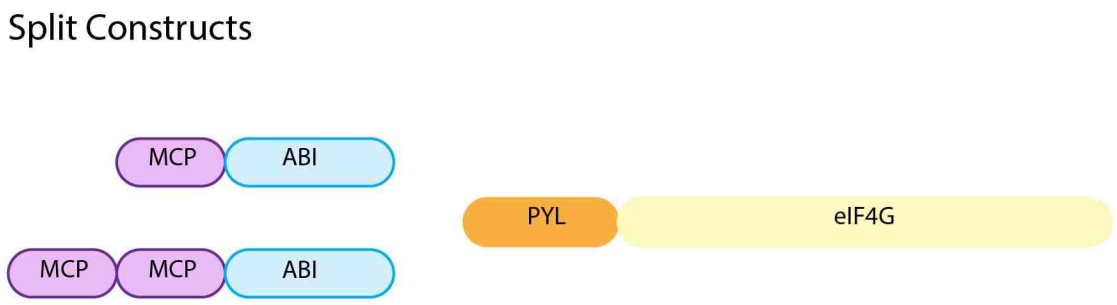

Figure 3.13. The ABA dependent dimerizing proteins ABI and PYL were fused to MCP and eIF4G domains to create ABA dependent translation.

Testing ABA inducible translation: B35 cells were transfected with the MCP-ABI and PYL-eIF4G constructs as well as the CM3G reporter. Cells that received ABA showed an increase in GFP translation compared to cells that did not receive ABA Figure 3.14.

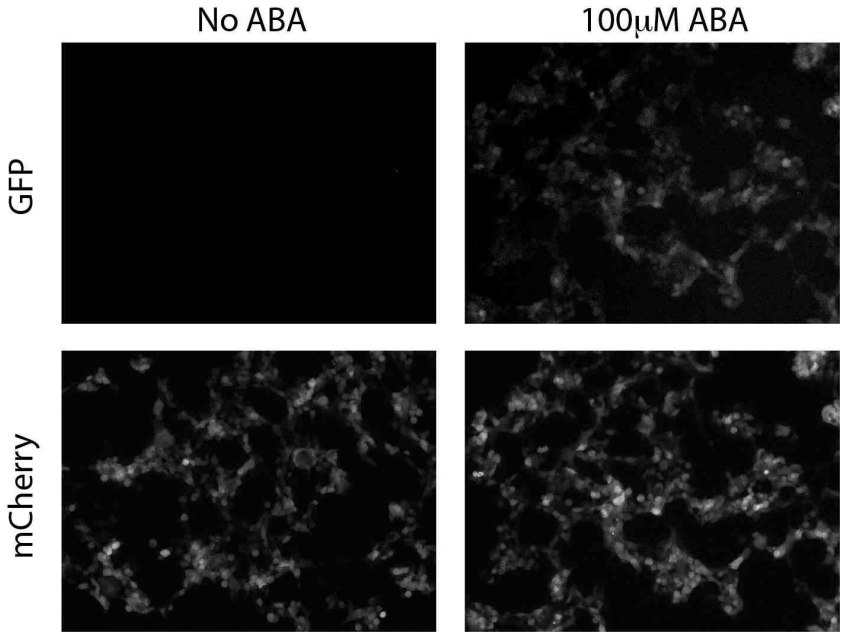

Figure 3.14. B35 cells were transfected with MCP-ABI and PYL-eIF4G along with the mCherry-$MS2_3$-GFP reporter construct. Cell incubated with 100μM ABA for 24 hours showed an increase in GFP fluorescence compared to cell that did not receive ABA.

I wanted to see which of the MCP-ABI fusion proteins showed greater induction of translation from the addition of ABA. Cells were transfected with PYL-eIF4G, either MCP-ABI or 2xMCP-ABI, and either CM1G or CM3G. Without ABA the reporter CM1G and MCP-ABI show the highest levels of background, and also show the highest fold change in translation of GFP with ABA when normalized to the lowest negative control, in this case CM3G with 2xMCP-ABI and PYL-eIF4G without ABA, Figure 3.15. The CM1G construct shows lower levels of background translation of GFP with the 2xMCP-ABI protein. The levels of background without ABA and induction with ABA were similar when using the

CM3G reporter construct with either of the MCP-ABI fusion proteins. It may be that there is better binding with the MCP fused dimer with the stem loop, which decreases the read through of the ribosome from mCherry.

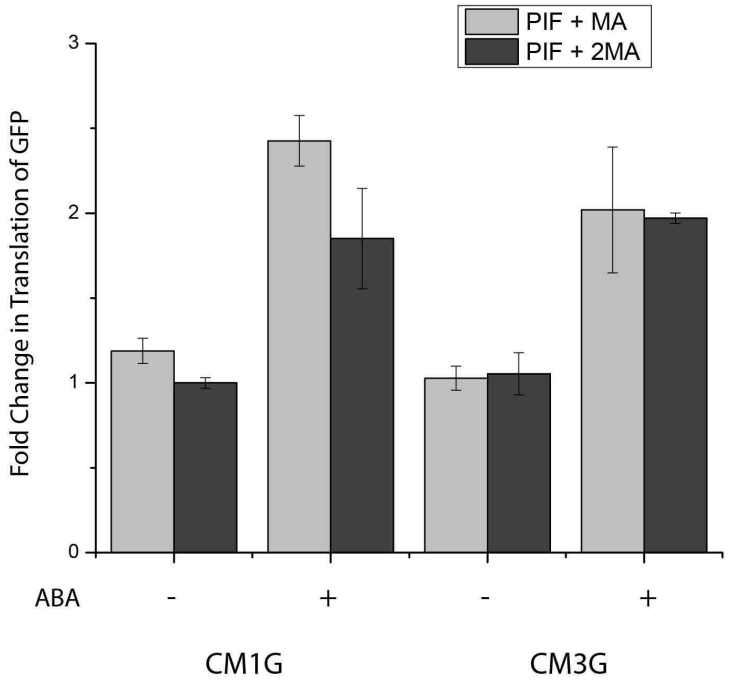

Figure 3.15. Whole well fluorescence analysis of B35 cells that had been transfected with either MCP-ABI (MA) or 2xMCP-ABI (2MA) along with PYL-eIF4G (PIF) and the reporter mCherry-$MS2_3$_GFP (CM3G). There was low expression of GFP when there is no ABA present, but shows increased levels of GFP when incubated with 100μM ABA.

Testing transfection ratios for PYL-eIF4G and 2xMCP-ABI: I wanted to make a bicistronic construct containing both halves of the dimerizing system. I thought that this would improve the system by increasing the probability that a cell will get all three components necessary for ABA inducible translation. The use of the hepatitis C virus (HCV) IRES allows the production of both proteins from the same mRNA transcript, thus assuring co-expression.

Translation from an IRES is still not quite as strong as normal cap-dependent translation, and so the second gene will always have slightly lower amounts. I wanted to find out which gene should come first and which should come second, so I tested the amount of induction from relative amounts of each constructs, Figure 3.16.

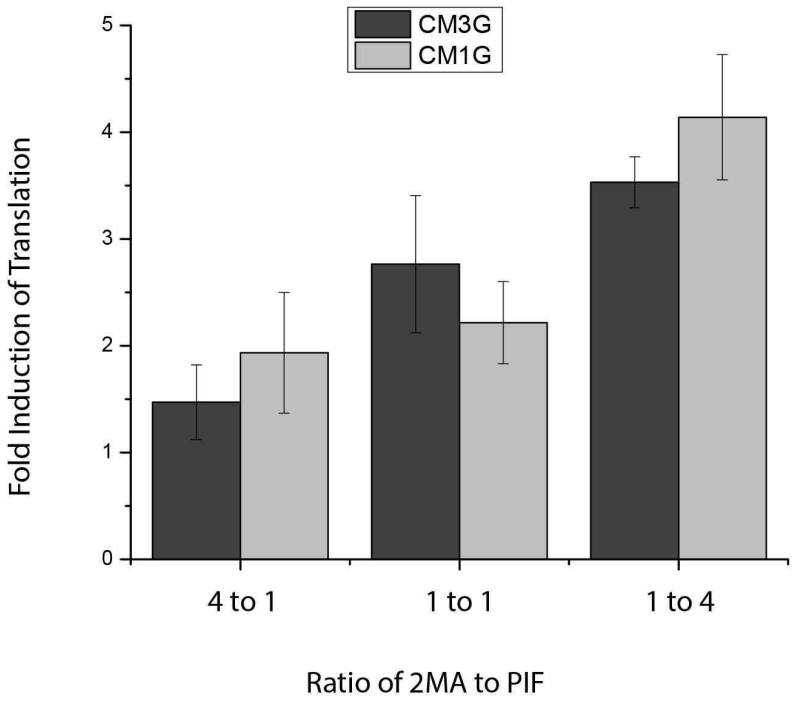

Figure 3.16. B35 cells transfected with mCherry-$MS2_1$-GFP (CM1G) or mCherry-$MS2_3$-GFP (CM3G) and different ratios of 2xMS2-ABI (2MA) and PYL-eIF4G (PIF). Cells were analyzed by whole well fluorescence to find optimal ratios for the dimerizing proteins 2MA and PIF. Fold change of translation is normalized to negative controls without ABA for each transfection condition. There is a greater amount of change in translation of GFP when greater amounts of PYL-eIF4G are transfected compared to 2xMCP-ABI.

I transfected cells with different ratios of DNA for the inducer constructs. I used .1µg of DNA for the reporter construct for each condition, but varied the amount of DNA for 2xMCP-ABI and PYL-eIF4G. I used ratios of 4:1, 1:1, and 1:4, in which the total amount of inducer construct DNA was equal to 0.5µg. I took half the transfected cells and added 10µM ABA and incubated for 24 hours. I then normalized each transfection condition with ABA to the same transfection condition without ABA as the negative control to get the fold change for ABA induced translation.

I found that the amount of translation of GFP increased the most when the amount of PYL-eIF4G transfected was the greatest, Figure 3.16. Therefore I concluded that the PYL-eIF4G would go before the IRES and the 2xMS2-ABI gene should go after the IRES, Figure 3.17.

Figure 3.17. PYL-eIF4G was inserted upstream from the IRES to attempt to have higher expression of this protein. 2xMCP-ABI was inserted downstream from the IRES, which will cause lower levels of expression of this protein.

Testing the bicistronic inducer construct: I wanted to test the effectiveness of duel transfection with the bicistronic construct and the reporter in comparison to triple transfection with all of the components on separate plasmids. B35 cells were transfected with the CM3G reporter construct and

either the bicistronic incuder PIFi2MA or the two constructs 2MA and PIF used in a 1 to 4 ratio. Fluorescence analysis of the whole well showed that the amount of translation of GFP induced with the PIFi2MA construct was greater than that of the separate constructs 2MA to PIF, and nearly reached that of the positive control with 2MIF, Figure 3.18. This may be due to the fact that the positive control scenario only requires the acquisition of two plasmids for a cell to be able to translate GFP, which is more likely than aquiring all three plasmids.

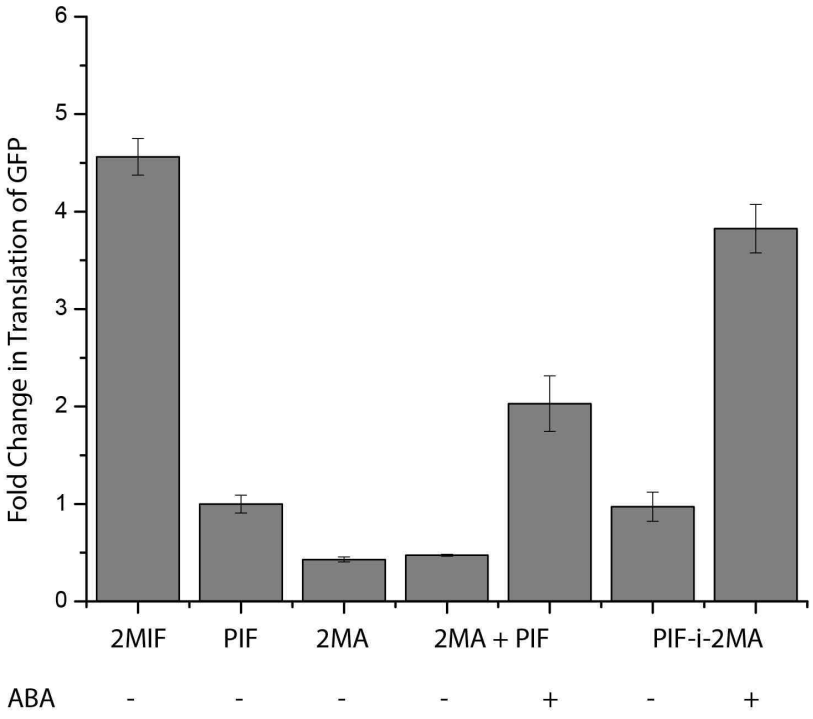

Figure 3.18. Whole well fluorescence was used to analyze the effectiveness of the bicistronic inducer construct. Cells transfected with the mCherry-MS2$_3$-GFP (CM3G) reporter construct and the bicistronic inducer, PYL-eIF4G-ires-2xMCP-ABI (PIFi2MA), showed a greater fold change of ABA dependent GFP translation than the separate constructs 2xMS2-ABI (2MA) and PYL-eIF4G (PIF). The bicistronic inducer does show a slight increase in the background translation of GFP, similar to the cells transfected with only PYL-eIF4G.

I repeated this experiment using the flow cytometer and expected to get similar results seen in whole well analysis. When the amount of translation induction was calculated with the flow cytometer a different pattern was observed. The cells that induced translation with all three plasmids showed greater GFP expression than those transfected with the bicistronic inducer, Figure 3.19. These results reveal that on a per cell basis the bicistronic inducer is less effective, but on a whole well level it is more effective.

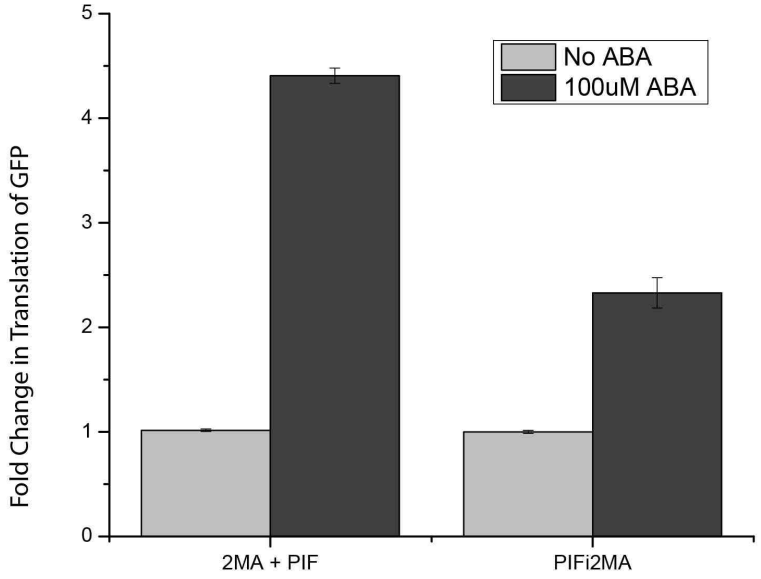

Figure 3.19. Flow cytometry was used to further analyze the bicistronic inducer's effectiveness. Cells were transfected with the reporter construct mCherry-$MS2_3$-GFP and either the bicistronic inducer PYL-eIF4G-ires-2xMCP-ABI (PIFi2MA) or separate constructs 2xMCP-ABI (2MA) and PYL-eIF4G (PIF). The levels of ABA induced GFP expression per cell are greater for those

transfected with the seperat constructs for 2MA and PIF compared to the ABA induction from the bicistronic inducer PIFi2MA.

This lead me to look into the amount of cells in each condition that show GFP expression above backgound levels. The bicistronic construct causes more cells to be able to translate GFP ,Figure 3.20, but to a lesser intensity per cell than transfecting the constructs seperately at a 1 to 4 ratio of 2MA to PIF as seen in Figure 3.19.

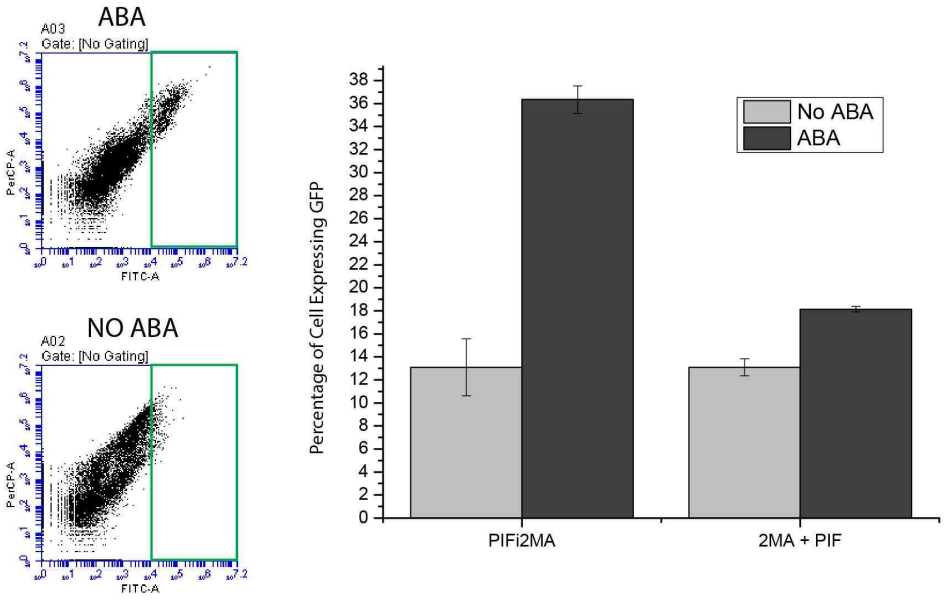

Figure 3.20. Cells were transfected with the reporter construct mCherry-$MS2_3$-GFP and either the bicistronic inducer PYL-eIF4G-ires-2xMCP-ABI (PIFi2MA) or separate constructs 2xMCP-ABI (2MA) and PYL-eIF4G (PIF). Further analysis from flow cytometry shows the percentage of cells in each condition that have GFP fluorescence greater than background levels (green box). The bicistronic inducer construct causes more cells to increase their translation of GFP compared to transfection with separate constructs when incubated with 100μM ABA.

Characterizing ABA Inducible Translation

I wanted to determine the optimal conditions to use for inducing translation of GFP. I wanted to see if there was a time point after the addition of ABA that would show high induction of GFP translation and low background translation of GFP without ABA. I also wanted to see how rapidly the system could elevate levels of GFP above background levels. In addition I wanted to see if there was a correlation between the concentration of ABA and the amount of GFP produced, similar to the results seen from ABA induced transcription.

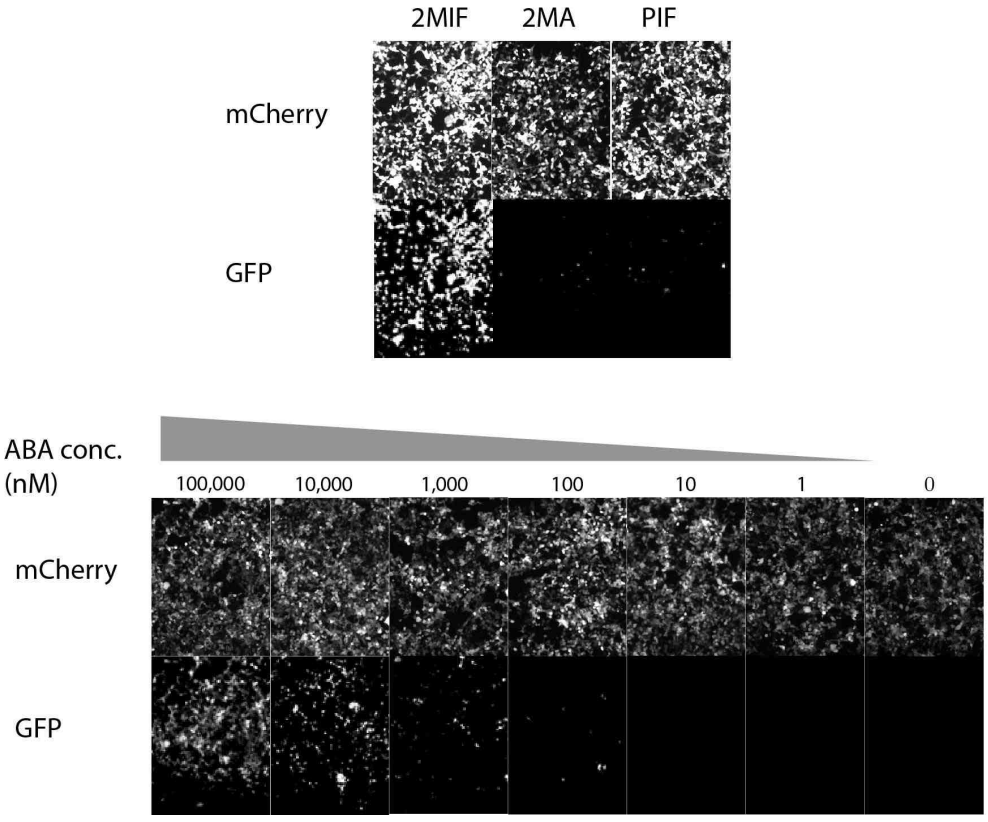

Figure 3.21. Cells were transfected with the reporter construct mCherry-$MS2_3$-GFP the bicistronic inducer PYL-eIF4G-ires-2xMCP-ABI (PIFi2MA). Cells were incubated with ABA in a range of concentrations from 1nM to 100μM for 24 hours. An increase in the expression of GFP was seen with increasing ABA concentration.

Testing optimal ABA concentration: B35 cells were transfected with the CM3G reporter construct and the bicistronic inducer construct PIFi2MA. A wide range of ABA concentrations were used, from 1 nM to 100 μM. There was an increase in the amount of GFP with an increase in concentration of ABA, Figure 3.21. Cells analyzed with flow cytometry showed an increase of fold change in translation for concentration up to the μM range, Figure 3.22.

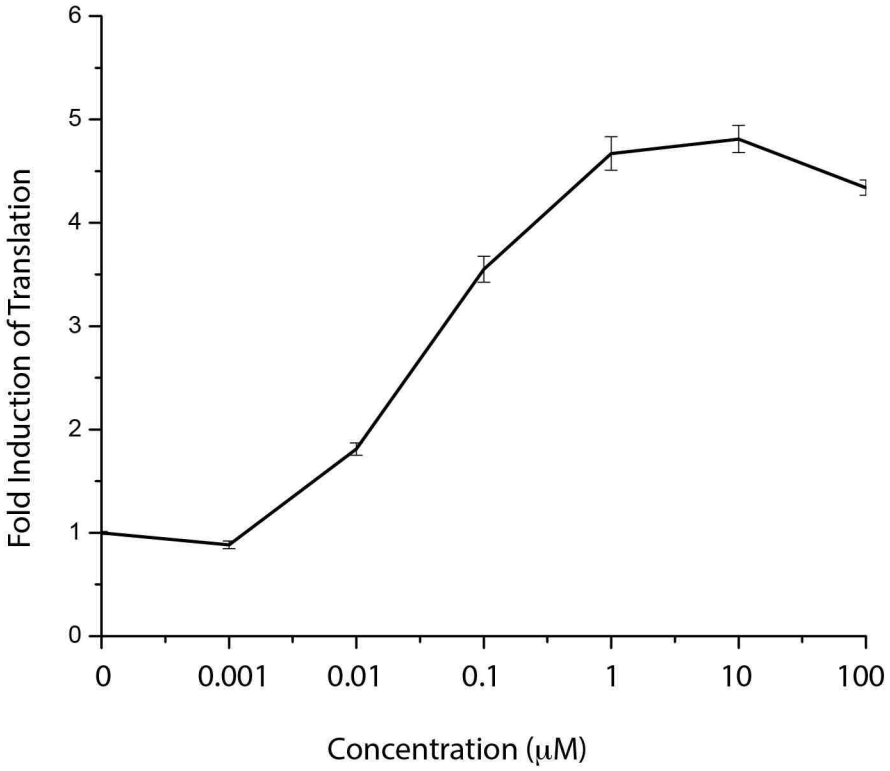

Figure 3.22. Cells were transfected with the reporter construct mCherry-$MS2_3$-GFP the bicistronic inducer PYL-eIF4G-ires-2xMCP-ABI (PIFi2MA). Cells were incubated with ABA in a range of concentrations from 1nM to 100μM for 24 hours. Flow cytometry analysis confirms that there is a relationship between ABA concentration and GFP expression. The peak responses are in the μM range of ABA, and induction of GFP translation drops off in the low nM range.

Testing the time course of protein translation: I wanted to measure the responsiveness of the system to ABA and so measured the induction of translation after incubating for various timepoints and various concentrations. ABA was added to cell cultures 12 hours after transfection with CM3G and inducer constructs in order to give cells time to produce inducing proteins. The cells transfected with the direct fusion construct already showed robust expression of GFP. The cells were collected at various time points after the addition of ABA at a concentration of 10μM. Translation of GFP increases above background levels after 6 hours after the addition of ABA, and reaches its maximum fold change in translation after twelve hours, Figure 3.23. The absolute level of GFP continues to increases after 12 hours, but the absolute levels of mCherry may be increasing faster such that the ratio of GFP fluorescence over mCherry fluorescence decreases past that time point.

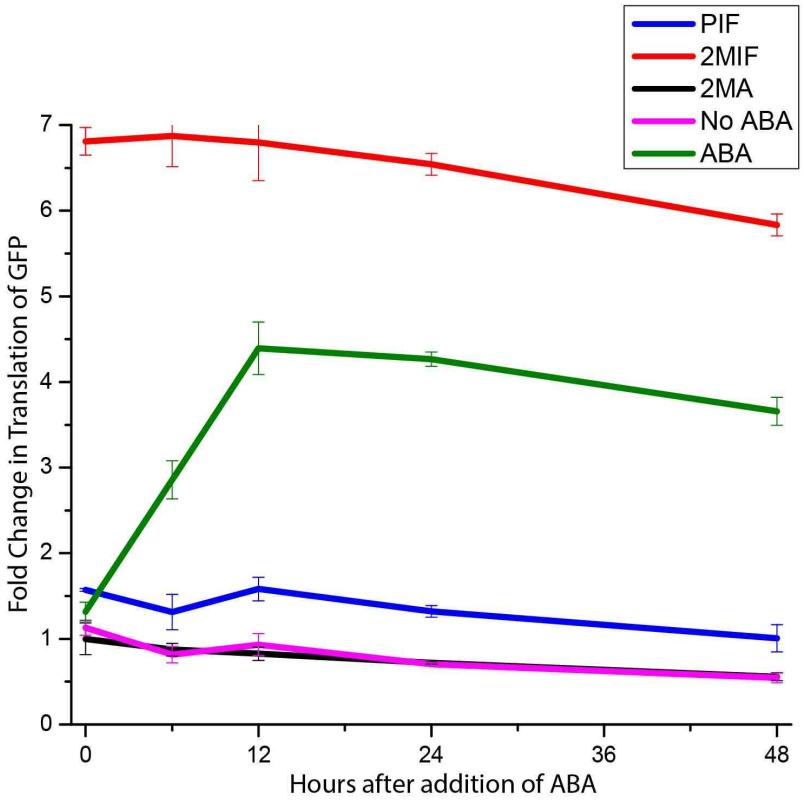

Figure 3.23. Cells were transfected with the reporter construct mCherry-MS2$_3$-GFP and the bicistronic inducer PYL-eIF4G-ires-2xMCP-ABI (PIFi2MA). Cells were incubated with ABA at a concentration of 10μM or given no ABA. Levels of translation peak 12 hours after the addition of ABA to cell cultures transfected with the reporter and inducer constructs.

3.3 Conclusion and Discussion

Reporter constructs were created to measure the difference in the amount of cap-dependent translation compared to induced cap-independent translation. GFP was expressed when the translational machinery was targeted to a specific RNA structure upstream from the start codon. RNA binding proteins from viruses were used to target cognate RNA stem loop structures. These proteins were either directly fused to the ribosome recruiting domain of eIF4G or two one of the dimerizing pair. In this way I could control the proximity of the translational machinery to the GFP sequence.

Chemically inducible dimerization from ABA is capable of controlling cap-independent translation. Fusion of the ABI protein to an MCP RNA binding domain targets the system to a MS2 stem loop, while fusion of the PYL protein to eIF4G, amino acids 642 to 1560, recruits the translation machinery. Addition of ABA dimerizes the proteins bringing the translation complex to a gene downstream of the RNA binding site initiating the production of the downstream GFP gene.

The stem loops and RNA binding proteins can be interchanged and optimized to increased translation of the reporter gene. In addition, combing both genes for the inducer proteins into one bicistronic construct allows better expression of the system. Further work to control the trafficking of the inducer proteins and the reporter mRNA could be used to allow sub-cellular regulation of translation.

The system induces the translation of the reporter gene to visible levels within hours of induction. The intensity of translation expression can be controlled by the dosage of ABA used. The intensity of activation of the system can be tuned by controlling how much ABA is present and for how long. This could be used to allow translation of a gene at a specific time and at a desired intensity to modulate biological events.

Chemically induced dimerization has been used to control biological events on a sub-cellular scale by using photocleavable cages. The development of a system to chemically induce translation of a protein allows the combination of these techniques. This opens up the possibility of sub-cellular control of specific transcripts independently of global cellular translation. Optogenetic control of translation could be used to investigate the role of a specific transcript and its protein product at a given time and place.

3.4 Methods

Materials

Restriction enzymes and polymerases were purchased from NEB. In-Fusion kit was purchase from Clonetech. Cell culture plates and tubes are from Grenier-Bio One. Cell culture reagents such as media, trypsin, and PBS were purchase from Gibco. Chemicals were purchased from Sigma unless otherwise noted. (+)-Abscisic acid was obtained from Gold Biotechnology.

DNA Plasmids Construction

DNA primers and g-block fragments were purchased from IDT.

Ac-BoxB$_1$-GFP – A g-block fragment was purchased containing a 70 nucleotide spacer followed by one functional BoxB stem loop and 40 nucleotide spacer with the following sequence

CTCAAGCTTCGAATTCTGCAGGGATCCCTGGACGGTACCCGGCTATTTAAC
CTCTTCCAACCCAAAGGCCTCTTCGAGTTCGAAGTTAACGATATCGGCGCG
CCACGCGTGATCCGGGCCCTGAAGAAGGGCCCTTTCCTTTGATCCCCCGG
GTGAAGAACCCGGGTTTCCTTTACGCGTCTCGAGTCTAGAGTCAGCTTCGA
CGAGATTTTCAGGAGCTAAGGAAGCTAAATGGCCACAACCATGGTGAGCA.

In-Fusion (Clonetech) was used to insert the fragment into Ac-ires-GFP that had been restricted with BamHI and MscI to remove the ires fragment to produce the vector Ac-BoxB$_1$-GFP.

Ac-mCherry-BoxB$_1$-GFP- The mCherry PCR product was produced using the primers CCGACAGAGCTCGCCACCATGGTGAGCAAGGGCGAGGAG and CCGACAGGATCCTTACTTGTACAGCTCGTCCATGCC. This was ligated to the Ac-BoxB$_1$-GFP vector that had been restricted with SacI and BamHI to produce Ac-mCherry-BoxB$_1$-GFP

Ac-mCherry-BoxB$_2$-GFP. The BoxB insert was created by annealing two oligonucleotides CGCGTGATCCGGGCCCTGAAGAAGGGCCCTTTCCTTTA and TAAAGGAAAGGGCCCTTCTTCAGGGCCCGGATCACGCG that were phosphorylated on their 5' ends. This double stranded DNA was ligated to the Ac-mCherry-BoxB-GFP vector that had been restricted with MluI to remove the BoxB$_1$ region. A plasmid was selected that had two copies of the BoxB insert and was named Ac-mCherry-BoxB$_2$-GFP.

Ac-mCherry-MS2$_1$-GFP & Ac-mCherry-MS2$_3$-GFP– pCR4-24XMS2SL-stable was a gift from Robert Singer (Addgene plasmid # 31865). The MS2 stem loop sequence was created by restricting this plasmid with MluI to produce fragments that contained the MS2 stem loop sequence. This fragment has one stem loop sequence in the middle of the fragment and another copy that was split by the restriction site, so that fusion of multiples of this fragment rejoined the whole stem loop sequence. Constructs were created that had one and two copies of the fragment and therefore had one and three copies of MS2. These constructs were named Ac-mCherry-MS2$_1$-GFP & Ac-mCherry-MS2$_3$-GFP.

Ac-mCherry-RL-MS2$_3$-GFP – The vector mCherry-MS2$_3$-GFP was restricted at the AscI site just upstream of the MS2 stem loops. The restriction site was then blunted using Klenow (NEB). The palindromic oligonucleotide AAACGCCTAGGCCGGAGCGCCCAGATCTGGGCGCTCCGGCCTAGGCGTTT with a 5' phosphate was annealed to form the double stranded DNA that was then ligated to the vector.

SV40-MCP-eIF4G- The MCP PCR product was created using the primers GTATATCCATTTTCGGAATTCGCCACCATGGCTTCTAACTTTACTCAG and CCCATACAGGGGGACACGCGTGCTGCCGCCGTAGATGCCGGA using pMS2-GFP, which was a gift from Robert Singer (Addgene plasmid # 27121) as the PCR template. In-Fusion (Clonetech) was used to insert the PCR product into the PYL-eIF4G vector that has been restricted with EcoRI and AscI to remove the PYL sequence and replace it with MCP.

SV40-2xMCP-eIF4G- Another MCP PCR product was created using the primer ATCTACGGCGGCAGCGGCGCGGCCATGGCTTCTAACTTTACTCAG along with the same C-terminal primer as before CCCATACAGGGGGACACGCGTGCTGCCGCCGTAGATGCCGGA. In-Fusion was used to insert the PCR product into the MCP-eIF4G vector that been restricted with AscI to insert another MCP in between the first MCP and eIF4G.

SV40-2xλN-eIF4G- The 2xλN fragment is a dimer of λN and was synthesized as a g-block by IDT with the following sequence, GTATATCCATTTTCGGAATTCGCCACCATGGATGCTCAGACAAGACGCAGG GAGAGGCGGGCCGAGAAGCAGGCCCAGTGGAAGGCCGCCAATGGCGGCA GCGGCATGGACGCCCAGACCAGAAGAAGAGAGAGAAGAGCCGAGAAGCA GGCCCAGTGGAAGGCCGCCAACGGCGCGCCAGGGCCCCCAAGGGGTGGG CCAGGTGGGGAATT. In-Fusion (Clonetech) was used to insert the fragment into the PYL-eIF4G that has been restricted with EcoRI and AscI.

SV40-PYL-eIF4G – The PYL-eIF4G construct was made by Dr. Liang and was used as the starting point for making the direct fusion constructs.

SV40-MCP-ABI & SV40-2xMCP-ABI – The constructs were made by inserting an ABI fragment created by using PCR primers with the sequence CCGACAGGCGCGCCAGTCCCCCTGTATGGGTTCACC and CCGACAGGATCCTCACTTCAGGTCCACGACGAC. This was inserted through ligation into the MCP-eIF4G and 2MCP-eIF4G vectors that had been restricted with Asc1 and BamH1 to remove eIF4G.

Ac -ires-2xMCP-ABI- To get the 2xMCP-ABI product I first tried using a primer to the N-terminal sequence of MCP, AACACGATGATAATATGGCCAATGGCTTCTAACTTTACTCAG, but this PCR reaction gave mostly the product with one copy of MCP. The 2xMCP-ABI product

was produced in such low amounts from this reaction that it could not be collected for downstream cloning. To get the 2xMCP-ABI PCR product a primer was designed upstream from the MS2 coding sequence, AACACGATGATAATATGGCCACCATTTTCGGAATTCGCCACC, that gave only the 2xMCP-ABI product when used with the same reverse primer, TTATGATCTAGAGTCGCGGCCGCTCACTTCAGGTCCACGACGAC . The MCP-ABI and 2xMCP-ABI fragments were inserted into the Ac-ires-GFP vector that had been restricted with MscI and NotI to remove the GFP DNA.

Ac-PYL-eIF4G-ires-2xMCP-ABI- The PYL-eIF4G PCR fragment was created using the primers TTTGGCAAAGAATTCCTCGAGGCCACCATGACCCAGGACGAG and GGGAGGGAGAGGGGCGGATCCTCAGTTGTGGTCAGACTCCTC. In-Fusion (Clonetech) was used to insert the PYL-eIF4G fragment into the plasmid Ac-ires-2xMCP-ABI that was restricted with XhoI and BamHI.

Cell Culture and Transfection

B35 cells were cultured in Dulbecco's modified Eagle's medium (DMEM) (Gibco) with 10% FBS (Atlanta Biologicals), 1x GlutaMAX (Gibco), and 1x penicillin/streptomycin (Pen/Strep; Gibco). Cells (100,000) were plated in wells of a 24well plate for 24 h before transfection. DNA constructs (0.1 µg to 0.5 µg) were added to 50x (v/w) Opti-MEM (Gibco) and then 3x (v/w) PEI (Polysciences)

was mixed with the DNA. The mixture was incubated for 20 min at the room temperature before adding it to cell cultures. The cells were grown for 1 day after transfection before experiments were performed.

Whole Well Fluorescence Measurement

Cells were harvested from 24 well plates by washing the cells from the surface and collecting the media. Cells were spun at 3000g for 5 min at 4°C and the media was aspirated. Cells were washed three times with PBS and spun down at 3000g for 5 min at 4°C. The cells were resuspended in 100µL of PBS and transferred to a black 96 well plate(Greiner Bio-One). The fluorescence of EGFP and mCherry were analyzed using Spectra Max i3 microplate reader with Soft Max Pro 6.3 software. EGFP fluorescence was measured using excitation at 485nm and measuring emission at 525nm while mCherry fluorescence was measured using excitation at 585nm and measuring emission at 625nm, Figure 3.24.

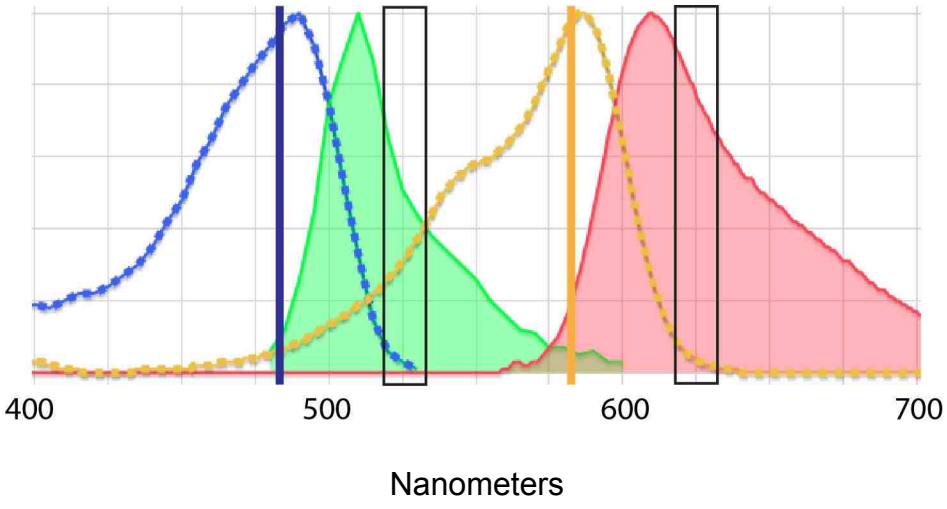

Figure 3.24. The Spectra Max i3 microplate reader has tunable excitation and emission spectra. The GFP is measured by exciting at 485nm and measuring emissions at 525nm, while the mCherry is measured by exciting at 585nm and measuring emissions at 625nm.

Flow Cytometry Measurement

To harvest the cells from a 24 well plate the media was aspirated and cells were incubated with 200µL 0.25% trypsin-EDTA (Gibco) for 15 minutes at 37°C. Cells were then spun down at 3000g for 5 min at 4°C and the trypsin was aspirated. The cells were washed with PBS and then pelleted at 3000g for 5 min at 4°C. The cells were fixed with 4% PFA (Sigma) for 15 minutes at room temperature. The cells were washed three times with PBS and then resuspended in 150µL PBS.

The cells were analyzed using a BD Accuri C6 Plus Flow Cytometer to measure the fluorescence of EGP and mCherry. The relative fluorescence of EGFP was measured using the FITC channel of the flow cytometer, while the relative mCherry fluorescence was measured using the PerCP channel of the flow cytometer. The fluorescence is excited with a 488nm laser and data was collected with the FL1 filter, 533/30, of the FITC channel and the FL3 filter, 670 LP, for the PerCP channel, Figure 3.25.

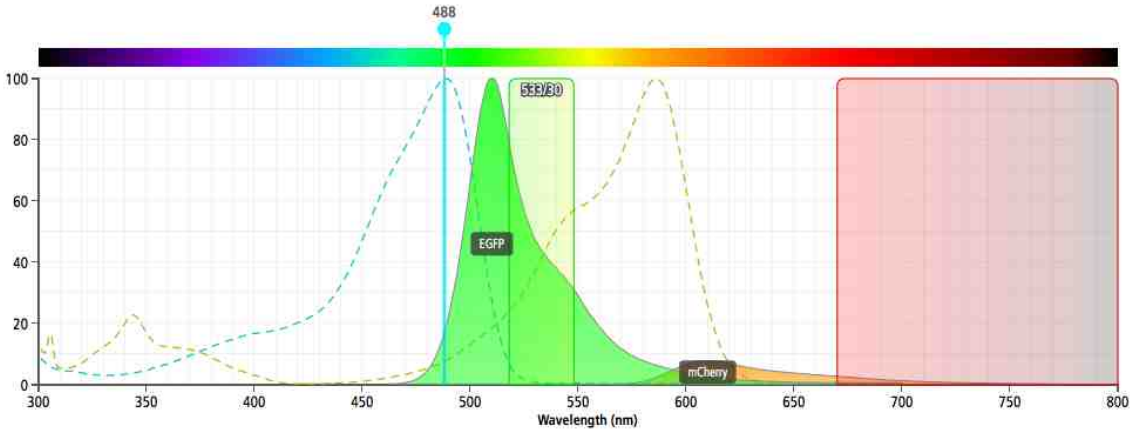

Figure 3.25. The flow cytometer has an excitation laser at 488nm that excites GFP at 99.8% of maximum and excites mCherry at 7.6% of maximum. The FL1 filter is at 533nm and has a band width of 30nm and collects 33.7% of the GFP emission. The FL3 filter is at 670nm and is a long pass filter and collects 20.1% of the mCherry emission.

Cells that were not transfected with the reporter construct showed most mCherry fluorescence below 10,000. The analysis of the change in fluorescence excluded the cells that had mCherry fluorescence below 10,000, Figure 3.26.

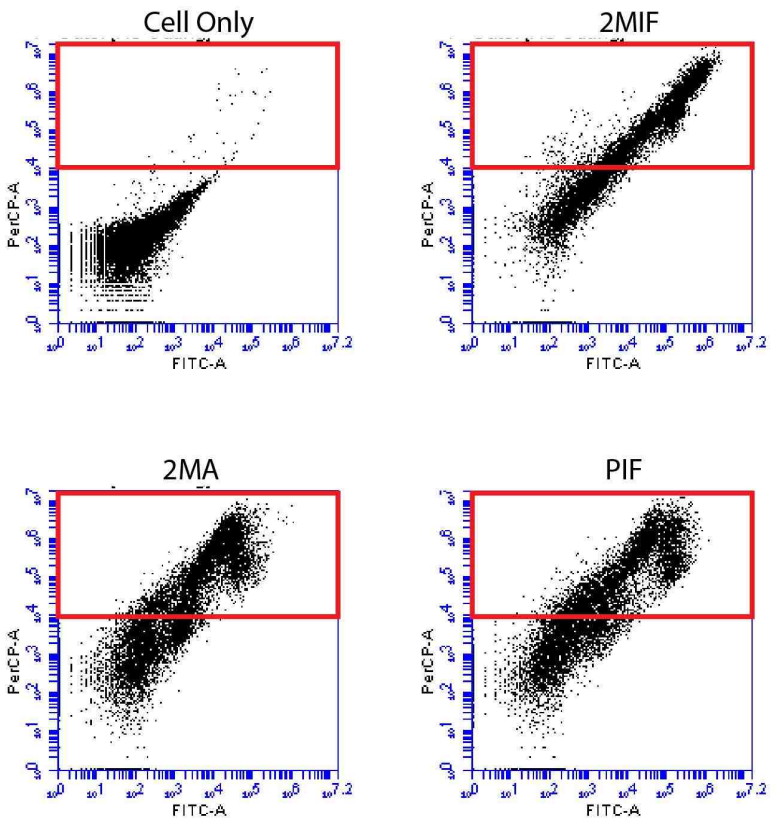

Figure 3.26. Cells were analyzed by flow cytometry based upon their GFP and mCherry fluorescence measured with the FITC and PerCP channels respectively. Statistics were calculated for cells showing mCherry expression above the levels seen for the untransfected cells (area shown in red box). The presence of the direct fusion protein 2xMCP-eIF4G causes translation of the GFP gene and is shifted further to the right than the negative controls.

Fluorescence Analysis

The amount of cap-dependent translation of mCherry is not affected by the amount of cap-independent translation of a downstream gene. Therefore the amount of mCherry expressed serves as a control for transfection and transcription of the reporter construct and can be used as a standard to the

amount of EGFP produced. Thus the relative amount of translation induction is found by dividing the EGFP fluorescence by the mCherry fluorescence.

$$\frac{cap-independent\ translation}{cap-dependent\ transltion}=\frac{EGFP\ Fluorescence}{mCherry\ Fluorescence}$$

$$relative\ amount\ of\ translation\ induction=\frac{cap-independent\ translation}{cap-dependent\ transltion}$$

Taking the relative amount of cap-independent translation of the experimental condition and dividing it by the relative amount of cap-independent translation of the control can measure the change in cap-independent translation. This normalizes the value and gives us the fold change in ABA inducible translation.

$$fold\ change\ in\ translation=\frac{relative\ amount\ of\ translation\ induction\ (experimental)}{relative\ amount\ of\ translation\ induction\ (control)}$$

3.5 References

1. De Gregorio, E.; Preiss, T.; Hentze, M.W. Translation driven by an eIF4G core domain in vivo. *EMBO J*. **1999**, 18, 4865-74.

2. Pantopoulos, K. Iron metabolism and the IRE/IRP regulatorysystem: an update. *Ann. N. Y. Acad. Sci*. **2004**, 1012, 1–13.

3. Barik, S.; Ghosh, B.; Whalen, W.; Lazinski, D.; Das, A. Anantitermination protein engages the elongating transcriptionapparatus at a promoter-proximal recognition site. *Cell* **1987**, 50, 885–899.

4. Lazinski, D.; Grzadzielska, E.; Das, A. Sequence-specificrecognition of RNA hairpins by bacteriophage antiterminatorsrequires a conserved arginine-rich motif. *Cell* **1989**, 59, 207–218.

5. Tan, R.; Frankel, A.D. Structural variety of arginine-richRNA-binding peptides. *Proc. Natl. Acad. Sci. U.S.A.* **1995**, 92, 5282–5286.

6. Chattopadhyay, S.; Garcia-Mena, J.; DeVito, J.; Wolska, K.; Das,A. Bipartite function of a small RNA hairpin in transcriptionantitermination in bacteriophage lambda. *Proc. Natl. Acad.Sci. U.S.A*. **1995**, 92, 4061–4065.

7. Bernardi , A.; François, P. Nucleotide Sequence at the Binding Site for Coat Protein on RNA of Bacteriophage R17. *Proc. Natl. Acad. Sci. USA* **1972**, 69, 3033–3037.

8. Bertrand, E.; Chartrand, P.; Schaefer, M.; Shenoy, S.M.; Singer,R.H.; Long, R.M. Localization of ASH1 mRNA particlesin living yeast. *Mol. Cell* **1998**, 2, 437–445.

9. Carey, J.; Cameron, V.; de Haseth, P.L.; Uhlenbeck, O.C. Sequence-specific interaction of R17 coat protein with itsribonucleic acid binding site. *Biochemistry* **1983**, 22, 2601–2610.

10. Peabody, D.S.; Ely, K.R. Control of translational repression by protein-protein interactions. *Nucleic Acids Res*. **1992**, 20,1649-1655.

11. Peabody, D.S. The RNA binding site of bacteriophage MS2 coat protein. *EMBO J*. **1993**, 12, 595–600.

12. Lim, F.; Peabody, D.S. Mutations that increase the affinity of a translational repressor for RNA. *Nucleic Acids Res.* **1994**, 22, 3748-3752.

13. Valegard, K.; Liljas, L.; Fridborg, K.; Unge, T. The three-dimensional structure of the bacterial virus MS2. *Nature* **1990**, 345, 36–41.

14. Peabody, D.S.; Lim, F. Complementation of RNA binding site mutations in MS2 coat protein heterodimers. *Nucleic Acids Res*. **1996**, 24, 2352–2359.

15. Romaniuk, P.J.; Lowary, P.; Wu, H.N.; Stormo, G.; Uhlenbeck,O.C. RNA binding site of R17 coat protein. *Biochemistry* **1987**, 26,1563–1568.

16. Uhlenbeck, O.C.; Carey, J.; Romaniuk, P.J.; Lowary, P.T.; Beckett, D. Interaction of R17 coat protein with its RNA binding site for translational repression. J. *Biomol. Str. and Dyn*. **1983**, 1, 532-552.